An investigation of hydrogen generation via steam reforming of liquid fuels

Von der Fakultät für Energie-, Verfahrens- und Biotechnik der Universität Stuttgart
zur Erlangung der Würde eines Doktors der Ingenieurwissenschaften (Dr.-Ing.)
genehmigte Abhandlung

vorgelegt von

Stefan Martin

aus Kaufbeuren

Hauptberichter: Prof. Dr. rer. nat. habil. André Thess

Mitberichter: Prof. Dr. techn. Günter Scheffknecht

Tag der mündlichen Prüfung: 15.12.2016

Institut für Energiespeicherung der Universität Stuttgart

2017

Für Claudia, Karin, Alexander und Thomas

Table of contents

Preface

The present doctoral thesis is based on three peer-reviewed journal papers which I have published as lead author in the International Journal of Hydrogen Energy (ISSN: 0360-3199). In particular, the following contributions are included:

- S. Martin, G. Kraaij, T. Ascher, D. Wails, A. Wörner: An experimental investigation of biodiesel steam reforming, International Journal of Hydrogen Energy 40, (2015), 95–105

- S. Martin, G. Kraaij, T. Ascher, G. Karagiannakis, P. Baltzopoulou, D. Wails, A. Wörner: Direct steam reforming of diesel and diesel-biodiesel blends for distributed hydrogen generation, International Journal of Hydrogen Energy 40, (2015), 75–84

- S. Martin, F. G. Albrecht, P. van der Veer, D. Lieftink, R.-U. Dietrich: Evaluation of on-site hydrogen generation via steam reforming of biodiesel: Process optimization and heat integration, International Journal of Hydrogen Energy 41, (2016), 6640–6652

Apart from the above papers which were largely adopted for the present work, a chapter containing a comprehensive discussion has been included supplemented by additional material where necessary.

I hereby certify that the dissertation entitled "An investigation of hydrogen generation via steam reforming of liquid fuels" is my own work with minor contributions of the co-authors of the above-mentioned papers. Intellectual properties including graphs and data sets originating from other sources have been clearly indicated.

Nomenclature

Latin symbols

Symbol	Description	Unit
a	side length	m
A	area	m^2
c	concentration	kg m^{-3}
c$_p$	specific heat capacity	J kg^{-1} K^{-1}
$\dot{C}_p$	heat capacity flow rate	W K^{-1}
d	diameter	m
G	Gibbs free energy	J
$\dot{H}$	heat load	W
l	length	m
L	characteristic length	m
$\dot{m}$	mass flow rate	kg h^{-1}
M	molar weight	g mol^{-1}
p	pressure	Pa
P	power	W
$\dot{Q}$	heat flux	W
Re	Reynolds number	-
S/C	steam-to-carbon ratio	-
t	time	s
T	temperature	K

U	heat transfer coefficient	W m^{-2} K^{-1}
$\bar{v}$	mean flow velocity	m s^{-1}
$\dot{V}$	volume flow rate	m^3 s^{-1}
vol. %	volume percent	-
wt. %	weight percent	-

Greek symbols

β	film diffusion coefficient	m s^{-1}
δ	boundary layer thickness	mm
Δ	difference	-
η	efficiency	-
μ	chemical potential	J mol^{-1}
ν	stoichiometric coefficient	-
ξ	extent of reaction	mole
υ	kinematic viscosity	m^2 s^{-1}

Subscripts

ads	adsorbed
BD	biodiesel
c	cold
C	carbon
Cat	catalyst
cond	condensed
diff	diffusive
Dod	dodecane
eff	effective

el	electric
eq	equilibrium
g	gas phase
h	hot
HC	hydrocarbon
hyd	hydraulic
i	index
l	liquid
LM	logarithmic
max	maximum
min	minimum
p	at constant pressure
rec	recuperative
R	reaction
Ref	reformer
s	solid
Syst	system

Abbrevations

ATR	autothermal reforming
B	burner
BT	benzothiophene
COND	condensate
DBT	dibenzothiophene
DHG	distributed hydrogen generation
EDX	energy dispersive X-ray spectroscopy

EN	European Norm
FAME	fatty acid methyl ester
FCEV	fuel cell electric vehicle
FCH JU	Fuel Cells and Hydrogen Joint Undertaking
FS	full scale
FCR	fuel conversion rate
GC	gas chromatography
GHSV	gas hourly space velocity
HEX	heat exchanger
LHV	lower heating value
MFC	mass flow controller
MFM	mass flow meter
NEMESIS2$^+$	New Method for Superior Integrated Hydrogen Generation System 2$^+$
OxBFR	oxygen-biodiesel molar feed ratio
POX	partial oxidation
PSA	pressure swing adsorption
PSC	paper structured catalyst
SEM	scanning electron microscopy
SOFC	solid oxide fuel cell
SR	steam reforming
SRK	Soave-Redlich-Kwong
STP	standard temperature and pressure
SV	space velocity
WBFR	water-biodiesel molar feed ratio
WGS	water gas shift
YSZ	yttria-stabilized ZrO_2

Abstract

Within the present work steam reforming of biodiesel, diesel and bioethanol is investigated experimentally and on process level. Liquid fuels have the advantage of a high volumetric and gravimetric energy density and an existing distribution infrastructure. On-site hydrogen generation from liquid fuels by means of reforming can help accelerate the market breakthrough of fuel cell electric vehicles. Besides, there is an increasing demand for industrial applications such as the production of high quality flat glass.

The experimental investigations of the current thesis aim at a thorough understanding of catalyst deactivation during direct steam reforming of liquid fuels. Suitable operating conditions are derived in order to avoid initiation of coke deposition on the catalyst surface. The experimental results show a detrimental effect of low temperature and high fuel mass flow rate on catalyst deactivation induced by coke deposition. Results clearly indicate that coking tendency increases in the order bioethanol < biodiesel < diesel. By adjusting the temperature and the fuel mass flow rate, a stable product gas composition close to chemical equilibrium has been achieved during 100 hours of operation. Catalyst deactivation was not observed. The reformer catalyst activity is higher when using desulphurized diesel, indicating an appreciable effect of organic sulphur compounds on long-term reformer performance.

The experimental work is accompanied by a simulation study, the main emphasis which is placed on evaluating a 50 Nm^3/h on-site hydrogen generation system based on steam reforming of biodiesel. The system consists of a steam reformer, a water gas shift stage, a pressure swing adsorption unit and a dual fuel burner. A positive effect of high pressure on thermal system efficiency is observed. For given operating conditions (p=13 bar, T=825 °C) sensitivity analysis with Aspen Plus reveals an optimum steam-to-carbon ratio of 2.78. Upon process optimization a heat-integrated near-optimum fuel processor system is developed with a thermal system efficiency of 75.6 % (based on lower heating value).

Zusammenfassung

Im Rahmen der vorliegenden Arbeit wurde die Dampfreformierung von Biodiesel, Diesel und Bioethanol experimentell und theoretisch untersucht. Flüssige Brennstoffe zeichnen sich durch eine hohe volumetrische und gravimetrische Energiedichte und eine bereits vorhandene Verteilungsinfrastruktur aus. Die dezentrale Wasserstofferzeugung aus Flüssigbrennstoffen durch Reformierung kann mit dazu beitragen, die Marktdurchdringung von Brennstoffzellen-fahrzeugen zu beschleunigen. Weitere Anwendungsmöglichkeiten bestehen im industriellen Sektor, etwa für metallurgische Prozesse oder für die Herstellung von Flachglas.

Im Rahmen der experimentellen Arbeiten wurde ein vertieftes Verständnis der Katalysator-deaktivierung erzielt. Insbesondere wurden geeignete Betriebsbedingungen ermittelt, um die initiale Kohlenstoffbildung auf der Katalysatoroberfläche zu verhindern. Geringe Temperaturen und hohe Brennstoffmassenströme begünstigen eine Katalysatordeaktivierung durch Verkokung. Die Kohlenstoffbildungsneigung nimmt in der Reihenfolge Bioethanol < Biodiesel < Diesel zu. Durch entsprechende Wahl der Katalysatoreintrittstemperatur und des Brennstoffmassenstromes wurde für die jeweiligen Flüssigbrennstoffe ein stabiler Versuchsbetrieb (100 Stunden) nahe am chemischen Gleichgewicht nachgewiesen. Im Falle von fossilem Diesel hat sich gezeigt, dass die Langzeitstabilität der Dampfreformierung durch eine vorhergehende Entschwefelung des Kraftstoffs weiter verbessert werden kann.

Die experimentellen Arbeiten werden ergänzt durch eine Simulationsstudie. Ziel der Untersuchung ist die verfahrenstechnische Optimierung einer Wasserstofferzeugungseinheit aus Biodiesel (50 Nm^3/h H$_2$) bestehend aus den Komponenten Dampfreformierung, Wassergasshift-Stufe, Druckwechseladsorption und Gas-Flüssig-Brenner. Neben einem positiven Druckeinfluss zeigen die Ergebnisse ein Optimum des molaren Dampf:Kohlenstoff-Verhältnisses bei 2,78. Aufbauend auf einem verfahrenstechnisch optimierten System wird ein wärmeintegrierter Wasserstoffgenerator entwickelt mit einem thermischen Systemwirkungsgrad von 75,6 % (bezogen auf den unteren Heizwert).

1.   Introduction

1.1   Motivation

Hydrogen is considered to be a promising energy carrier for future energy requirements as it can be produced from a wide variety of resources including renewable and non-renewable feedstock. Hydrogen is the most abundant element in the universe (75 wt. %) and accounts for 0.14 wt. % of the earth's crust [Audesirk 1999, Lide 2005]. It occurs mainly in combination with carbon and oxygen, most of the hydrogen which is bonded to water and organic compounds. Thus, any hydrogen supply chain requires a primary hydrogen production step followed by compression, transportation and distribution. The currently available hydrogen production technologies can be broadly divided into three categories [Kırtay 2011, Dutta 2014, Sterner 2014, Dincer 2015]:

- Thermochemical hydrogen production: reforming, gasification and pyrolysis of biomass and biomass-derived products, thermal dissociation of water, thermochemical water splitting cycles, hybrid thermochemical cycles

- Electrochemical hydrogen production: water electrolysis, chlor-alkali electrolysis, photoelectrolysis

- Biochemical hydrogen production: dark fermentation, photofermentation, biophotolysis

Approximately 65 million tons of hydrogen are produced annually worldwide [Navarro 2011], large quantities of which are needed for the chemical and petrochemical industry, in particular for ammonia production, oil refining and methanol synthesis. Besides, hydrogen is increasingly discussed as an energy carrier for transport applications [Holladay 2009].

Today, 48 % of the global hydrogen demand is supplied by steam reforming (SR) of natural gas, 30 % from heavy oil and naphta reforming, 18 % from coal gasification, 3.9 % from water electrolysis and 0.1 % from other sources [Navarro 2011].
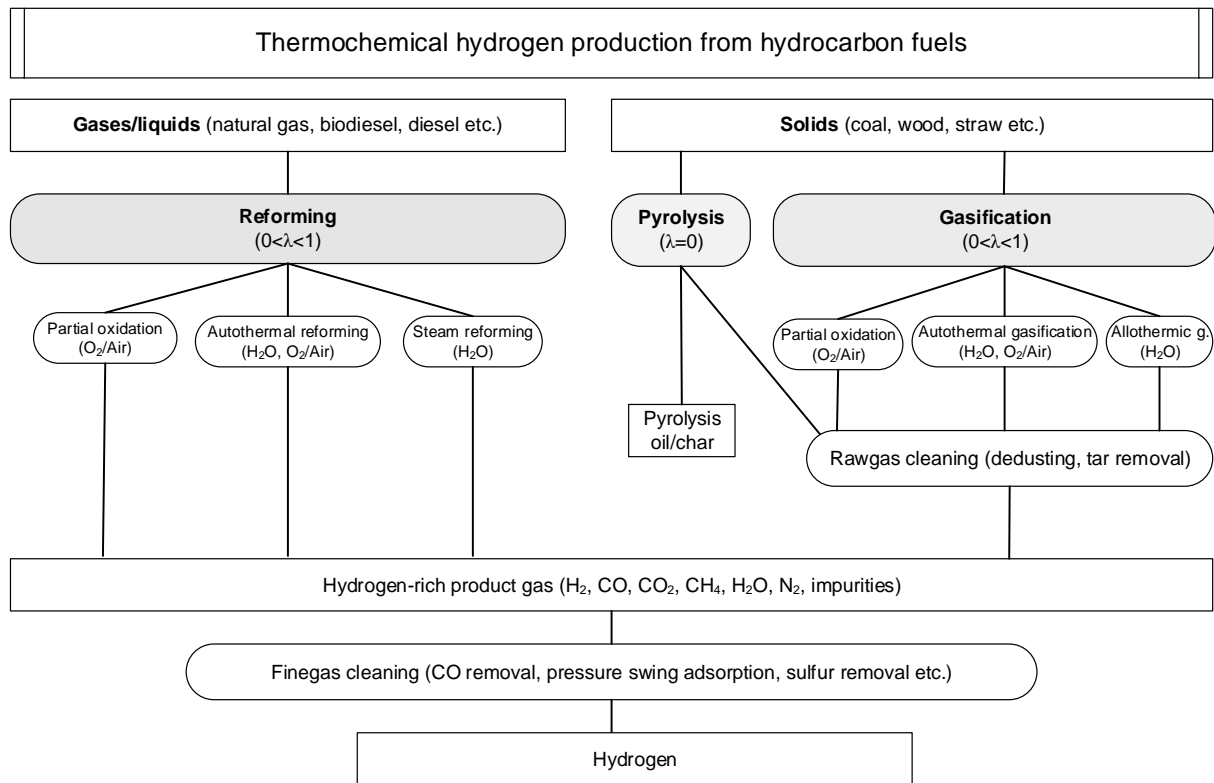
```
┌─────────────────────────────────────────────────────────────────────────────┐
│          Thermochemical hydrogen production from hydrocarbon fuels            │
└─────────────────────────────────────────────────────────────────────────────┘
```

Figure 1 – Main thermochemical hydrogen production routes

Thermochemical hydrogen production routes based on reforming and gasification (Fig. 1) are currently among the most mature and cost effective technologies [Chaubey 2013]. Reforming/gasification involves the conversion of hydrocarbon fuels in the high temperature range under lack of oxygen using steam, air/oxygen or the combination of both as gasifying agents. In the particular case of liquid fuel steam reforming, liquid hydrocarbons are catalytically transformed into a hydrogen-rich gas by reaction with steam in the absence of oxygen. (Details of the SR reaction system are given in chapter 2.2) Rapid catalyst deactivation induced by coke deposition on the catalyst surface is one of the main obstacles that prevents the industrial use of liquid fuel SR. The current thesis particularly addresses this issue (see chapter 1.4).

Electrolysis of water, which is widely considered as a promising future hydrogen production technology allowing to balance fluctuating renewable energy sources, still suffers from high costs of electricity resulting in increased hydrogen net production costs [Carmo 2013].

Recently, biochemical hydrogen production has attracted increasing attention. However, it is still in an early stage of development leaving room for significant improvements. Low efficiencies and high production costs are among the main challenges to be resolved [Dincer 2015].

The prevailing hydrogen production method – steam reforming of natural gas – mainly takes place in large-scale, central production plants. However, with an increasing share of fuel cell electric vehicles (FCEVs) in the market, which is expected to happen in Germany in the next decade [Pfropfe 2013], central hydrogen production will suffer from additional costs associated with the distribution of gaseous-phase hydrogen by trailer over long distances [Yeh 2014]. Taking into account that transportation costs significantly contribute to the overall hydrogen production costs, distributed hydrogen generation (DHG) from logistic fuels is a viable alternative in the transition phase towards a fully renewable hydrogen production economy [Ogden 2001, Hulteberg 2008, Schjølberg 2012]. DHG at fueling stations offers the advantage of using readily available liquid fuels such as diesel, biodiesel and bioethanol with high energy densities and already existing infrastructure. Rostrup-Nielsen [2004] considers decentralized SR of hydrocarbons in compact units a promising vehicle for bridging the gap to a future hydrogen economy.

Hydrogen generation from liquid fuels is applicable but not limited to decentralized hydrogen production at fueling sites. There is an increasing demand for annealing applications, in particular for metal treatment processes and for the production of high quality flat glass. According to Neumann [2003] conventional hydrogen generation processes up to 300 Nm^3/h H_2 are being increasingly substituted with advanced reforming technologies.

1.2   Historical perspective and current research activities

Steam reforming of liquid fuels was first introduced in the 1960s for the production of town gas and substitute natural gas from naphta [Davies 1967, Moseley 1972]. Today, SR of heavy hydrocarbons for industrial applications is usually accomplished using an adiabatic pre-reforming step prior to the tubular main reformer [Rostrup-Nielsen 2004]. Typically, Nickel containing catalysts are used in the low temperature range between 350 °C and 500 °C. During pre-reforming the long-chain hydrocarbons are converted into a methane-rich gas, thereby avoiding carbon formation in the subsequent tubular main reformer. Since the 1980s adiabatic pre-reforming of heavy hydrocarbons has become an established process in syngas production. In modern steam reforming plants, natural gas is the most commonly used feedstock. However, naphta is also used, depending on feedstock availability [Bartholomew 2006].

Recent research activities focus on catalytic reforming of methanol, ethanol, butanol, vegetable oil, biodiesel, glycerol and different types of bio-oil for fuel cell applications [Blasi 2014, Frusteri 2015]. Besides, fossil fuels such as diesel and kerosene have attracted considerable attention. Although fossil fuels are not sustainable, they can be used during the transition phase while the renewable hydrogen production techniques are being developed [Dincer 2015], thus securing a smooth transition from the current fossil based economy to a future hydrogen economy based on renewables. It is generally agreed that fuel processing of fossil and renewable fuels will play a crucial role in distributed energy generation in the short and mid-term perspective [Specchia 2014].

1.3   Literature survey

1.3.1   Steam reforming of diesel

In 1996 T. S. Christensen was the first to show steam reforming of diesel and jet fuel in an adiabatic reactor using a Ni catalyst supported on magnesium oxide [Christensen 1996]. Since then successful pre-reforming of diesel in the low temperature range using Ni-based catalysts has been demonstrated by several working groups [Piwetz 1996, Boon 2011, Koo 2014]. By contrast, direct SR of diesel at high temperatures ($\sim 800\,°C$) is still at an early research and development stage and needs further improvement [Specchia 2014]. Typically, diesel SR catalysts become deactivated within a few hours of on-stream exposure [Fauteux-Lefebvre 2011] due to rapid catalyst deactivation induced by coking, sulphur poisoning and/or sintering [Bartholomew 2006].

Ming et al. [2002] carried out SR of diesel surrogate hexadecane using a proprietary catalyst formulation in a packed-bed reactor. Stable catalyst performance was shown for 73 hours on stream without observing deactivation or carbon deposition. Goud et al. [2007] conducted SR of hexadecane using a Pd/ZrO_2 catalyst coated on metal foils at steam-to-carbon ratios (S/C) of $3-6$ and $T = 750\,°C - 850\,°C$. A first-order kinetic model with a first-order deactivation rate was obtained. The catalyst deactivation rate was found to be accelerated by the presence of sulphur, low S/C and at low temperatures.

In recent years, research groups have propagated the use of microstructured reactors for SR of diesel-like fuels, thereby circumventing problems related to heat and mass transfer limitations. Thormann et al. [2009, 2012] investigated hexadecane SR over a Rh/CeO_2 catalyst using microstructured devices. The experiments revealed a fast transient response, thereby making it an interesting option for mobile APU applications. However, the reformer system suffered from high heat losses. Kolb et al. [2009] developed a microstructured plate heat exchanger composed of stainless steel metal foils. Oxidative diesel steam reforming (molar O/C-ratio: $0.12 - 0.2$) was performed using Euro V diesel supplied by Shell and using commercial catalysts provided by Johnson Matthey. Although a diesel conversion of 99.9 % was achieved, formation of light hydrocarbons started after only a few hours of operation at S/C < 4 indicating the onset of catalyst deactivation. In a follow-up study, Grote et al. [2011] carried out further steam reforming tests ($4 - 10$ kW thermal input) using a diesel surrogate mixture, accompanied by computational fluid dynamics modeling. The results show an increase of residual hydrocarbons (caused by a reduction of catalyst activity) with decreasing temperature. In order to prevent the formation of higher hydrocarbons, a reformer outlet temperature in excess of 1013 K was required. Long-term performance data is not presented by the authors. In a second follow-up study, Maximini et al. [2012] tested four downscaled microchannel diesel steam reformers ($1\,kW_{th}$) with different precious metal coatings at S/C ratios of 3 and 4. Increased carbon formation was observed when reducing the temperature from 800 °C to 700 °C. This was accompanied by the formation of higher hydrocarbons like C_2H_4, C_2H_2 and C_3H_6. The same group of authors presented experimental results of a microstructured diesel SR fuel processor coupled with a PEM fuel cell [Engelhardt 2012]. The $10\,kW_{th}$ reformer consisted of 35 reformer channels with a channel height of 0.6 mm and 34 combustion channels being operated at S/C $= 5$ and 6 and a reactor outlet temperature of 765 °C $-$ 800 °C. The results indicate a clear trend toward increasing residual hydrocarbon formation in the reformate gas for higher feed mass flow rates causing a decline of the mean cell voltage of the stack.

Other research groups used Ni-based catalysts for SR of diesel as Nickel is less expensive and more readily available than precious metals [Fauteux-Lefebvre 2010/2011, Xu 2011, Achouri 2013, Zyryanova 2013]. Fauteux-Lefebvre et al. [2010] tested an Al_2O_3-ZrO_2-supported nickel-alumina spinel catalyst in a lab-scale isothermal packed-bed reactor at various operating conditions. Mixing of fuel and water was achieved by feeding in a stabilized hydrocarbon-water

emulsion, which successfully prevented undesired pre-cracking. Product concentrations close to equilibrium for up to 20 hours of on-stream exposure were reported at severe operating conditions (T < 720 °C, S/C < 2.5). Steam reforming of commercial diesel was carried out for more than 15 hours at S/C < 2. Carbon formation on the catalyst surface was not observed, although measured diesel conversion was lower than 90 % [Fauteux-Lefebvre 2011].

Boon et al. [2011] were the first to report stable diesel SR for more than 100 hours at temperatures of 800 °C using commercial precious metal catalysts. The experiments were carried out in a packed-bed reactor at gas hourly space velocities (GHSV) of $1000 \, h^{-1} - 2000 \, h^{-1}$. Diesel evaporation was achieved by spraying diesel in a hot gas phase, thereby preventing self-pyrolysis during the evaporation step. Stable conditions with no sign of deactivation were reported for 143 hours on stream at 1.2 bar, 800 °C and S/C = 4.6 and 2.6 using Aral Ultimate diesel with an added 6.5 ppm sulphur. Similar experiments with commercial BP Ultimate diesel containing 6 ppm sulphur turned out to be more challenging due to problems with blocking of the diesel capillary and the nozzle. By using a medium sized diesel capillary (0.25 mm internal diameter) continuous operation was achieved for 180 hours without observing any sign of deactivation, although deactivation occurred at larger diameters. The authors concluded that the observed deactivation was caused by the poor spraying of diesel, resulting in fluctuations of diesel conversion, thus initiating coke deposition.

1.3.2 Steam reforming of biodiesel

Amongst the available logistic fuels, biodiesel, which is a fatty acid methyl ester (FAME) produced from transesterification of vegetable oil with methanol, appears to be a promising feedstock for distributed hydrogen generation by means of SR [Qi 2007, Nahar 2012]. Biodiesel is a renewable, non-polluting resource with a low sulphur content (typically below 5 ppmw), a high energy density and an already existing infrastructure. Currently, biodiesel is produced at a rate of approximately 33 billion litres per year, thus representing 20 % of world's biofuel production [Diop 2013]. Nahar & Dupont [2012] reviewed the use of steam reforming to convert liquid bio-feedstock to a hydrogen-rich product gas. According to the authors, biodiesel is among the least explored liquid feedstocks for hydrogen production.

The reported literature treating hydrogen production from biodiesel is almost entirely related to ATR of biodiesel for fuel cell applications [Sgroi 2005, Specchia 2005, Colucci 2006, Kraaij 2009, Nahar 2010, Siefert 2012, Lin 2013, Gonzalez 2013, Lin 2014]. Although promising concepts have been identified, challenges remain with regard to incomplete biodiesel conversion, formation of higher hydrocarbons and catalyst coking. In contrast, hydrogen production from biodiesel by means of SR is very recent and offers significant room for further development [Xuan 2009, Nahar 2012].

Nahar [2010] carried out a thermodynamic analysis of biodiesel SR and ATR using Gibbs free energy minimization method. The water-biodiesel molar feed ratio (WBFR) was varied between 3 and 12, oxygen-biodiesel molar feed ratio (OxBFR) between 0 and 4.8 and reaction temperature between 300 °C and 800 °C under atmospheric pressure. Hydrogen yield and selectivity were found to be highest for SR conditions with a maximum hydrogen yield at WBFR=12 and T=800 °C. Increased coke selectivity is reported for SR compared to ATR conditions.

Martin & Wörner [2011] report a plateau for thermal hydrogen efficiency for a heat integrated biodiesel SR system (including water gas shift and burner) of 76 % at S/C=3 in the temperature range 700 °C − 850 °C.

Abatzoglou et al. [2011] investigated biodiesel SR using a newly developed Al_2O_3/YSZ supported $NiAl_2O_4$ spinel catalyst. Work was performed in a fixed-bed isothermal reactor. Biodiesel/water was emulsified prior to being injected at room temperature into the reactor preheating zone maintained at 550 °C. The molar S/C-ratio was varied between 1.9 and 2.4, the temperature between 700 °C and 725 °C and space velocity (SV) between 5,500 and 13,500 $cm^3_{reac} g_{cat}^{-1} h^{-1}$ at atmospheric pressure. Results show that complete biodiesel conversion has been achieved during 4 hours of operation at S/C=1.9, SV=5,500 and T=725 °C. Coke deposition and catalyst deactivation were not observed.

Shiratori et al. [2013-1] evaluated paper structured catalysts (PSCs) for steam reforming of biodiesel. Catalytic activity of the Ni-PSC could be significantly improved by Ni-MgO loading and introducing Cs as an inorganic binder. The inorganic fiber network of the PSC with a mean pore size of 20 μm leads to an effective three-dimensional diffusion and a good dispersion of the

metal catalyst particles, resulting in efficient biodiesel conversion. 50 hours of biodiesel SR was achieved using a Ni-MgO loaded PSC at 800 °C and S/C=3.5 with 90 % fuel conversion. Although formation of C_2H_4 could be avoided, CH_4 levels started to rise after 28 hours of operation, indicating the onset of catalyst deactivation. However, Ni agglomeration and carbon deposition on the PSC were not observed.

In a follow-up study, Shiratori et al. [2013-2] evaluated SOFC performance connected with PSC in the direct feed of wet oleic fatty acid methyl ester ($C_{19}H_{36}O_2$). By application of two PSCs in series (Ni-MgO loaded and Ru-loaded $BaTiO_3$ containing PSC) prior to a single cell SOFC, stable cell voltage has been observed for 100 hours at 800 °C and S/C=2. Carbon formation was not observed on the SOFC anode surface nor on the PSCs. Data on reformate gas composition prior to the SOFC is not available.

Recently, Nahar et al. [2015] evaluated the feasibility of hydrogen production from steam reforming of biodiesel feedstock on Ni-supported catalysts. Effects of temperatures of biodiesel preheating/vaporizing (190 °C − 365 °C) and reforming (600 °C − 800 °C), molar S/C ratio (2 − 3), and residence time in the reformer were examined for 2 hours of on-stream exposure. Although steady-state conditions have been achieved, the product gas composition was not in equilibrium and significant amounts of carbon had deposited on the catalyst. An increase of S/C ratio positively affected the hydrogen yield and reduced carbon deposition.

1.3.3 Small-scale H_2 production from liquid fuels

Research efforts have been carried out in recent years regarding small-scale hydrogen production systems targeting a high system efficiency and low hydrogen production costs.

Katikaneni et al. [2014] conducted a detailed performance study comparing on-site hydrogen generation from liquid fuels by different process routes. Calculations were based on a 1000 kg/d hydrogen filling station (approximately 250 FCEVs per day). The hydrogen generation efficiency was found to be highest for a concept based on SR with upstream hydrodesulphurization. For diesel fuel a thermal H_2-efficiency of 65.2 % was calculated. In terms of hydrogen production costs, the authors conclude that on-site diesel SR is competitive with centralized hydrogen production from natural gas with pipeline transport ($ 6.72 per kg vs. $ 6.23 per kg). Finally,

the authors present a hydrogen roadmap starting with a small-scale 50 Nm^3/h H_2 generation system (\$ 28.8 per kg H_2), the costs of which can be reduced dramatically by design optimization and heat integration.

Persson [2007] investigated an integrated 20 kW hydrogen production system based on feedstock methane using a catalytic converter (steam reformer, water gas shift reactor, catalytic burner) and a pressure swing adsorption (PSA) unit. The Aspen Plus calculations were carried out at a pressure of 4 bar assuming a reformer catalyst inlet temperature of 550 °C and an outlet temperature of 850 °C. In the downstream WGS reactor the carbon monoxide content was reduced to below 1.5 vol. %. The PSA off-gas and methane were burned with air at 900 °C in order to provide the necessary heat for the endothermic steam reforming reaction. Parasitic power consumption amounted for 520 W with estimated heat losses of 710 W.

The S/C ratio and the system pressure were identified to be crucial parameters for achieving a high system efficiency. A maximum theoretical efficiency (based on lower heating value LHV) of 79.1 % is reported at an S/C ratio of 2.2. Hulteberg et al. [2008] carried out an experimental investigation based on a similar system using Fischer-Tropsch-Diesel for the production of 7 Nm^3/h H_2. The catalytic converter was operated at a pressure of 5 bar and an S/C ratio of $3.1 - 4.1$. Reforming catalyst temperature ranged from 650 °C at the catalyst inlet to $750 - 800$ °C at the catalyst outlet. High heat and mass transfer were ensured by using a noble metal catalyst supported on a patented thermally sprayed woven wire mesh system. With the given experimental set-up, a maximum system efficiency of 58 % (based on LHV) was achieved assuming a parasitic power consumption of 500 W.

In the industrial field, stand-alone fuel processors for distributed hydrogen generation from readily available liquid fuels (methanol, ethanol, diesel, biodiesel) are currently being developed by several companies including Helbio S.A. (Greece), HyGear B.V. (The Netherlands), SerEnergy (Denmark), PowerCell AB (Sweden), Innovatek (United States) and Precision Combustion (United States). Although considerable progress has been made in terms of system durability, the development of low-cost DHG systems based on liquid fuels is still in an early stage leaving room for further development [Bolat 2014, Dincer 2015]. Regarding SR of biodiesel, there is no literature data available for heat integrated on-site hydrogen production systems including PSA in the kilowatt range.

1.4   Aim of this thesis

Literature study indicates that coke deposition on the catalyst surface, sulphur poisoning and sintering are among the main reasons for catalyst deactivation during steam reforming of diesel and biodiesel. In particular, deactivation by carbon deposition is a significant barrier to commercialization of fuel cell technologies based on liquid fuel reforming [Lakhapatri 2009]. Bartholomew [1982], Trimm [1999] and Yoon et al. [2009] consider minimization of catalyst coking as one of the major issues to enhance the application of industrial steam reforming. Therefore, a profound knowledge of carbon formation (from combined experimental and thermodynamic analysis) is essential in order to identify operating conditions that avoid carbon formation [Lin 2013, Parmar 2009]. Kauppi et al. [2010] point out "the importance of experimental research in evaluating coke formation since thermodynamic calculations alone do not provide accurate knowledge about the outcome of the complicated set of reactions involved in coking".
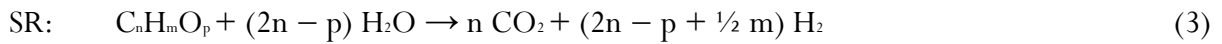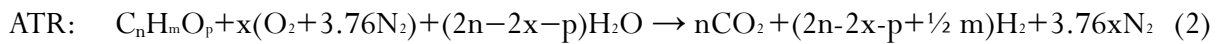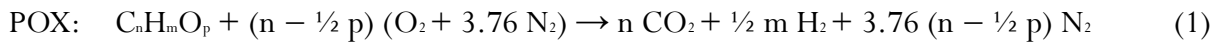
The aim of this thesis is to provide a fundamental understanding of hydrogen generation via steam reforming of liquid fuels. In particular, the applicability of direct steam reforming of biodiesel, diesel and bioethanol is investigated at various operating condition. Direct steam reforming in the high temperature range (> 800 °C) is the preferred option for steam reforming of liquid fuels since it eliminates the need of an additional pre-reforming step [Boon 2011, Katikaneni 2014]. The experimental study includes variation of reforming temperature, pressure, steam-to-carbon ratio, sulphur content and feed mass flow rate. The main emphasis is placed on finding suitable operating conditions for coke-free operation. The initiation of catalyst deactivation is evaluated in detail including measurement of carbon deposition on the catalyst surface and post mortem analysis.

The experimental work is complemented by a simulation study, the aim of which is to evaluate a 50 Nm^3/h hydrogen generation system based on SR of biodiesel. The main emphasis is placed on maximizing system efficiency through extensive parameter variation (including variation of pressure and S/C ratio). Additionally, a heat exchanger network is developed ensuring a maximum internal heat recovery and a minimum external heating/cooling demand.

2.   Theoretical Background

2.1   Reforming options

Conversion of hydrocarbon fuels into a hydrogen rich gas can be achieved via partial oxidation (POX), autothermal reforming (ATR) or steam reforming (SR). Eqs. 1-3 represent an idealized reaction stoichiometry assuming full conversion of the reactants to CO_2 and H_2 [Ahmed & Krumpelt 2001]. One has to keep in mind that under real conditions the achievable hydrogen yield is limited by the thermodynamic equilibrium depending on the actual operating conditions.

POX: $C_nH_mO_p + (n - \frac{1}{2} p) (O_2 + 3.76 N_2) \rightarrow n\ CO_2 + \frac{1}{2}\ m\ H_2 + 3.76\ (n - \frac{1}{2} p)\ N_2$ (1)

ATR: $C_nH_mO_p + x(O_2 + 3.76N_2) + (2n - 2x - p)H_2O \rightarrow nCO_2 + (2n - 2x - p + \frac{1}{2} m)H_2 + 3.76xN_2$ (2)

SR: $C_nH_mO_p + (2n - p)\ H_2O \rightarrow n\ CO_2 + (2n - p + \frac{1}{2} m)\ H_2$ (3)

Among the available reforming options, SR is the most established hydrogen production technology [Nahar 2012]. SR offers the advantage of a high partial pressure of hydrogen in the product gas ($70 - 80$ vol. % on a dry basis compared to $40 - 50$ vol. % for ATR and POX) which is beneficial for fuel cell applications [Ersoz 2006]. Both POX and ATR suffer from the dilution with nitrogen which is unfavourable for the performance of fuel cells. Among the drawbacks of the SR technology are its poor dynamic behaviour and a comparatively high level of system complexity. Taking further into account that compressing liquid fuels is less energy intensive than compressing gaseous feeds, SR of liquid fuels is widely considered to be the preferred reforming option for stationary hydrogen generation [Hulteberg 2008, Holladay 2009, Martin 2011].
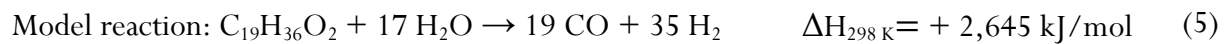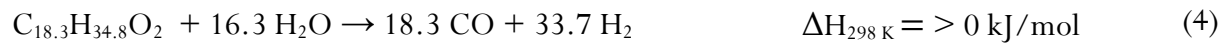
Various types of catalysts appear suitable for liquid fuel reforming, including noble, non-noble and bimetallic catalysts [Navarro 2011, Hulteberg 2012]. Rh and Ni catalysts are commonly considered to be most suitable for SR of liquid fuels [Blasi 2014, Kaynar 2015]. The main challenge related to liquid fuel SR is unwanted coke deposition on the catalyst surface resulting

in a loss of catalyst activity. Catalyst deactivation may be further caused by sintering and/or sulphur poisoning [Bartholomew 2006]. The deactivation mechanisms will be reviewed in more detail in chapters $2.3 - 2.5$. The following section provides a description of the main chemical reactions involved in the catalytic SR process.
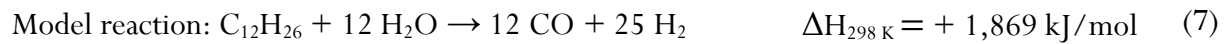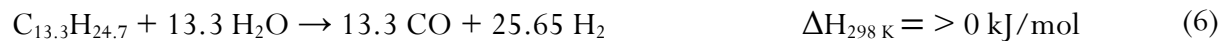
2.2   Chemical reaction system

SR of liquid hydrocarbons can be described by three linearly independent equations, namely the conversion into CO and H_2 (Eqs. $(4 - 7)$), the water gas shift (WGS) reaction (Eq. (8)) and the methanation reaction (Eq. (9)). While the WGS and the methanation reaction are exothermic being favoured at low temperatures, the SR reaction is strongly endothermic, being favoured at high temperatures. The overall SR reaction including WGS and methanation is endothermic and therefore requires an external heat source. The reformate gas composition is mainly controlled by thermodynamics. High temperatures and a high S/C favour a high hydrogen yield whereas the application of high pressure reduces the achievable hydrogen yield [Bartholomew 2006].

Biodiesel steam reforming reaction[1]:

$$C_{18.3}H_{34.8}O_2 + 16.3\ H_2O \rightarrow 18.3\ CO + 33.7\ H_2 \qquad \Delta H_{298\ K} = > 0\ kJ/mol \qquad (4)$$

$$\text{Model reaction: } C_{19}H_{36}O_2 + 17\ H_2O \rightarrow 19\ CO + 35\ H_2 \qquad \Delta H_{298\ K} = +\ 2{,}645\ kJ/mol \qquad (5)$$

Diesel steam reforming reaction[2]:

$$C_{13.3}H_{24.7} + 13.3\ H_2O \rightarrow 13.3\ CO + 25.65\ H_2 \qquad \Delta H_{298\ K} = > 0\ kJ/mol \qquad (6)$$

$$\text{Model reaction: } C_{12}H_{26} + 12\ H_2O \rightarrow 12\ CO + 25\ H_2 \qquad \Delta H_{298\ K} = +\ 1{,}869\ kJ/mol \qquad (7)$$

Water gas shift reaction:

$$CO + H_2O \leftrightarrow H_2 + CO_2 \qquad \Delta H_{298\ K} = -\ 41\ kJ/mol \qquad (8)$$

Methanation reaction:

$$CO + 3\ H_2 \leftrightarrow CH_4 + H_2O \qquad \Delta H_{298\ K} = -\ 206\ kJ/mol \qquad (9)$$

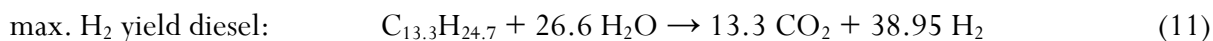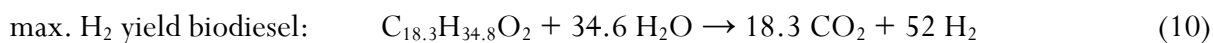[1] molecular formula is based on chemical analysis of biodiesel (see chapter 3.1)

[2] molecular formula is based on chemical analysis of diesel (see chapter 3.1)

By combining SR and WGS reaction (Eqs. 4/6 and 8) the maximum hydrogen yield for biodiesel and diesel SR is obtained as follows:

max. H_2 yield biodiesel: $\qquad C_{18.3}H_{34.8}O_2 + 34.6\ H_2O \rightarrow 18.3\ CO_2 + 52\ H_2$ $\qquad$ (10)

max. H_2 yield diesel: $\qquad C_{13.3}H_{24.7} + 26.6\ H_2O \rightarrow 13.3\ CO_2 + 38.95\ H_2$ $\qquad$ (11)

The exact mechanism of diesel and biodiesel steam reforming is not completely understood, involving hundreds of elementary gas phase and surface reactions [Parmar 2009]. However, it is generally agreed that steam reforming of higher aliphatic hydrocarbons takes place by irreversible chemisorption on the catalyst surface resulting in C_1 compounds [Rostrup-Nielsen 1973]. According to this mechanism, which was first proposed for methane steam reforming, hydrocarbons adsorb dissociatively on the metal surface forming a methylene group that undergoes further stepwise dehydrogenation. Simultaneously, H_2O reacts with metal atoms producing adsorbed oxygen and gaseous hydrogen. Finally, the $CH-$ species formed by the dehydrogenation step react with adsorbed oxygen to yield gaseous CO [Navarro 2011, Thormann 2009] which is subsequently converted to CO_2 through WGS reaction (Eq. (8)). In parallel, the methanation reaction (Eq. (9)) takes place.

2.3   Side reactions associated with carbon/coke deposition

Apart from the main reactions which involve hydrocarbon adsorption and dissociation on the catalyst surface followed by WGS and methanation reaction, formation of carbonaceous residues (usually referred to as coke or carbon) by undesired side reactions may occur, leading to a gradual coverage of the active sites and subsequent catalyst deactivation (Fig. 2).
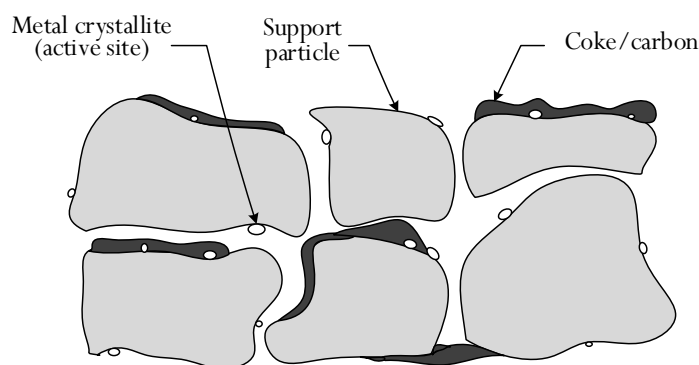

Figure 2 – Conceptual model of coke/carbon deposition (reproduced from Bartholomew [2006])

$$C_nH_m \rightarrow C + H_2 + CH_4 + Olefins + Aromatics \qquad \Delta H_{298\,K} = > 0 \text{ kJ/mol} \qquad (12)$$

$$2\,CO \leftrightarrow C + CO_2 \qquad \Delta H_{298\,K} = -172 \text{ kJ/mol} \qquad (13)$$

$$CO + H_2 \leftrightarrow C + H_2O \qquad \Delta H_{298\,K} = -131 \text{ kJ/mol} \qquad (14)$$

$$CH_4 \leftrightarrow C + 2\,H_2 \qquad \Delta H_{298\,K} = +75 \text{ kJ/mol} \qquad (15)$$

Olefins/Aromatics $\rightarrow$ Polyaromatics (Coke)

$\rightarrow$ Amorphous carbon $\rightarrow$ Graphitic carbon $\qquad \Delta H_{298\,K} = > 0 \text{ kJ/mol} \qquad (16)$

Carbon can be formed by non-catalytic thermal cracking of higher hydrocarbons in the gas phase (Eq. (12)) or by decomposition of carbon monoxide (Eqs. (13), (14)) and methane (Eq. (15)) [Navarro 2011, Parmar 2009]. Berry et al. [2003] argue that CH_4 decomposition is due to thermal cracking while Christensen [1996] and Trane et al. [2012] claim that CH_4 as well as CO decomposition is catalyzed by the active sites of the catalyst. Irrespective of the catalytic or non-catalytic nature of the process, the decomposition of higher hydrocarbons and methane (Eqs. (12), (15)) is thermodynamically favoured at high temperatures whereas carbon formation through decomposition of CO (Eqs. (13), (14)) predominantly occurs in the low temperature range. Non-catalytic formation of gas-phase carbon (Eq. (12)) is slow compared to the catalytic coke formation reactions on the catalyst surface [Trimm 1997]. According to Kang et al. [2011] gas phase reactions are likely to be unimportant as long as the temperature in the mixing zone is less than 800 K (527 °C). Concurrently, Navarro et al. [2011] report that thermal cracking of higher hydrocarbons is initiated at temperatures higher than 500 °C.

Depeyre et al. [1985] investigated the thermal cracking of the diesel model substance hexadecane in the presence of steam (which may occur in the mixing zone upstream of an SR catalyst). They found that the formation of coke can be kept to a minimum by increasing the amount of steam, decreasing the residence time and using a catalytically inactive wall material. The favourable effect of high S/C is mainly attributed to the fact that steam inhibits the formation of high molecular weight compounds which otherwise would promote the production of coke.

It should be noted that reactions $13-15$ may also serve to remove carbon through gasification by reaction with CO_2, H_2O or H_2 [Shekhawat 2007]. The reaction of carbon with CO_2 and H_2O is thermodynamically favoured (criterion: $\Delta G^0 < 0$) at high temperatures (> 703 °C; > 677 °C,

respectively) whereas carbon removal with H_2 is thermodynamically favoured at low temperatures (< 544 °C) (see Fig. A1, Tab. A1). Regarding the overall chemical reaction system (including carbon forming reactions) the heterogeneous gas-solid reactions with carbon (reverse reactions of Eqs. $13 - 15$) are the slowest reactions, thus limiting the overall conversion rate [Higman 2003]. Results from a recent study related to ATR of n-hexadecane with mono- and bimetallic noble metal (Rh, Pt) catalysts indicate that reduced coke formation at high temperatures (800 °C) predominantly arises from gasification of coke with H_2O [Kauppi 2010]. Concurrently, Frusteri et al. [2015] report that an increased partial pressure of H_2O reduces coke formation by increasing the coke gasification rate.

The term coke is a broader definition of the term carbon. Coke is often referred to deposits originating from decomposition and condensation of polyaromatic compounds (Eq. (16)) which strongly adsorb on the metal active sites resulting in reduced catalytic activity. Coke, which is described by Xu et al. [2013] as a high-molecular-weight polymer with a low hydrogen content, may be further converted to more stable amorphous and graphitic type carbon. Thus, actual coke forms vary from high molecular weight hydrocarbons such as condensed polyaromatics to graphite type carbon [Bartholomew 1982].

Olefins and aromatic compounds, which are known to be the main precursors for coke formation, are originally present in liquid fuels such as diesel and biodiesel. In addition, the formation of olefins and/or aromatics can be caused by improper mixing of the reactants upstream of the catalyst resulting in fuel-rich zones leading to the formation of ethylene and aromatics through pyrolysis reactions [Norinaga 2007, Kang 2011]. With regard to diesel ATR Yoon et al. [2009] report that ethylene formation is mainly caused by non-catalytic homogenous decomposition (homolytic fission) of paraffins. Ethylene may be further converted to high molecular weight compounds such as benzene which in turn accelerate the ethylene formation as they are strongly bond to the active sites, thus limiting the catalytic reactions of other hydrocarbons and favouring the non-catalytic cracking of paraffins. Long residence times of the feed mixture prior to the catalyst bed are reported to enhance the formation of the coke precursor ethylene [Kang 2011].

Most importantly, surface carbon is a reaction intermediate in the reforming of higher hydrocarbons originally present in the liquid fuel (Fig. 3) [Kauppi 2010, Wu 2010]. The surface

carbon $C(s)_{ads}$ which arises through the adsorption and dissociation of the carbon originally present in the liquid fuel ($C(l)$) can be subsequently gasified by reaction with CO_2, H_2O or H_2 resulting in gaseous carbon $C(g)$. In essence, the formation of coke is a kinetic competition between the carbon forming reactions and the gasification reactions [Christensen 1996].
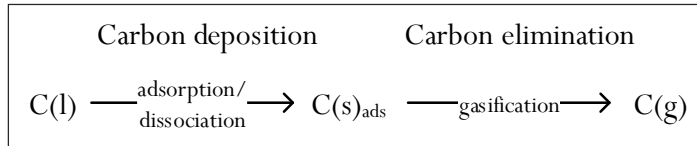

Figure 3 – Carbon deposition - carbon elimination kinetic model [Wu 2010]

From the above it can be concluded that in order to avoid the initiation of coke deposition on the catalyst surface during liquid fuel reforming it is decisive to

- ensure proper mixing of steam and fuel

- avoid long residence times in the mixing zone upstream the SR catalyst

- realize operating conditions which guarantee complete conversion of aromatic compounds

- use highly active catalyst material

Proper feed mixing can be achieved by various technical measures including sophisticated fuel injectors, fuel atomizers and customized nozzles [Lin 2013-2]. Complete conversion of aromatic compounds is favoured at high temperatures (> 750 °C) and high S/C ratios [Gonzalez 2013]. High temperatures are at the same time favourable for enhancing the rate of coke gasification, especially for reactions with H_2O and/or CO_2 (see Fig. A1).

It is important to note that catalyst deactivation through coking is different for non-noble and noble metals [Trimm 1997]. According to Christensen [1996] there is a temperature window for carbon free operation when using Ni-catalysts. If the temperature exceeds an upper limit, filamentous whisker carbon is likely to form whereas in the low temperature range polymerization and/or gum formation can occur. The formation of whisker type carbon results from the diffusion of carbon through Ni leading to carbon filaments on the back side. As noble metals do not dissolve carbon significantly, less carbon is formed and coke morphology is different [Alvarez-Galvan 2008].

Knowledge about the nature of deposited coke during SR of liquid fuels using noble metal catalysts is limited. Maier et al. [2011] report the formation of a full carbon monolayer at a certain position downstream the catalyst, the position of which depends on the flow rate. Zheng et al. [2014] carried out SEM analysis of spent catalysts after SR of dodecane revealing poorly structured amorphous carbon and well-structured graphitic carbon. They observed a gradual change of coke morphology from amorphous, moss-like coke with diameters less than 1 μm to crystallized graphitic type carbon (average diameters: $1 - 6$ μm) with increasing time on stream and increasing sulphur concentration. Kauppi et al. [2010] found that bimetallic Rh-Pt catalysts are more effective in preventing coke formation than monometallic catalysts suggesting that the coke formed on monometallic catalysts differs from the coke formed on bimetallic catalysts. Moreover, they consider it possible that the formation of surface carbon and its gasification may be differently catalyzed. Kaynar et al. [2015] investigated SR of kerosene using bimetallic Ru-Ni catalysts and compared them with monometallic catalysts containing only Ni or Ru. In line, they observed less coke deposition on the catalyst surface and improved catalyst stability in the case of the bimetallic Ru-Ni catalysts.

Brief summary of carbon/coke deposition

Coke deposition on the catalyst surface arises from thermal, non-catalytic cracking in the gas phase and from heterogeneous catalytic reactions on the catalyst surface. Non-catalytic coke forming reactions mainly involve the decomposition of hydrocarbons in the high temperature range. Catalytic carbon formation involves the adsorption and dissociation of hydrocarbons and carbon monoxide on the catalyst surface. In particular, it is induced by coke precursors such as ethylene, propylene and aromatic compounds which are particular prone to coking. Qualitatively, coking tendency increases as the proportion of high molecular weight hydrocarbons, unsatured molecules and aromatic species increase [Rostrup-Nielsen 2011].

Literature data indicates that the bulk of the coke formation occurs on the catalyst surface [Trimm 1997, Shi 2008, Schädel 2009]. Considering that the same intermediates are involved in the main reactions as are involved in coking [Eßmann 2012], the higher hydrocarbons can either react on the metal surface to give C1-compounds or they remain as coke deposits on the surface. Further taking into account that in the catalytic steam reforming process carbon deposition and

carbon elimination co-exist, the coke formation rate is apparently determined by the competition of these two reactions [Wu 2010]. Avoidance of catalyst coking thus demands "increasing the rate of coke gasification so that the coke formation rate is less than or equal to the rate of coke deposition" [LeValley 2014].

With regard to practical applications it is desirable to be able to select appropriate operating conditions that guarantee coke-free operation based on macroscopic properties, thus eliminating the need to derive the reaction kinetics of the individual reactions involved in SR of liquid fuels.

2.4   Sulphur poisoning

Apart from coking, catalyst deactivation can be caused by sulphur poisoning which involves strong chemisorption of the sulphur-containing molecule on the metal sites (Eq. (17)), leading to a stable and inactive metal sulfide species on the catalyst surface (Eq. (18)) [Navarro 2011].

The main sulphur compounds present in logistic fuels are mercaptanes, sulphides, disulphides, thiophenes, benzothiophenes (BTs) and dibenzothiophenes (DBTs) [Hulteberg 2012]. The prevailing sulphur species in commercial diesel are BTs and DBTs. Sulphur poisoning is more severe at lower temperatures due to the increased strength of sulphur adsorption. Contrary to catalyst coking, sulphur poisoning is very difficult to reverse, requiring harsh conditions for catalyst regeneration [Fauteux-Lefebvre 2011].

$$M + \text{S-R} \rightarrow M + \text{R'} + H_2S \tag{17}$$

$$H_2S + M \rightarrow \text{M-S} + H_2 \tag{18}$$
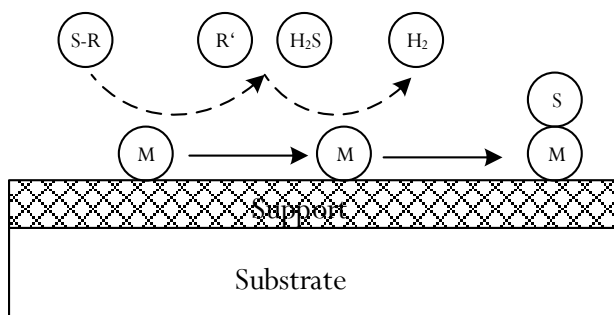
Figure 4 – Catalyst deactivation by sulphur poisoning

2.5   Catalyst sintering

Thermal degradation by catalyst sintering refers to the loss of catalyst active surface due to crystallite growth of either the support material or the active phase (Fig. 5). Sintering of supported metal catalysts occurs via surface diffusion of atoms, particle migration followed by coalescence and/or interparticle transport by volatilization or surface migration [Moulijn 2001].
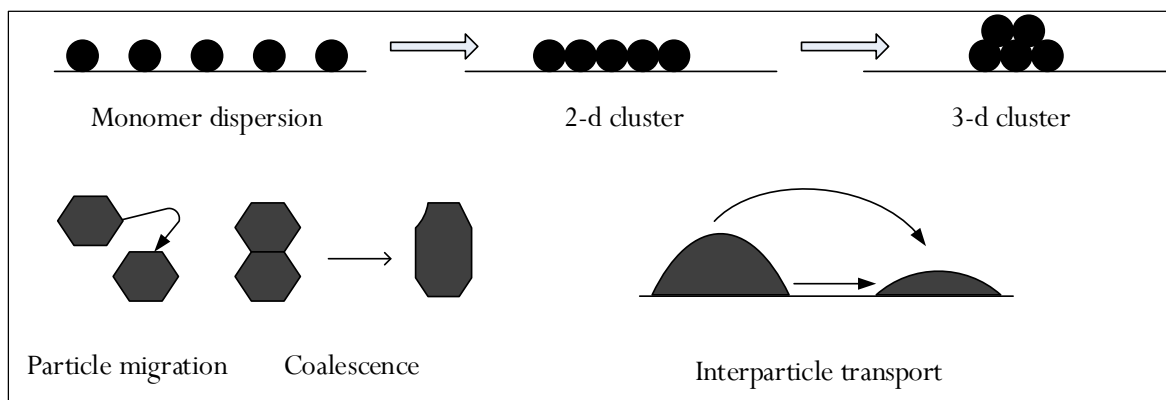

Figure 5 – Catalyst sintering (reproduced from Moulijn [2001])

Sintering during SR of hydrocarbons strongly depends on the actual operating conditions, in particular on temperature and type of atmosphere. Moreover, time plays an important role as it is well known that sintering typically occurs on a larger time scale (hours, days) than coking and/or sulphur poisoning [Contreras 2012]. Further factors which affect sintering are morphology of the support, metal dispersion and the presences of impurities. According to Forzatti et al. [1999] species such as C, O, Ca, Ba, Ce or Ge may decrease metal atom mobility, while others such as Pb, Bi, Cl, F or S can increase the mobility. The presence of water vapor strongly accelerates sintering. Therefore it is desirable to minimize water vapor concentrations, especially at high temperatures and with high surface-area catalysts.

Attempts have been made to correlate the propensity of sintering to characteristic physical properties of the catalyst material. Regarding the relative thermal stability, two semi-empirical relations have been derived, both of which are directly related to the melting temperature.

$$T_{Hüttig} = 0.3\,T_{Melting} \tag{19}$$

$$T_{Tamman} = 0.5\,T_{Melting} \tag{20}$$

When the Hüttig temperature (Eq. (19)) is reached, less strongly bound surface atoms at defect sites dissociate and diffuse readily over the surface, while at the Tamman temperature (Eq. (20)), atoms in the bulk become increasingly mobile until the melting point is reached [Argyle 2015]. The Tamman temperature of metals increases in the order Ni < Fe < Pd < Pt < Rh < Ru indicating that precious metals such as Ru and Rh are thermally more stable than non-noble metals such as Ni.

3. Methodology

In this chapter the physicochemical properties of the liquid fuels investigated within this study (biodiesel, diesel, bioethanol) are presented. In addition, the experimental set-up and the methodology of the simulation study are described.

3.1 Fuel properties

a) Biodiesel

Biodiesel produced by transesterification of soybean oil (40 %) and palm oil (60 %) was used as a feedstock for the steam reforming experiments. A selection of physical and chemical biodiesel properties is shown in Tab. 1. From the fatty acid spectrum (main components: oleic acid: 34.2 %, palmitic acid: 30.9 %, linolic acid: 26.0 %) the molecular formula $C_{18.3}H_{34.8}O_2$ (average molecular weight: 287.2 g/mol) was derived.

Table 1 – Biodiesel properties		
Property	**Value**	**Test method**
Density at T=15 °C (kg/m^3)	878.6	EN ISO 12185
Sulphur content (ppmw)	1.5	ASTM 5453-09
Lower heating value LHV (MJ/kg)	37.79	DIN 51 900-1,3
Fatty acid methyl ester content (wt. %)	99.5	EN 14103
Methanol (wt. %)	0.09	EN 14105

b) Diesel

Fossil diesel is a complex mixture of paraffins, olefins, cycloalkanes and aromatics, containing up to 400 different hydrocarbon species, including organic sulphur compounds and additives [Parmar 2009]. Different empirical chemical formulas have been reported in the literature:

$C_{13.4}H_{26.3}$ [Pereira 2000], $C_{14.342}H_{24.75}O_{0.0495}$ [Sahin 2008], $C_{13.57}H_{27.14}$ [Brown 2001], $C_{16.2}H_{30.6}$ [Lindermeir 2007], $C_{12}H_{20}$ [Fauteux-Lefebvre 2011]. In the present study, a Shell diesel fulfilling EN 590 is used with the main properties given in Tab. 2. Based on the chemical analysis, a molecular formula of $C_{13.3}H_{24.7}$ (average molecular weight: 185 g/mol) was derived.

Table 2 – Diesel properties		
Property	**Value**	**Test method**
Density at T=15 °C (kg/m³)	836.4	ASTM D4052-11/ISO 12185-96
Lower heating value LHV (MJ/kg)	42.93	DIN 51 900-1,3
Monoaromatic content (wt. %)	21.5	EN 12916
Polyaromatic content (wt. %)	2.5	EN 12916
Total aromatic content (wt. %)	24.0	EN 12916
Sulphur content (ppmw)	7.0	ASTM D4294/EN 20884
Initial boiling point (° C)	169.9	EN ISO 3405
Final boiling point (° C)	361.9	EN ISO 3405

Regarding the chemical composition of biodiesel and fossil diesel, the differences are considerable. Biodiesel predominantly consists of fatty acid methyl esters (Tab. 1) whereas fossil diesel is a mixture of many different chemical compounds with a high total aromatic content (Tab. 2).

The distillation curve of diesel has a broad range (170 °C – 362 °C) compared to a narrow range of biodiesel (347 °C – 357 °C, [Yuan 2005]). The heating value of diesel (42.93 MJ/kg) is 13.6 % higher than that of biodiesel (37.79 MJ/kg). The sulphur content (7 ppmw) is slightly higher than the sulphur content of biodiesel (1.5 ppmw).

c)   Bioethanol

Additional experiments have been carried out with bioethanol, the properties of which are given in Tab. A2. The lower heating value of ethanol (26.8 MJ/kg) is significantly lower compared to biodiesel and diesel. The sulphur content is similar to biodiesel (1 ppmw).

3.2   Experimental set-up

A schematic of the test-rig used for liquid fuel steam reforming is shown in Fig. 6 (for photographic view see Fig. A2). Water and liquid fuel are supplied to the system by micro annular gear pumps using mass flow controllers (MFCs). Diesel at $T=0\,°C$ (biodiesel: room temperature) is mixed with superheated steam of $T_{H2O}=390\,°C$ (biodiesel: $T_{H2O}=550\,°C$). In the subsequent mixing zone the feed is homogeneously mixed at a constant temperature of $450\,°C$ before being heated up to the desired SR temperature.

The catalytic conversion into H_2, CO, CO_2 and CH_4 is accomplished by using a catalyst monolith which is mounted inside a heat resisting chrome-nickel steel tube (EN 10095: 1.4841, X15CrNiSi25-21, $d=2.1\,cm$). The heat for the endothermic reforming reaction is supplied by an electrical oven.
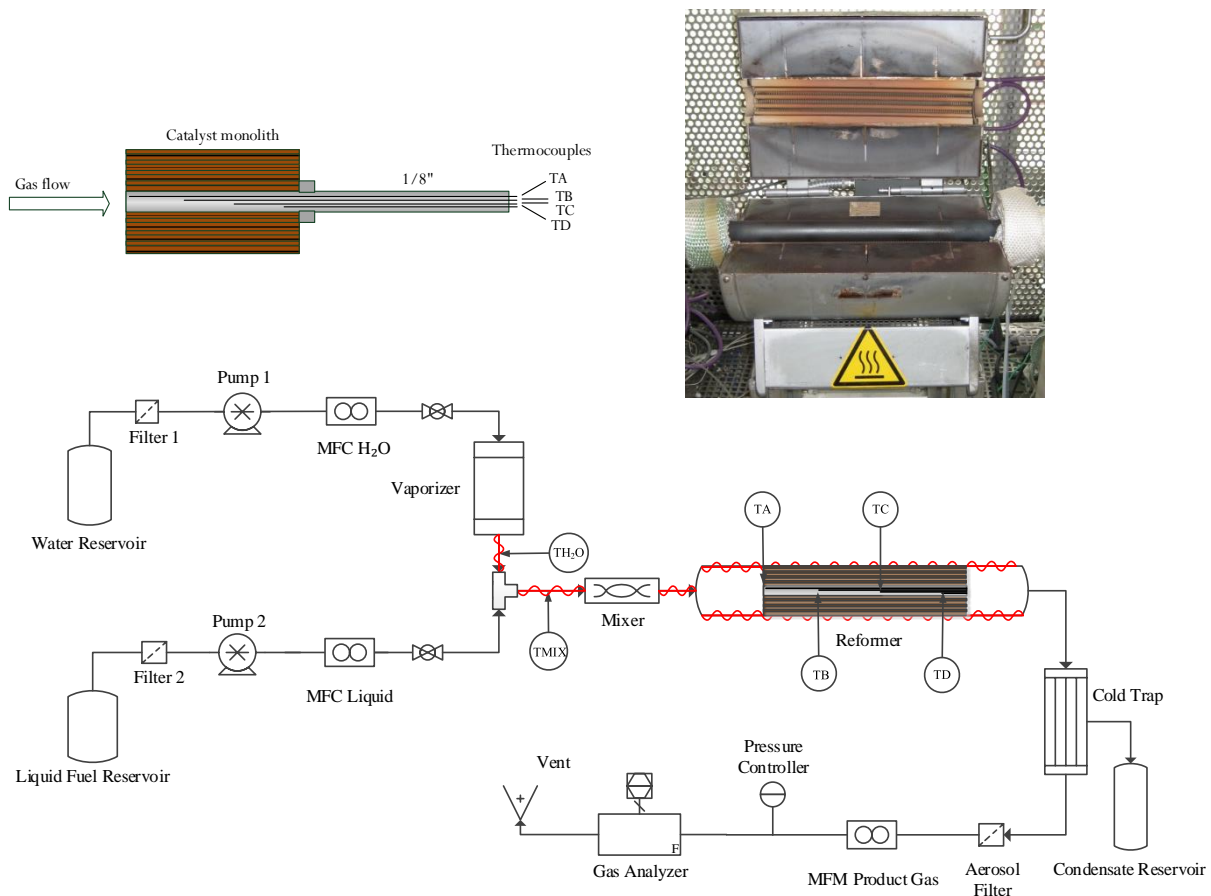
Figure 6 – Schematic of test-rig for steam reforming of liquid fuels; upper right: electrical oven with stainless steel tube (catalyst monolith is mounted centrally inside); upper left: cross section view of the catalyst monolith with thermocouples mounted along the centre line of the catalyst piece

Commercial precious metal catalyst monoliths supplied by Johnson Matthey have been used for the experimental investigations (Fig. 7). The ceramic and metallic based catalyst monoliths are impregnated with finely distributed platinum group metals (including Pt, Pd and Rh) on a high surface area $(140 \ \mathrm{m^2/g})$ alumina based mixed metal oxide support (including silicon and zirconium). It is coated on the monolith at a loading of 0.122 g catalyst/cm^3 with an overall Rh loading of 0.00224 g/cm^3. The channels of the ceramic based monoliths (900 cells per square inch) can be approximated as rectangle cross sections with a diameter of 0.9 mm. The channels of the metallic based catalyst monoliths (600 cells per square inch) can be approximated as equilateral triangles with a uniform side length of 1 mm.
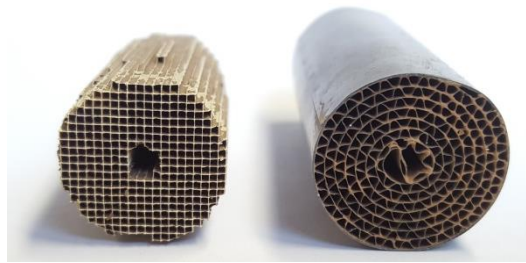
Figure 7 – Ceramic based cordierite catalyst monolith (left) and metallic based fecralloy catalyst monolith (right)

Four thermocouples (Nickel alloy, type k, specified measurement error: $\pm$ 2.5 K) have been placed along the center line of the catalyst piece (TA, TB, TC, TD, see Fig. 6) in order to measure the temperature profile over time on stream. The temperature measured at the rear end (TD) was used to control the reformer temperature. The obtained axial temperature profile provides valuable information on the catalyst activity. After initiation of the reforming reaction, the temperature at the catalyst front TA (located 1 mm from the catalyst entrance in flow direction) drops due to the endothermic heat demand. A stable catalyst front end temperature over time indicates stable catalyst activity.

Upon leaving the reformer section, water and unconverted liquid fuel are condensed in a cold trap at T=10 °C and stored in a condensate reservoir (Fig. 6). Before each experiment, the cold trap is filled with 100 ml of organic solvent (dodecane, mixture of isomers). The fuel conversion rate FCR (Eq. (21)) is subsequently derived from gas chromatography (GC) analysis of the organic phase that accumulates in the cold trap during the test ($m_{\mathrm{Fuel,cond.}}$).

In addition, carbon deposition on the catalyst surface and the tube walls (m_C) and higher hydrocarbons leaving the cold trap (m_{HC}) are considered for FCR calculation:

$$FCR = \frac{m_{Fuel} - (m_{Fuel,cond.} + m_C + m_{HCs})}{m_{Fuel}} \qquad (21)$$

The amount of condensed liquid fuel $m_{Fuel,cond.}$ (including cracking products) in the cold trap is derived from the area proportion $x_{Fuel,cond.}$ in the gas chromatogram (which is assumed to be equivalent to the mass proportion) and the amount of dodecane m_{Dod} according to Eq. (22). The amount of deposited carbon m_C is obtained by flushing the system with air after each test and detecting the resulting CO_2 evolution. Higher hydrocarbons m_{HCs} (C_2-C_4) passing the cold trap were measured periodically via GC analysis (Varian Micro CP-4900, accuracy: $\pm$ 0.1 % of the upper limit range).

$$m_{Fuel,cond.} = m_{Dod} \cdot \left(\frac{1}{1 - x_{Fuel,cond.}} - 1 \right) \qquad (22)$$

Subsequent to the cold trap, any remaining moisture is removed by an aerosol filter. The dry reformate gas flow is measured with a mass flow meter (MFM) before it enters the online gas analyzer unit (Rosemount Analytical NGA 2000 MLT), which is equipped with an infrared adsorption detector for CO, CO_2 and CH_4 and a thermal conductivity detector for the measurement of H_2. The specified measurement error of the MLT is $\pm$ 1 % relative to the full scale value. System pressure is regulated using a pressure control device.

In case of the tests with ceramic based catalyst monoliths the carbon deposition on the spent catalyst after each experiment was measured using an elemental analyzer (EA 5000, Jena Analytik). Therefore, the catalyst piece as a whole was pulverized and the deposited carbon was oxidized to CO_2 and subsequently detected.

The mass balance of the process is given by:

$$\dot{m}_{Fuel} + \dot{m}_{Water} = \dot{m}_{Condensate} + \dot{m}_{Residual\ moisture} + \dot{m}_{Dry\ reformate} \qquad (23)$$

A mass balance error (defined as $|1 - m_{Product}/m_{Feed}|$) of < 2 % was ensured for all experimental tests within this study.

Evaluation parameters

Thermal hydrogen efficiency based on the lower heating value (LHV) is calculated according to Eq. (24) (assuming that CO is completely converted into H_2 through water gas shift reaction):

$$\eta_{H_2} = \frac{\dot{m}_{H_2} \cdot LHV_{H_2}}{\dot{m}_{FUEL-REF} \cdot LHV_{FUEL-REF}} \tag{24}$$

$\dot{m}_{H_2}$: hydrogen mass flow; $\dot{m}_{FUEL-REF}$: fuel mass flow to reformer

The gas hourly space velocity (GHSV) at standard temperature and pressure (STP) and the molar steam-to-carbon ratio (S/C) are defined according to Eqs. (25) and (26):

$$GHSV = \frac{\dot{V}_{Feed,STP}}{V_{Catalyst,void}} \tag{25}$$

$$S/C = \frac{\dot{n}_{H_2O}}{\dot{n}_{Fuel,C}} \tag{26}$$

3.3   Simulation of biodiesel steam reforming in Aspen Plus ®

A hydrogen generation system based on feedstock biodiesel is evaluated with Aspen Plus ® using the Soave-Redling-Kwong (SRK) property method [Soave 1972] with Kabadi-Danner mixing rules to handle the interaction between water and hydrocarbon components [Kabadi 1985]. The SRK property method is a two-parameter equation of state derived from the van der Waals equation. It is particularly suitable in the high temperature and high pressure regions, i.e. for gas-processing, refinery and petrochemical applications. The SRK method allows for computing thermodynamic properties such as fugacity, entropy, Gibbs energy and molar volume through fundamental thermodynamic equations. For a detailed description of the underlying calculation procedures please refer to AspenTech [2010].

Chemical equilibrium calculations are based on minimization of Gibbs free energy. The Gibbs minimization method offers the advantage of not necessarily knowing the chemical reactions involved. Instead, the SR product gas composition is calculated based on the input specifications of the feed streams, the thermodynamic state (p, T) of the reaction system and possible product

gas species. Minimization of Gibbs free energy is applicable to gaseous, liquid and solid state components. It is particularly suitable for calculating equilibrium coke formation of liquid fuel reforming [Nahar 2010-2].

The total Gibbs free energy G of a thermodynamic system is given by the following equation:

$$G_{System} = \sum_{i=1}^{m} n_i \cdot \mu_i \tag{27}$$

n_i : mole number of species i; μ_i : chemical potential of species i

Minimization of Gibbs free energy at constant temperature and pressure is equivalent to:

$$\left(\frac{dG}{d\xi}\right)_{p,T} = \sum_{i=1}^{m} \nu_i \cdot \mu_i \tag{28}$$

ξ : extent of reaction; ν_i : stoichiometric coefficient of species i

The Aspen Plus algorithm used for Gibbs minimization is Gautam-Seider [1979]. Gautam & Seider use the tangent plane criterion first proposed by Gibbs in 1873 in conjunction with the minimization of the Gibbs free energy and then combine a phase-splitting algorithm. Thereby the probability of finding the global minimum of Gibbs free energy is strongly increased compared to Newton-type algorithms which are highly dependent on the starting value.

The following products were considered for the Gibbs minimization calculations using Aspen Plus: H_2, CO, CO_2, CH_4, H_2O, C_2H_4, C_2H_6, C_3H_6, C_3H_8, C_4H_{10}, $C_{19}H_{36}O_2$, C_{solid}.

3.3.1 Biodiesel model substance

Methyl-oleate was chosen as a model substance for biodiesel (Fig. 8). Chemically speaking, methyl-oleate is a fatty acid methyl ester (FAME) produced from transesterification of triolein, the triglyceride of oleic acid, which is known as the dominating fatty acid in vegetable oil.
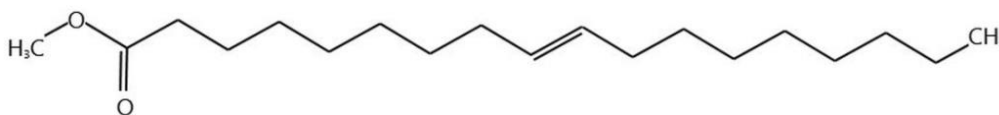

Figure 8 – Chemical structure of methyl-oleate ($C_{19}H_{36}O_2$)

Taking into account that the equilibrium product gas composition is not path dependent and solely a function of the thermodynamic state defined by temperature, pressure and atomic ratio C:H:O in the feed [Parmar 2009], methyl-oleate is considered to be a suitable model substance for modeling biodiesel SR. The heating values of biodiesel and methyl-oleate differ by less than 1 %. A comparison of selected properties is given in Tab. 3.

Table 3 – Selected properties of biodiesel and model substance methyl-oleate		
	Biodiesel	Methyl-oleate
Mass density at T=15 °C (kg/m³)	878.6	872.0
Molecular weight (g/mol)	287.2	296.5
Lower heating value (MJ/kg)	37.790	37.438
O_2-content (wt. %)	10.8	10.7
Chemical formula	$C_{18.3}H_{34.8}O_2$	$C_{19}H_{36}O_2$
C:H:O molar ratio	9.2 : 17.4 : 1	9.5 : 18.0 :1

As discussed in chapter 2.2, SR of methyl-oleate can be described by three linearly independent chemical equations, namely the steam reforming reaction (Eq. (5)), the water gas shift reaction (Eq. (8)) and the methanation reaction (Eq. (9)). Apart from these main reactions, coking of the catalyst can occur (Eqs. (12-16)) being favoured at low reforming temperatures and low S/C ratios.

3.3.2 Aspen Plus Flowsheet

The Aspen Plus flowsheet consists of a steam reformer (SR), a water gas shift reactor (WGS), a pressure swing adsorption unit (PSA) and a burner (B) (Fig. 9). The system is operated at pressures higher than 6 bar (up to 13 bar) in order to ensure a high PSA efficiency. The molar S/C ratio is varied from 2.5 to 5. All feed streams are supplied at an initial temperature of 20 °C. Water is vaporized and overheated prior to being mixed with biodiesel. By overheating the steam to 400 °C, complete vaporization of the incoming biodiesel is ensured. The water-biodiesel feed stream is then heated up to 650 °C by recuperative heat exchange, making use of

the reformate enthalpy. The steam reformer is operated at 825 °C taking into account that coke formation is less pronounced at higher temperatures.

Upon leaving the reformer section, the hydrogen rich gas is cooled down to a WGS inlet temperature of 300 °C. The WGS reactor is operated in an adiabatic mode resulting in a temperature increase of 50 °C up to 100 °C depending on the actual S/C ratio and CO concentration.

After leaving the WGS reactor, the gas stream is cooled down to 35 °C leading to a condensation of water. In the PSA unit the gas is divided into pure hydrogen and an off-gas stream containing H_2, CO, CO_2 and CH_4. The PSA unit is implemented as a splitter in Aspen Plus assuming a pressure dependent H_2 recovery rate ranging from 55 % at 6 bar to 78.3 % at 13 bar (Fig. A7).

The remaining heating value of the PSA off-gas is used for the burner, thus providing the necessary heat for the reformer section. The burner is operated in an adiabatic mode, the outlet temperature of which is kept at 1100 °C by adjusting the incoming air mass flow $\dot{m}_{Air-B}$. The flue-gas leaves the reformer section at an outlet temperature of 740 °C and can be further used for preheating water and/or air. If the required endothermic heat demand for the steam reforming section cannot be met by burning the off-gas with air, additional biodiesel $\dot{m}_{BD-B}$ has to be fed to the burner.
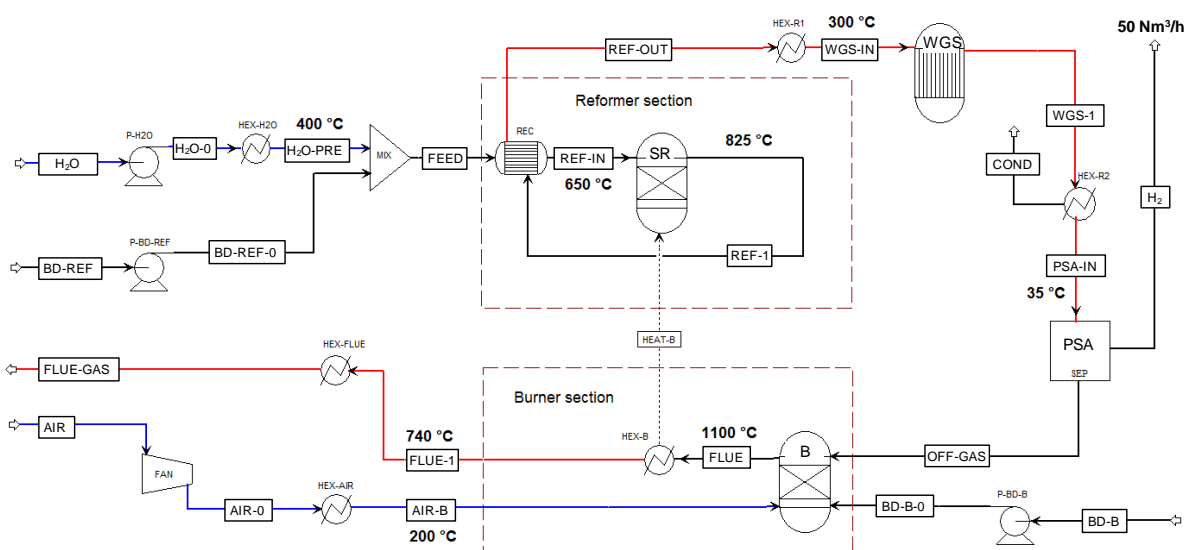
Figure 9 – Basic Aspen Plus flowsheet of a 50 Nm^3/h hydrogen generation system based on biodiesel feedstock

At a given S/C ratio, the targeted hydrogen output of 50 Nm³/h is ensured by adjusting the fuel mass flow $\dot{m}_{BD-Ref}$ accordingly. A brief overview of the underlying boundary conditions (based on experimentally derived values from a 50 Nm³/h hydrogen production system developed within the FCH JU project NEMESIS2⁺ [2015]) is given in Tab. 4.

Table 4 – Boundary conditions of basic Aspen Plus flowsheet	
Reformer	T_{REF-IN}=650 °C, T_{REF-1}=825 °C
WGS	T_{WGS-IN}=300 °C (adiabatic operation)
PSA	H_2-recovery: 55 % at 6 bar - 78.3 % at 13 bar
Burner	T_{FLUE}=1100 °C (adiabatic operation)
Flue-gas (after heat release to reformer)	T_{FLUE-1}=740 °C
Steam	$T_{H2O-PRE}$=400 °C
Air	T_{AIR-B}=200 °C (reference case)
H_2 output	50 Nm³/h

The thermal system efficiency is defined as follows:

$$\eta_{Syst} = \frac{\dot{m}_{H_2} \cdot LHV_{H_2}}{(\dot{m}_{BD-REF} + \dot{m}_{BD-B}) \cdot LHV_{BD}} \tag{29}$$

LHV: lower heating value; $\dot{m}_{H_2}$: hydrogen product gas mass flow; $\dot{m}_{BD-REF}$: biodiesel mass flow to the reformer; $\dot{m}_{BD-B}$: biodiesel mass flow to the burner

For the given system, the numerator of Eq. (29) is constant as the hydrogen output is fixed at 50 Nm³/h. Thus, the thermal system efficiency can be calculated from the biodiesel demand for the reformer and the burner. An additional electrical power demand P_{el} is needed for cooling the WGS outlet stream to the required PSA inlet temperature as well as for the biodiesel and water pump and for the air blower. Heat and pressure losses are not considered within this study.

3.3.3 Process heat integration

Pinch analysis is used in this work to achieve proper heat integration of the fuel processor system. It was conducted using the Aspen Plus ® energy analyzer [AspenTech 2009] which allows to extract the required stream data directly from the Aspen Plus flowsheet. Upon extracting the stream data, heat exchanger design networks are recommended based on user defined default values.

The Pinch method was first introduced by Linnhoff [1987] and has since then gained wide acceptance among engineers all over the world. By applying pinch method, the minimum required external heating and cooling demand (*hot* and *cold utility*) and the appropriate temperature levels can be derived for any given process. The following brief description of the Pinch methodology is based on the widely recognized user guide "Pinch Analysis and Process Integration" by Kemp [2007].

In a first step the process streams (criterion: change in heat load but not in composition) have to be extracted. The required stream data are temperature range ΔT (°C) and heat capacity flow rate $\dot{C}_p$ (kW/°C) or stream heat load $\Delta\dot{H}$ (kW). The differential change in heat load is given by:

$$d\dot{H} = c_p \cdot \dot{m} \cdot dT = \dot{C}_p \cdot dT \tag{30}$$

For $c_p = $ constant, the change in stream heat load $\Delta\dot{H}$ is given by:

$$\Delta\dot{H} = \int_{T_1}^{T_2} \dot{C}_p \cdot dT = \dot{C}_p \cdot (T_2 - T_1) \tag{31}$$

The streams that have to be heated up in the process (*cold streams*) and the streams that have to be cooled down (*hot streams*) can be combined to so-called hot and cold composite curves as shown in Fig. 10. In order to obtain the point of closest approach, the cold composite curve is shifted along the H-axis towards the hot composite curve until a minimum temperature approach ΔT_{min} is reached. The corresponding temperature is the so-called pinch temperature of the system.
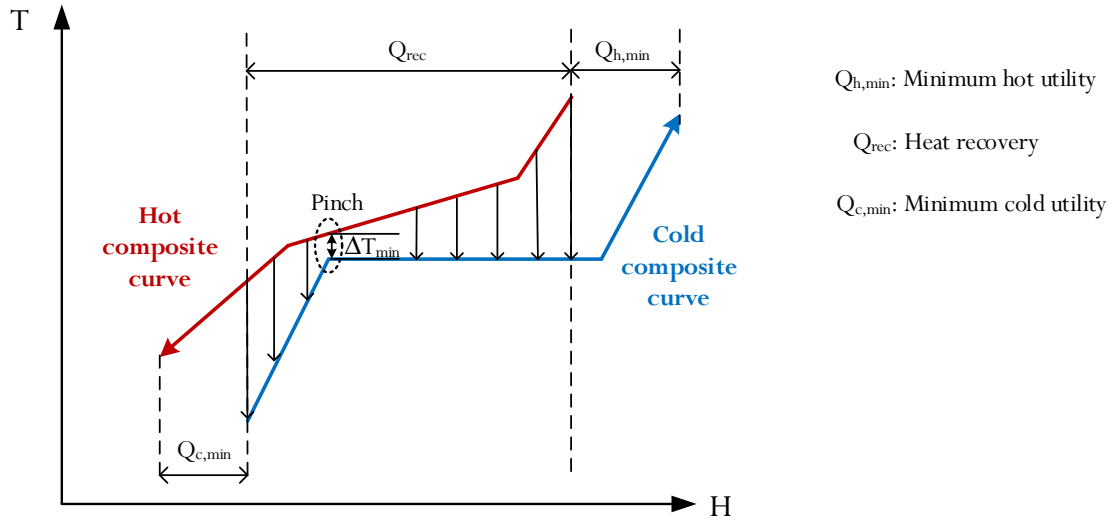
Figure 10 – Pinch analysis: Hot and cold composite curves, minimum cold and hot utility demand, heat recovery within the system

The pinch divides the process into two regions: Above the pinch the hot composite curve transfers all its heat to the cold composite curve leaving only hot utility $Q_{h,min}$ required. Thus the region above the pinch is a net heat sink. Conversely, below the pinch only cold utility $Q_{c,min}$ is required and the region is therefore a net heat source. It should be noted that any network design that transfers heat across the pinch requires an additional amount of hot and cold utility, thus reducing the amount of heat that can be recovered within the system.

The choice of ΔT_{min} is primarily an economic optimization problem. Higher values of ΔT_{min} lead to higher hot and cold utility requirements and thus higher energy costs. On the other hand, lower ΔT_{min} require larger and more costly heat exchangers as shown in Eqs. (32) and (33).

$$A = \frac{\dot{Q}}{U \cdot \Delta T_{LM}} \tag{32}$$

A is the heat exchanger area in m^2, $\dot{Q}$ is the transferred heat (kW), U is the overall heat transfer coefficient (kW m^{-2} K^{-1}) and ΔT_{LM} is the logarithmic mean temperature difference:

$$\Delta T_{LM} = \frac{\Delta T_h - \Delta T_c}{\ln \dfrac{\Delta T_h}{\Delta T_c}} \tag{33}$$

ΔT_h : temperature difference at the hot end of the heat exchanger; ΔT_c : temperature difference at the cold end of the heat exchanger
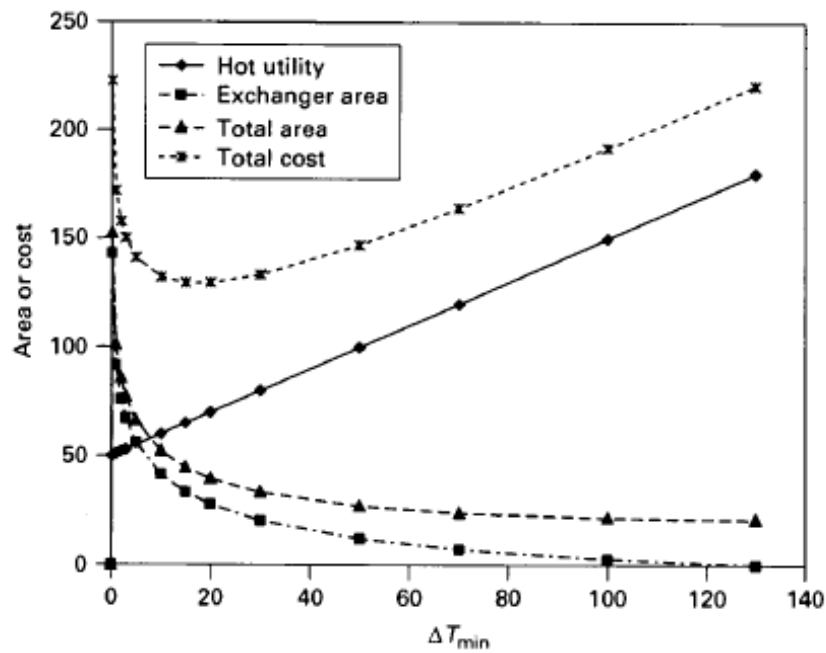
Figure 11 – Utility use, exchanger area and cost variation with ΔT_{min} (reprinted from "Pinch Analysis and Process Integration", Second Edition, Ian C. Kemp, chapter 2, p. 37, Copyright (2007), with permission from Elsevier)

In essence, the heat exchanger area is roughly inversely proportional to ΔT_{min}. Hence, low values of ΔT_{min} can lead to very large and costly heat exchangers, as capital cost is closely related to area. On the other hand, high values of ΔT_{min} can lead to high energy costs. By summing up the operating and capital costs a combined total cost graph is obtained with a typical optimum for ΔT_{min} in the range of 10 °C - 20 °C (Fig. 11).

Based on an appropriate ΔT_{min} the composite curves give energy targets for hot and cold utilities and determine the maximum achievable heat recovery within the system. Thereupon it is always possible to set up a heat exchanger network that fulfills the energy targets (minimum utility targets and maximum heat recovery) by obeying the three "golden rules":

- Don't transfer heat across the pinch
- Don't use cold utilities above the pinch
- Don't use hot utilities below the pinch

4. Results

4.1 An experimental investigation of biodiesel steam reforming

4.1.1 Preliminary tests with ceramic based catalyst monoliths

27 steam reforming experiments (test duration: 2.5 hours, biodiesel mass flow: 20 g/h) with ceramic based catalyst monoliths (l: 4 cm, d: 1.8 cm) have been conducted in order to detect the influence of pressure, temperature and steam-to-carbon ratio on hydrogen efficiency and carbon deposition. Pressure has been varied in the range of 1 bar to 5 bar, temperature from 600 °C to 800 °C and S/C from 3 to 5.

In line with thermodynamics, a decline of the thermal hydrogen efficiency with increasing pressure and decreasing temperature was observed at S/C=3 and S/C=4 (Figs. 12a, 13a). At S/C=5 (Fig. 14a), the lower residence time in the low pressure range seems to outweigh the effect of increased hydrogen yield. Generally, increasing the S/C from 3 to 5 has a positive effect on hydrogen efficiency at 600 °C, whereas the positive effect is almost negligible at 800 °C.
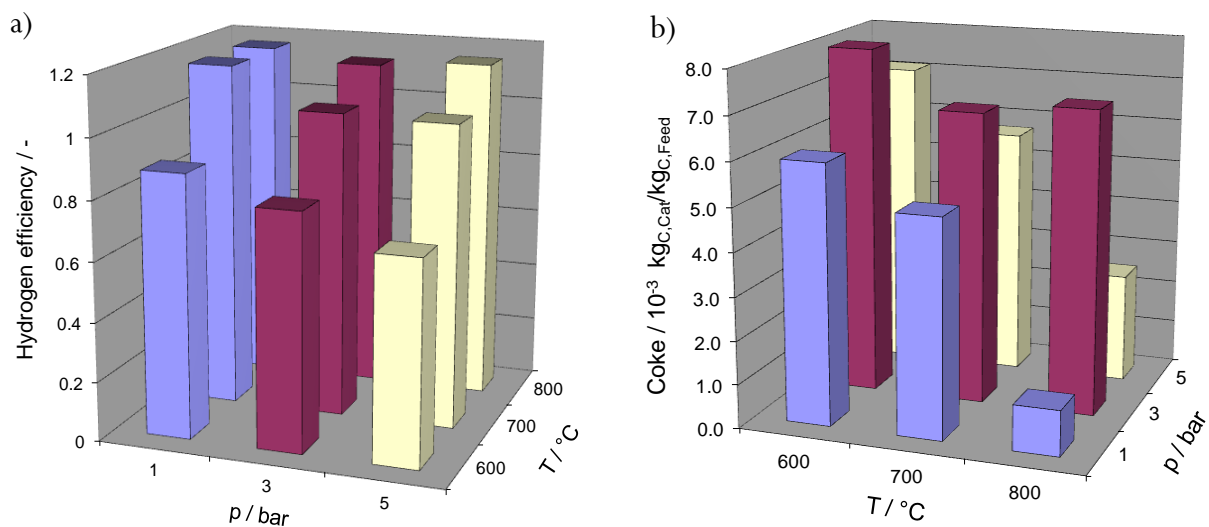
Figure 12 – Biodiesel steam reforming: Hydrogen efficiency (a) and coke deposition (b) at S/C=3
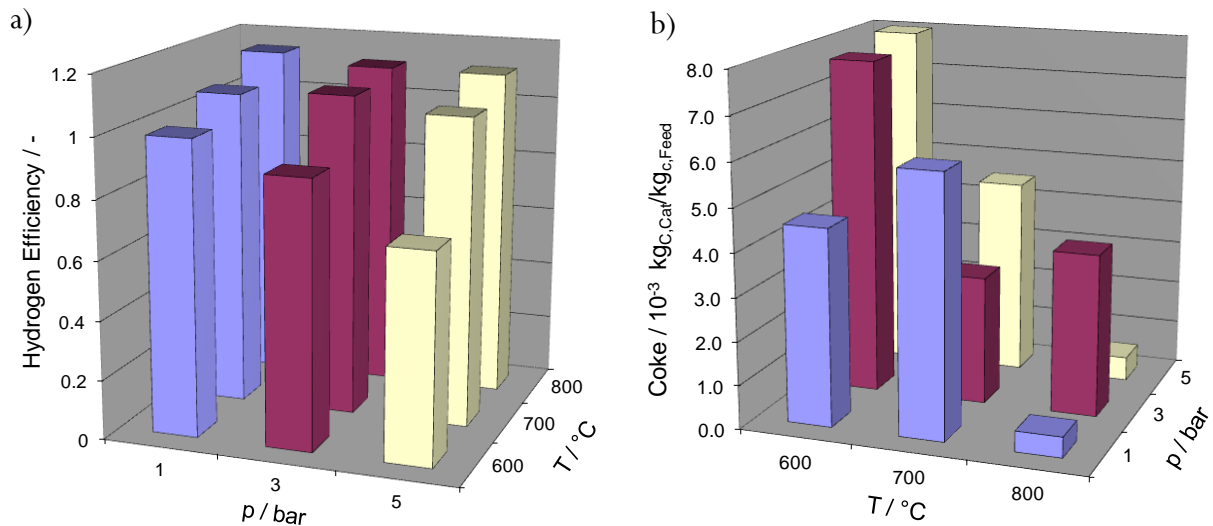
Figure 13 – Biodiesel steam reforming: Hydrogen efficiency (a) and coke deposition (b) at S/C=4
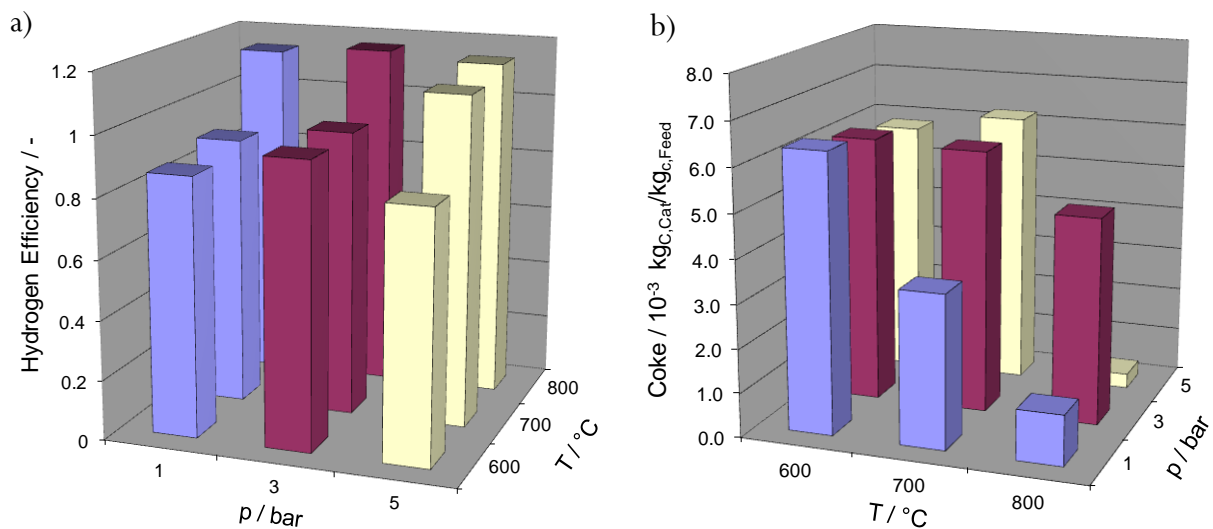
Figure 14 - Biodiesel steam reforming: Hydrogen efficiency (a) and coke deposition (b) at S/C=5

Coke deposition on the catalyst surface increases with decreasing temperature (Figs. 12b, 13b, 14b). This finding is in agreement with published literature. Lin et al. [2013, 2014] report an onset of carbon formation for ATR of biodiesel below 900 °C, accompanied by an increase in methane and ethylene production. Concurrently, Maximini et al. [2012] observed increased carbon formation for a microchannel diesel steam reformer when reducing the temperature from 800 °C to 700 °C.

In line with the experimental and literature findings, Aspen Plus calculations based on minimization of Gibbs free energy show increased coke formation at low temperatures and low

S/C ratios (Fig. 15). In the considered S/C range, the coke deposition maximum is shifted towards higher temperatures for decreasing values of S/C. Moreover, the coke formation boundary at elevated pressure is shifted slightly towards higher temperatures and higher S/C.
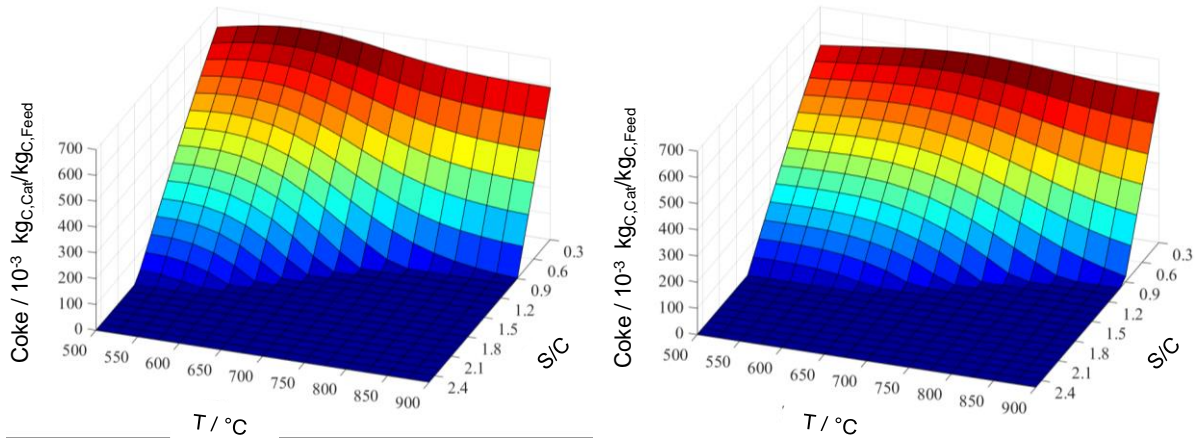
Figure 15 - Biodiesel steam reforming: Equilibrium coke formation at p=1 bar (left) and p=5 bar (right)

Obviously, the experimentally derived coke deposition (Figs. 12b − 14b) is higher than thermodynamically predicted (Fig. 15). In fact, at the given boundary conditions of the preliminary tests (T=600 °C − 800 °C, p=1 bar − 5 bar, S/C=3 − 5), carbon formation is not expected at thermodynamic equilibrium. Similarly, Lin et al. [2014] found that at S/C > 0.75 it is not possible to predict carbon formation accurately by thermodynamic equilibrium calculations which the authors attribute to heat transfer limitations in the catalyst bed and reaction kinetics.

4.1.2 Longevity tests with ceramic based catalyst monolith

Based on the preliminary experiments, a longevity test (100 hours, l: 8 cm, d: 1.8 cm, $\dot{m}_{BD}$: 5 g/h) has been carried out at operating conditions where coking on the catalyst surface was found to be least severe (T=800 °C, S/C=5, p=5 bar, see Fig. 14b). Although a stable product gas composition close to chemical equilibrium has been achieved, the axial temperature profile changed significantly over time on stream (Fig. 16). Please note that the observed fluctuations of axial temperatures are caused by pressure fluctuations which are induced by periodical condensate release.

After the start of the reforming reaction, the catalyst front temperature TA drops from 800 °C to 723 °C due to the required endothermic heat demand. Shortly afterwards, TA starts to rise indicating a severe loss of catalyst activity due to progressive catalyst deactivation. Subsequently the reaction front moves downwards in the axial direction. Within the considered time range, a deterioration of reformate gas composition was not observed with regard to the main components H_2, CO, CO_2 and CH_4, since the number of active metal particles on the catalyst surface was sufficiently high to ensure equilibrium gas concentration at the catalyst outlet.
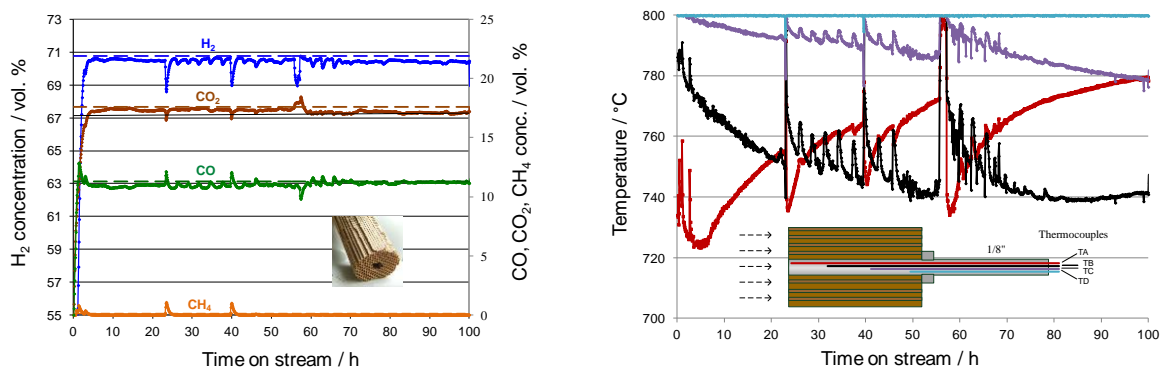
Figure 16 – Longevity test with ceramic based catalyst monolith (T=800 °C, p=5 bar, S/C=5); left: dry product gas composition (dotted lines: equilibrium concentrations); right: axial catalyst temperatures over time on stream
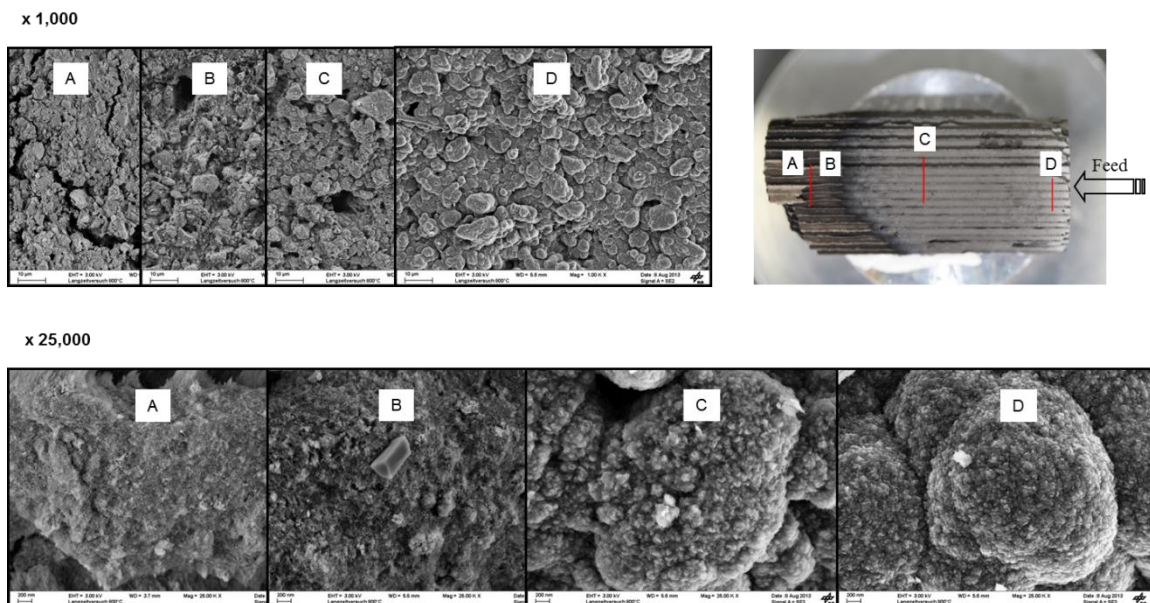
Figure 17 – Longevity test with ceramic catalyst monolith (T=800 °C, p=5 bar, S/C=5), Scanning electron microscopy of the catalyst surface

Scanning electron microscopy (SEM) of the catalyst surface shows sintering and coking (Fig. 17). Both sintering and coking occur predominantly at the catalyst inlet, leading to a reduction of

catalytically active sites for biodiesel conversion. As previously discussed, deactivation through coking can be caused by light hydrocarbons such as ethylene and propylene which are known to be the main precursors for coke formation [Blasi 2014, Yoon 2008]. Ethylene and propylene can be produced by thermal cracking of biodiesel or by decomposition of the fatty acids into saturated and unsaturated hydrocarbons, which can then be further converted into ethylene, propylene and other small hydrocarbons via ethylene elimination, isomerization and hydrogen transfer reactions [Berry 2003]. In addition, double bonds present in the fatty acid methyl esters enhance the formation of aromatics, which are coke precursors [Nahar 2010-1]. Temperatures higher than 750 °C are necessary in order to fully convert aromatic species [Gonzalez 2013].

Notwithstanding, higher hydrocarbons have not been detected in the product gas due to the sufficient catalyst length, allowing for a complete conversion into C_1 products. In contrast, during the preliminary tests at higher feed mass flow rates (see chapter 4.1.1), light hydrocarbons ($C_2 - C_4$) have been detected in 10 out of 27 experiments in the outlet stream. It is assumed that the low temperature at the catalyst inlet is the main cause of catalyst deactivation, since this favours the evolution of light hydrocarbons and an incomplete conversion of aromatics, resulting in catalyst coking. Concurrently, Lin et al. [2014] report a deterioration of reforming efficiency as the temperature at the front end of the catalyst bed is reduced due to the application of a higher S/C.

4.1.3 Longevity tests with metallic based catalyst monolith

In order to improve the long-term stability of biodiesel steam reforming, an experiment at similar conditions (T=840 °C, p=5 bar, S/C=5, $\dot{m}_{BD}$=5 g/h) has been conducted using a metallic based catalyst monolith (l: 5.1 cm, d: 2 cm). The metallic catalyst substrate offers the advantage of an improved heat transfer in both radial and axial directions, thus ensuring a more homogeneous temperature profile. As can be seen from Fig. 18, a stable product gas composition near chemical equilibrium has been achieved over 100 hours. After initiation of the reforming reaction, the catalyst front temperature TB decreases by 38 °C (compared to 77 °C for the ceramic monolith). Moreover, catalyst temperatures in axial directions are stable during time on stream indicating high and stable catalyst activity (Fig. 19).
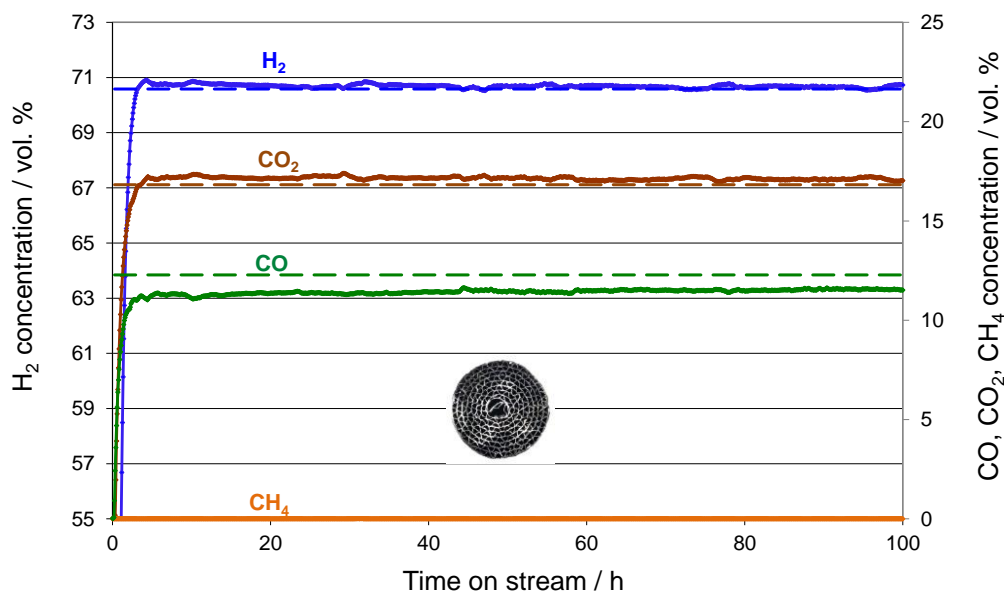
Figure 18 – Longevity test with metallic based catalyst monolith (T=840 °C, p=5 bar, S/C=5), dry product gas composition (dotted lines: equilibrium concentrations)

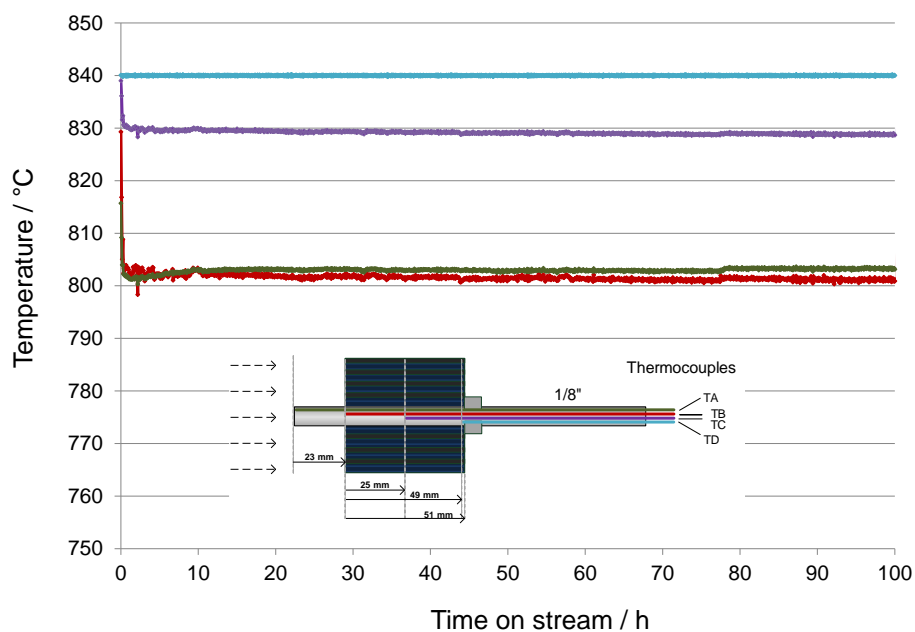**Figure 19** – Longevity test (T=840 °C, p=5 bar, S/C=5), axial temperatures over time on stream

Analysis of the unconverted biodiesel in the cold trap revealed 98.7 % biodiesel conversion. As can be seen from Fig. 20, the biodiesel peaks in the GC chromatogram have nearly vanished. 69 % of the unconverted biodiesel can be attributed to coke deposits on the catalyst surface and tube walls, the remaining 31 % is related to biodiesel and its cracking products. No higher hydrocarbons have been detected in the product gas.
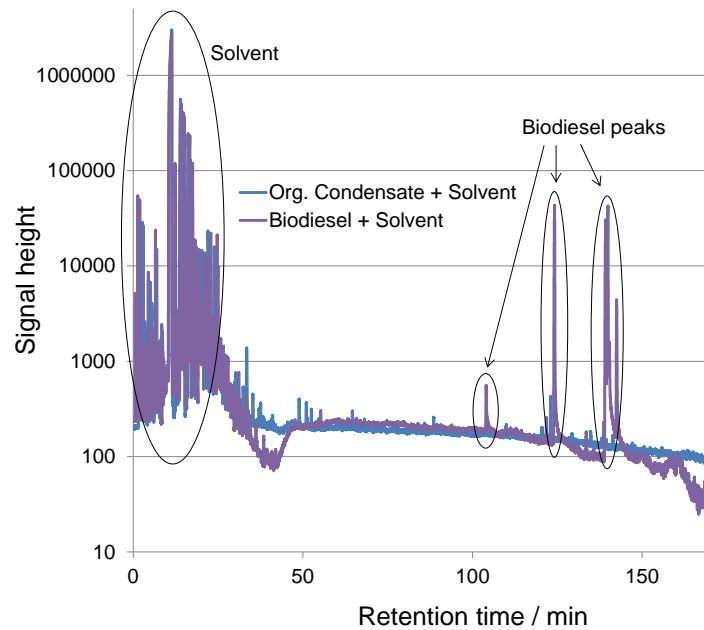
Figure 20 – Longevity test (T=840 °C, p=5 bar, S/C=5), GC analysis of original and unconverted biodiesel

In summary, by increasing the control temperature from 800 °C to 840 °C and using metallic instead of ceramic catalyst substrate, a significant improvement in catalyst stability was achieved. It is assumed that the high temperature at the catalyst front end mitigates coke formation due to improved kinetics of the gasification reactions, in particular the reaction of solid carbon with CO_2 and H_2O (Eqs. (13), (14)). The following hypothesis is derived: As a first step, coke is formed through chemisorption and dissociation of biodiesel. Subsequently, the deposited coke reacts with H_2O and CO_2 to form CO and H_2. If the reaction rate of the gasification reactions is slower compared to the coke forming reactions in the given temperature range, this will result in an accumulation of carbon on the catalyst surface. Obviously, the accumulation is induced at the catalyst front end. The decrease of coke with increasing temperature can be explained by a stronger increase of the reaction rate of gasification reactions compared to the coking reactions.

Taking into account the inverse relationship of the coking rate to coke formed [Mieville 1991] a drop of coking rate will be caused at the catalyst front end with time on stream. Carbon deposition then progresses in the axial direction until a point is reached where catalyst activity is significantly reduced due to a limited availability of active sites. Subsequently, reformate gas composition deteriorates, leading to an increase of methane and the evolution of light hydrocarbons. Finally, the biodiesel conversion rate decreases.

4.1.4 Feed mass flow variation

In order to better understand the effect of flow rate, a feed mass flow variation has been carried out. Therefore the biodiesel mass flow has been varied at a constant S/C ratio of 5. As can be seen from Fig. 21, the catalyst front temperature TB is stable for a biodiesel mass flow of 10 g/h over the whole temperature range, indicating stable catalyst activity. By contrast, increasing the biodiesel mass flow from 10 g/h to 15 g/h results in an increase of the catalyst front temperature being initiated at a threshold temperature of 730 °C. When the inlet temperature is further decreased stepwise from 730 °C to 693 °C, catalyst deactivation becomes more pronounced.
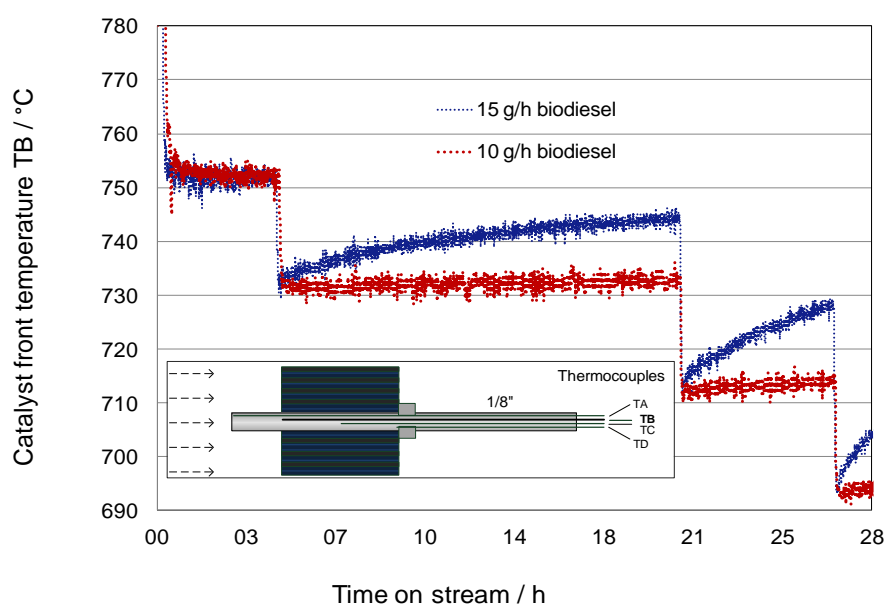

Figure 21 – Effect of biodiesel mass flow rate on catalyst deactivation (metallic catalyst substrate, p=5 bar, S/C=5)

This finding is in line with the above-mentioned hypothesis stating that deactivation induced at the catalyst front end is the result of kinetic limitations of the gasification reactions. At higher feed mass flows, the kinetic limitations of the reverse Boudouard reaction and the water gas reaction become more severe, resulting in a faster catalyst deactivation (this will be reviewed in more detail in chapter 5). Besides, formation of light hydrocarbons and aromatics is favoured in the low temperature range. Thus, the observations of Lin et al. [2014] and Berry et al. [2003] that high GHSV accelerates the formation of carbon can be confirmed for steam reforming of biodiesel. When comparing Fig. 21 with Fig. 16, it becomes evident that the metallic catalyst

substrate shows improved performance over the ceramic substrate at similar temperature conditions. Whilst the catalyst inlet temperature remains stable at a biodiesel mass flow of 10 g/h and a temperature of 730 °C (Fig. 21), it rises sharply at a similar front end temperature of 723 °C when using a ceramic based catalyst monolith (Fig. 16, right side).

4.1.5 Conclusions

Biodiesel steam reforming has been investigated at various operating conditions including variation of temperature, pressure, steam-to-carbon ratio and gas hourly space velocity. By directly mixing biodiesel at room temperature into superheated steam (T=550 °C), complete vaporization of biodiesel could be ensured. Thereby, self-pyrolysis and subsequent coke formation in the mixing zone was minimized and fluctuations in reformate flow rate were avoided.

Coke deposition on the catalyst surface and sintering are determined as main causes of catalyst deactivation. Preliminary experiments using ceramic catalyst monoliths indicate increased coking tendency with decreasing temperature which is in line with literature findings and thermodynamic calculations. A longevity test at conditions where coking was found to be least severe (T=800 °C, S/C=5, p=5 bar) showed a stable product gas composition. However, progressive blocking of the active sites by coke deposition occurred. By using a metallic catalyst substrate, a more homogenous axial and radial temperature profile could be ensured, leading to higher catalyst inlet temperatures (> 800 °C). Hence, coking of the catalyst was reduced to a minimum resulting in stable catalyst performance over 100 hours with 99 % biodiesel conversion. In addition, tests were carried out at varying mass flows in the temperature range 690 °C – 750 °C indicating a detrimental effect of high feed mass flows on catalyst activity. The observed effect is more pronounced in the low temperature range. Moreover, the metallic based precious metal catalyst shows improved performance over the ceramic based catalyst at similar inlet temperatures.

Based on the experimental findings, it can be concluded that catalyst deactivation primarily depends on catalyst inlet conditions, in particular on the catalyst front temperature and feed mass flow per open frontal area of catalyst. Gas hourly space velocity seems not to be an

adequate parameter for determining coke formation, as catalyst length is not decisive for the initiation of coking. Instead, feed mass flow per open catalyst area and fluid velocity are proposed as appropriate criteria for evaluating coking tendency.

The results of this study show that it is vital (at the given boundary conditions) to ensure a minimum threshold temperature of 750 °C (assuming a feed mass flow per open area of catalyst of 39 g/h·cm^2) at the catalyst inlet in order to avoid catalyst deactivation. Apart from ensuring a threshold temperature, small biodiesel flow rates are favourable in order to maintain high and stable catalyst activity. At a given catalyst inlet temperature of 730 °C a threshold mass flow of 10 g/h (corresponding to a mass flow per open area of catalyst of 26 g/h·cm^2, a fluid velocity of 6 cm/s or a gas hourly space velocity of 5,200 h^{-1}) must not be exceeded. Increasing the feed mass flow rate beyond a threshold mass flow rate causes immediate initiation of catalyst deactivation. Regarding practical applications, operating conditions should be targeted which avoid initial carbon formation at the catalyst front end.

It has to be taken into account that high reformer temperatures, high steam-to-carbon ratios and low feed mass flow rates are not favourable in terms of fuel processor efficiency and net hydrogen production costs. Therefore a trade-off between high catalyst durability and acceptable hydrogen production costs must be found.

Summarizing, catalyst deactivation of biodiesel steam reforming has been studied in detail. Accordingly, favourable operating conditions have been derived. Stable biodiesel steam reforming has been shown, thus laying the basis for reformer design studies targeting commercial applications.

4.2   Direct steam reforming of diesel and diesel-biodiesel blends

4.2.1   Steam reforming of pure diesel

Steam reforming at T=800 °C, p=3 bar and S/C=5 has been carried out using pure diesel ($\dot{m}_{Diesel}$: 5 g/h) the properties of which are described in Tab. 2 (chapter 3.1). As can be seen from Fig. 22 a stable product gas composition close to chemical equilibrium has been achieved over a period of 20 hours. No higher hydrocarbons were detected in the product gas stream, while methane production was also negligible.
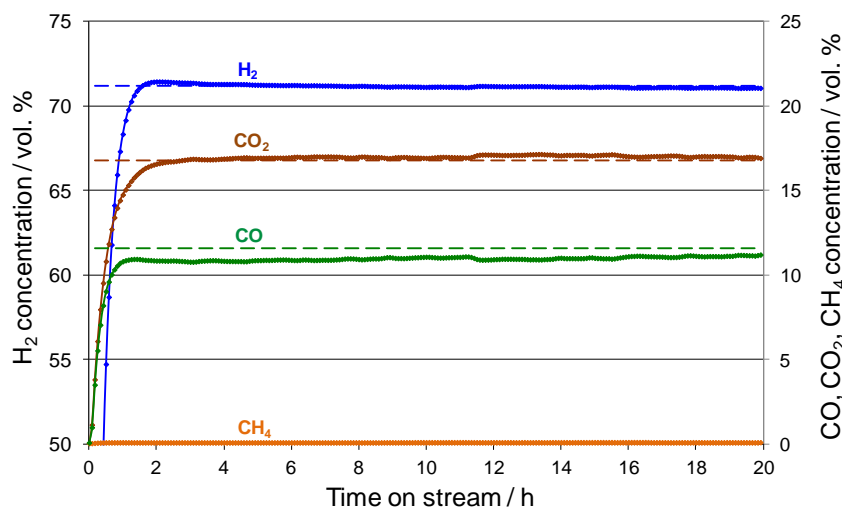
Figure 22 – Dry product gas composition of diesel steam reforming (T = 800 °C, p = 3 bar, S/C = 5), (dashed lines: chemical equilibrium concentrations)

It is well known that it is not possible to quantify the onset of catalyst deactivation by analyzing the product gas alone [Boon 2011], which is due to the fact that parts of the catalyst can already be heavily deactivated before a deterioration of the product gas composition (decrease of H_2, increase of CH_4, formation of higher hydrocarbons) is observed. A more precise method of determining the onset of catalyst deactivation is to measure the temperature at the center line of the catalyst. Fig. 23 depicts the axial catalyst temperatures over time on stream. Shortly after initiation of the reforming reaction, the catalyst front temperature TB drops by 27 °C due to the endothermic reforming reaction. Subsequently, it stabilizes at this level indicating a stable catalyst activity.

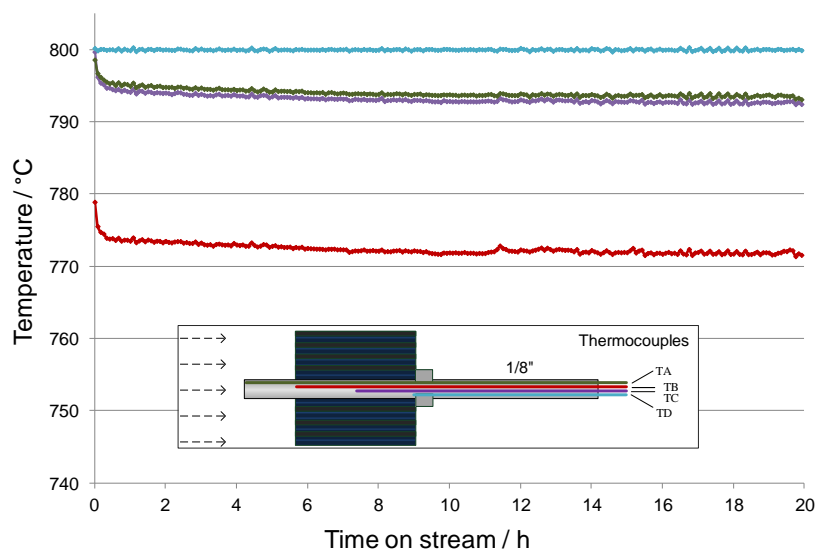**Figure 23** – Axial catalyst temperatures over time on stream (T = 800 °C, p = 3 bar, S/C = 5)

As can be seen from the results of the GC analysis of the condensate (Fig. 24) the diesel compounds (predominantly paraffins) are for the most part converted into gaseous products during steam reforming. Only small amounts of unconverted hydrocarbon species remain in the liquid organic condensate. Based on Eq. (21), a fuel conversion rate of 97.6 % was calculated. 85 % of the unconverted diesel is attributed to coke deposition on the catalyst surface and on the tube walls, whilst the remaining 15 % are attributed to unconverted diesel compounds and its cracking products.
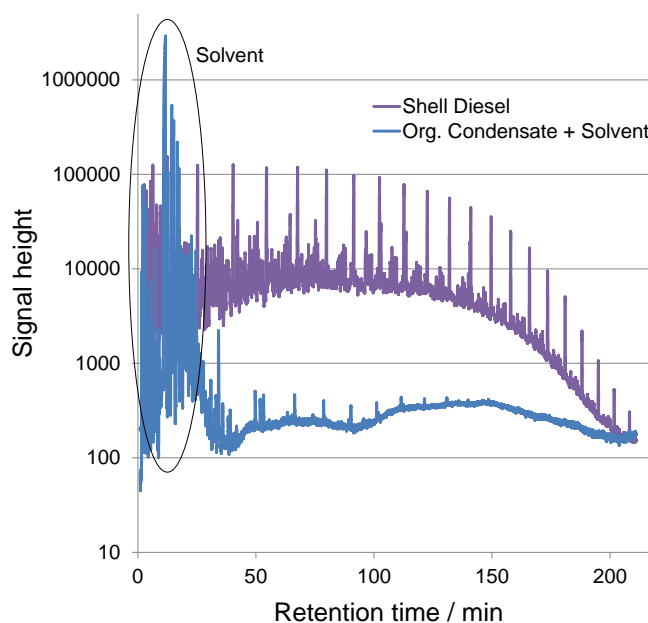

Figure 24 – Gas chromatography condensate analysis (T = 800 °C, p = 3 bar, S/C = 5)

In addition, the spent catalyst has been analyzed by scanning electron microscopy (SEM), revealing slight sintering at the catalyst inlet (Fig. 25), which is accompanied by a reduction of surface porosity. Steam reforming experiments with feedstock biodiesel revealed similar sintering effects (chapter 4.1.2). However, sintering was more severe in case of biodiesel, especially with the ceramic based catalyst monoliths, leading to a reduction of catalytically active sites. In the case of diesel SR with metallic monoliths, the observed sintering is not detrimental to catalyst stability in the given time period of 20 hours.
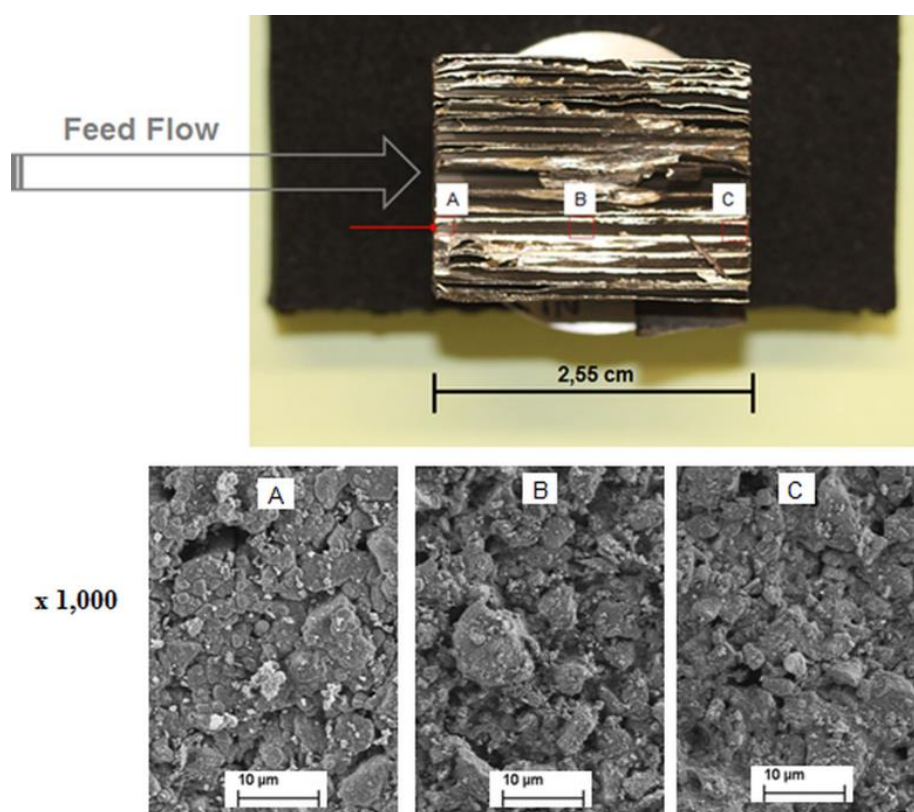

Figure 25 – Cross section of spent metallic catalyst monolith (top), scanning electron microscopy of the catalyst surface at different positions (bottom)

4.2.2   Steam reforming of diesel-biodiesel blends

In addition to the experiment with pure diesel, steam reforming tests with diesel containing 7 vol. % biodiesel (B7 diesel) were carried out. The B7 diesel was acquired from a local petrol station in Greece. The physical properties of the B7 diesel differ slightly from the Shell diesel (Tab. 5). 5 g/h of B7 diesel were fed into the reformer at S/C=5 and p=5 bar.

Table 5 – Comparison of pure diesel and B7 diesel properties		
Property	Pure Diesel	B7 Diesel / Desulphurized B7 diesel
Density at T = 15 °C (kg/m3)	836.4	831.5/828.4
Lower heating value LHV (MJ/kg)	42.93	42.63/43.11
Empirical formula	$C_{13.3}H_{24.7}$	$C_{13.5}H_{25.2}O_{0.1}$
Sulphur content (ppmw)	7.0	6.8/1.6
Fatty acid methyl ester FAME (vol. %)	< 0.3	7/7
Total aromatic content (wt. %)	24.0	18.7/15.3

As can be seen from Fig. 26, a stable product gas composition has been achieved over 100 hours of on stream exposure. H_2, CO_2 and CH_4 concentrations are in equilibrium, whereas CO shows slight deviations. As expected, CH_4 is not present in the product gas stream at the given catalyst outlet temperature of 850 °C, which is attributed to the exothermic nature of the methanation reaction (Eq. (9)). Higher hydrocarbons were not detected in the dry product gas stream after leaving the cold trap, nor are they expected from equilibrium calculations.
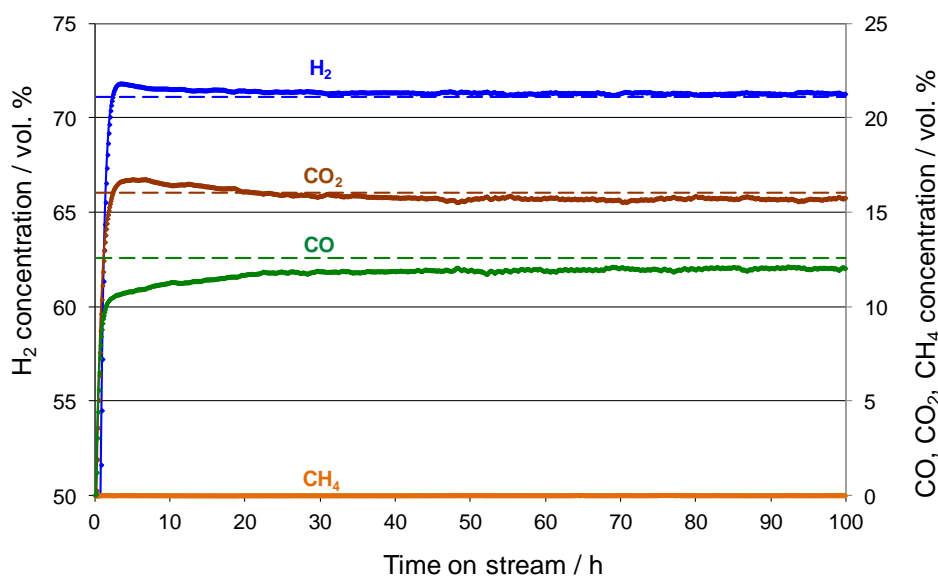

Figure 26 – Dry product gas composition (B7 diesel, 6.8 ppm sulphur, T = 850 °C, p = 5 bar, S/C = 5), (dashed lines: chemical equilibrium concentrations)
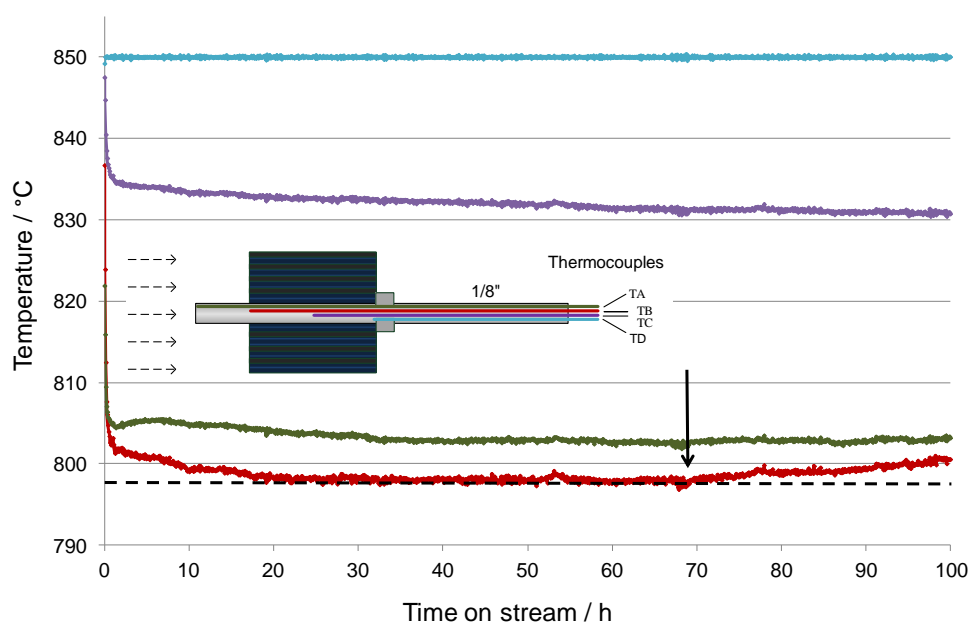
Figure 27 – Axial catalyst temperatures (B7 diesel, 6.8 ppm sulphur, T = 850 °C, p = 5 bar, S/C = 5)

After initiation of the reforming reaction, the catalyst front temperature TB drops by 52 °C, subsequently stabilizing at this level (Fig. 27). However, after 68 hours of on stream exposure, temperature TB (located 1 mm from the catalyst entrance in flow direction) starts to rise, indicating the onset of catalyst deactivation. Compared to the test with pure diesel (Fig. 23), the temperature drop at the catalyst front end is larger, which might be attributed to the higher catalyst loading (0.183 g/cm^3 for B7 diesel versus 0.122 g/cm^3 for pure diesel).

4.2.3 Effect of sulphur on long-term stability

In a test at similar operating conditions (T=850 °C, p=5 bar, S/C=5) with desulphurized B7 diesel (1.6 ppm sulphur, achieved via liquid-phase adsorption of organic diesel compounds using a specific activated carbon-based sorbent [Hoguet 2009]) a stable product gas composition was achieved over 100 hours (not shown here since the measured product concentration profiles were very similar to the ones depicted in Fig. 26), with no higher hydrocarbons being present in the dry reformate stream. The fuel conversion rate, as defined by Eq. (21), was similar to the test with sulphur-containing B7 diesel (98.7 % versus 98.5 %).

The catalyst front temperature TB, which is an appropriate indicator for initial catalyst deactivation, was found to be more stable compared to the 100 h test with sulphur containing

diesel (Fig. 28). Nevertheless, a minor increase in TB was observed after a test period of 96 hours. It is uncertain if this slight temperature increase is a sign of catalyst deactivation, considering that the deviation is still within the statistical range of fluctuations. It can therefore be hypothesized that the reformer catalyst activity is higher for the desulphurized diesel, indicating an appreciable effect of organic sulphur compounds on long-term reformer performance. This ties in well with the requirement to desulphurize petroleum-derived liquid fuels to sulphur levels of less than 1 ppmw in order to be used in fuel cell systems [Wang 2002].
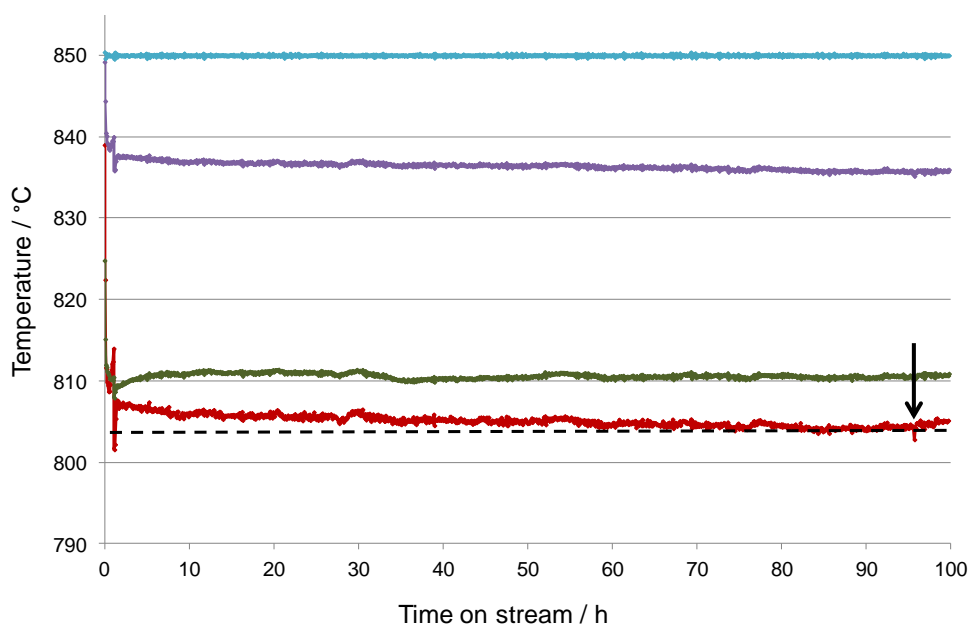

Figure 28 – Axial catalyst temperatures (B7 diesel, 1.6 ppm sulphur, T = 850 °C, p = 5 bar, S/C = 5)

Compared to the test with pure diesel (chapter 4.2.1) the fuel conversion rates for the B7 type diesel batches (original and desulphurized) were about one percentage point higher. This might be attributed to the higher reformer outlet temperature (850 °C vs. 800 °C) and to the fact that biodiesel, being present with a share of 7 vol. % in B7 diesel, can be more easily converted into gaseous products, as it is free of aromatics. Aromatic compounds are one of the main coke precursors, leading to coke deposition and subsequent catalyst deactivation [Nahar 2010-1]. Moreover, it is well known that aromatics are amongst the least reactive components in liquid fuels, thus requiring higher temperatures than non-aromatic compounds in order to be fully converted [Gonzalez 2013].

4.2.4   Feed mass flow variation

Recently, several authors have presented results of liquid fuel reforming, indicating a detrimental effect of high feed mass flow rates on catalyst activity. For ATR of diesel, Lin et al. [2014] reported initiation of carbon formation at GHSV > 48,500 h^{-1} (compared to > 44,000 h^{-1} for biodiesel), being accompanied by an increase of light hydrocarbons in the product gas. Ethylene, aromatics and naphtenes were identified as the main precursors for carbon formation. Concurrently, Engelhardt et al. [2012] observed a clear trend toward a higher amount of hydrocarbons for increasing diesel feed flow. For SR of biodiesel, initiation of catalyst deactivation occurs at GHSV levels in excess of 5,200 h^{-1} (corresponding to a mass flow per open area of catalyst of 26 g/h·cm^2 and a fluid velocity of 6 cm/s) at a catalyst inlet temperature of 730 °C (see chapter 4.1.4).

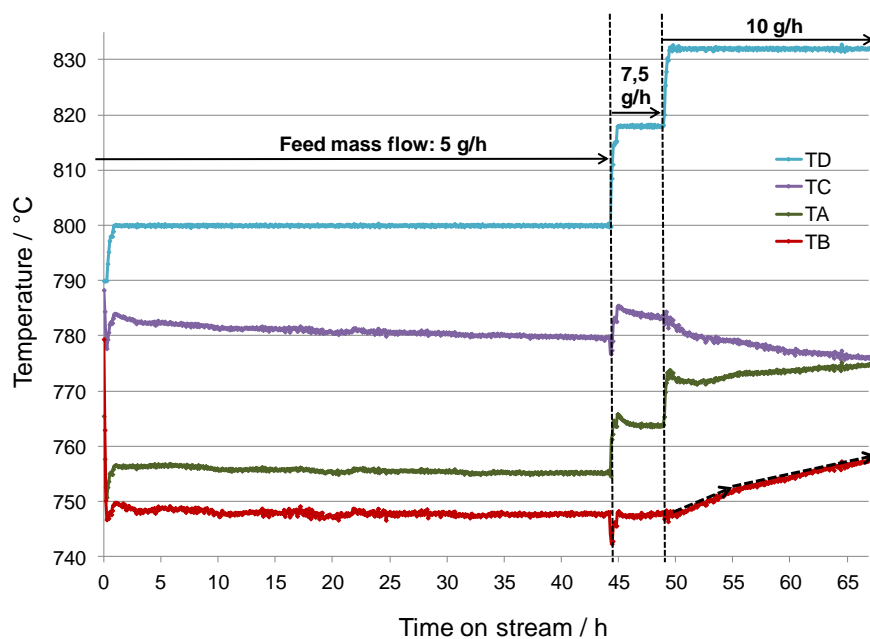**Figure 29** – Feed mass flow variation (B7 diesel, 6.8 ppm sulphur, TB = 750 °C, p = 5 bar, S/C = 5)

Within this work, the diesel mass flow has been increased stepwise from 5 g/h to 7.5 g/h and 10 g/h at an initial catalyst front temperature of 750 °C in order to evaluate the influence of increasing feed mass flow rates on catalyst deactivation. As can be seen from Fig. 29, the catalyst front temperature TB remains constant for diesel mass flows up to 7.5 g/h. Upon raising the mass flow to 10 g/h, the catalyst front temperature increases, indicating initiation of catalyst deactivation due to coking. Thus, a threshold mass flow per open area of catalyst of 21 g/h·cm^2

(corresponding to a fluid velocity of 5 cm/s and GHSV of 4,400 h^{-1}) must not be exceeded in order to prevent initiation of catalyst deactivation. Obviously, the threshold value for the diesel-biodiesel blend considered in this study is lower than for biodiesel (see chapter 4.1.4). Thus, high feed mass flows are a critical issue for diesel steam reforming.

4.2.5 Conclusions

Direct diesel steam reforming has been evaluated experimentally at various operating conditions using precious-metal-based catalyst monoliths. By cooling the feed diesel to 0 °C and mixing it directly into superheated steam (T=390 °C) coke deposition in the mixing zone and on the catalyst surface could be reduced to a minimum and fluctuations of the product gas flow were avoided.

Successful direct steam reforming of pure diesel and diesel-biodiesel blends (B7 diesel) with stable product gas composition near chemical equilibrium has been achieved by applying a steam-to-carbon ratio of 5, a high catalyst inlet temperature (~ 800 °C) and a low gas hourly space velocity (2,700 h^{-1} − 2,900 h^{-1}). Diesel conversion ranged from 97.6 % for pure diesel to 98.7 % for desulphurized B7 diesel. In the case of pure diesel, scanning electron microscopy revealed slight sintering effects at the catalyst inlet, which however, were not detrimental for catalyst performance in the time range studied.

Catalyst durability tests (100 hours) with diesel-biodiesel blends indicate a slightly higher catalyst activity for desulphurized B7 diesel (1.6 ppmw sulphur) compared to the original B7 diesel (6.8 ppmw sulphur). It is therefore recommended to desulphurize commercial diesel blends to less than 1 ppmw prior to steam reforming, in order to maintain a high and stable catalyst activity. Thereby, operation and maintenance costs for distributed hydrogen generation systems can be reduced substantially.

Furthermore, the experimental results reveal a detrimental effect of high feed mass flow rates on catalyst activity. At given boundary conditions (T=750 °C, p=5 bar, S/C=5) catalyst deactivation caused by coking is initiated at a threshold mass flow per open area of catalyst of 21 g/h·cm^2 (corresponding to a fluid velocity of 5 cm/s and gas hourly space velocity of 4,400 h^{-1}). As a rule of thumb, the maximum threshold feed mass flow for steam reforming of

diesel is less than half the threshold value of biodiesel, making biodiesel an interesting alternative feedstock for distributed hydrogen generation via SR. Summarizing, successful direct steam reforming of diesel and diesel-biodiesel blends at elevated pressures ($3 - 5$ bar) has been shown on a lab-scale level. Applying a high catalyst inlet temperature and low feed mass flow rates proved decisive for stable long-term operation.

4.3 Evaluation of on-site hydrogen generation via steam reforming of biodiesel: Process optimization and heat integration

The experimental work has been complemented by a simulation study with Aspen Plus ® covering on-site hydrogen generation based on biodiesel SR, the results of which are presented in this chapter.

4.3.1 Non-heat integrated system: Effect of pressure on system efficiency

Based on the $50\,\text{Nm}^3/\text{h}$ non-heat integrated Aspen Plus flowsheet (Fig. 9, chapter 3.3.2) a sensitivity analysis has been carried out at $S/C=5$ by varying system pressure from 6 bar to 13 bar. As can be seen from Fig. 30 the thermal system efficiency as defined by Eq. (29) increases from 53.9 % at 6 bar to 62.4 % at 13 bar which is mainly attributed to an improved PSA-efficiency resulting in a decreased amount of biodiesel needed for the reformer ($\dot{m}_{BD-REF}$). Despite a slight increase of the required biodiesel mass flow to the burner ($\dot{m}_{BD-B}$) which arises from the fact that the PSA off-gas heat load (based on LHV) drops from 127.2 kW at 6 bar to 48.3 kW at 13 bar (see Fig. 31a), total fuel consumption $\dot{m}_{BD-TOTAL}$ is reduced from 26.4 kg/h to 22.8 kg/h. The drop of the PSA off-gas heat load is mainly caused by a rapid decrease of the off-gas mass flow and an increased share of CO_2 (Fig. 31b). Obviously, applying high pressure is beneficial for the given H_2 generation system including a PSA unit.
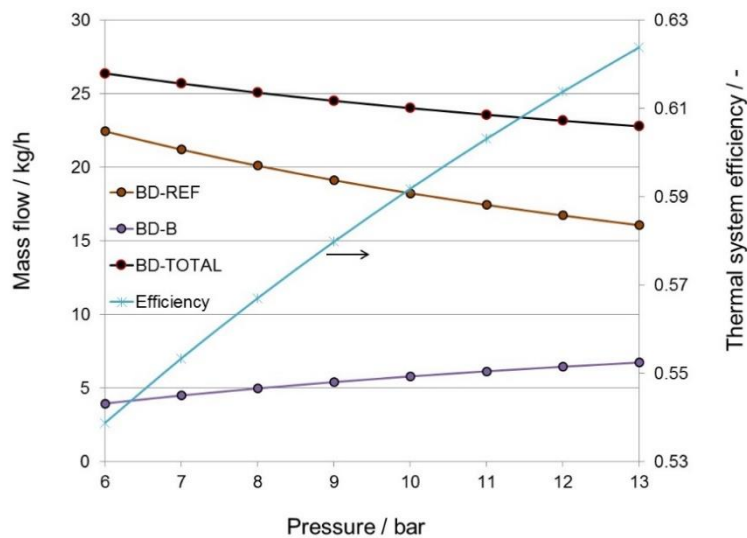

Figure 30 – Effect of pressure on fuel demand and thermal system efficiency (S/C=5)
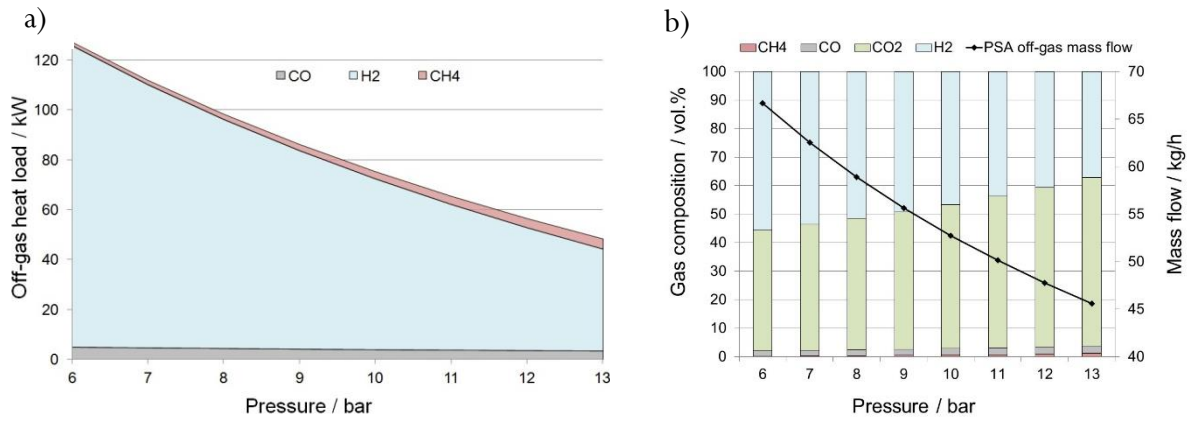
Figure 31 – Effect of system pressure on PSA off-gas heat load (a), PSA off-gas composition and PSA off-gas mass flow (b) at S/C=5 (further boundary conditions: see Tab. 4)

Based on the sensitivity analysis, a base case (=operating regime "0") is defined with the following operating parameters: p=13 bar, S/C=5, T_{AIR-B}=200 °C. Starting from this base case the system efficiency of a heat integrated system can be improved by raising the burner air preheating temperature T_{AIR-B} by making use of waste heat streams. As a result, less fuel $\dot{m}_{BD-B}$ is needed for the burner in order to provide the necessary heat for the endothermic SR reaction, while the amount of fuel needed for the reformer $\dot{m}_{BD-REF}$ remains unaffected. Accordingly, the thermal system efficiency rises.

4.3.2 Heat-integrated system

The flowsheet depicted in Fig. 9 (chapter 3.3.2) comprises two streams that have to be heated up (=*cold streams*) according to the process specifications, namely "H2O-0" to "H2O-PRE" and "AIR-0" to "AIR-B" and three streams which have to be cooled down (=*hot streams*), namely "FLUE-1" to "FLUE-GAS", "REF-OUT" to "WGS-IN" and "WGS-1" to "PSA-IN". Obviously, using the enthalpy of the hot streams for heating up the cold streams is decisive for system optimization.

As described in chapter 3.3.3 hot and cold streams can be combined to so-called hot and cold composite curves for any given process. For the Aspen Plus base case (p=13 bar, S/C=5, T_{AIR-B}=200 °C) the composite curves have been derived by extracting the respective streams from the flowsheet resulting in a thermal system efficiency of 62.4 % (Fig. 32).
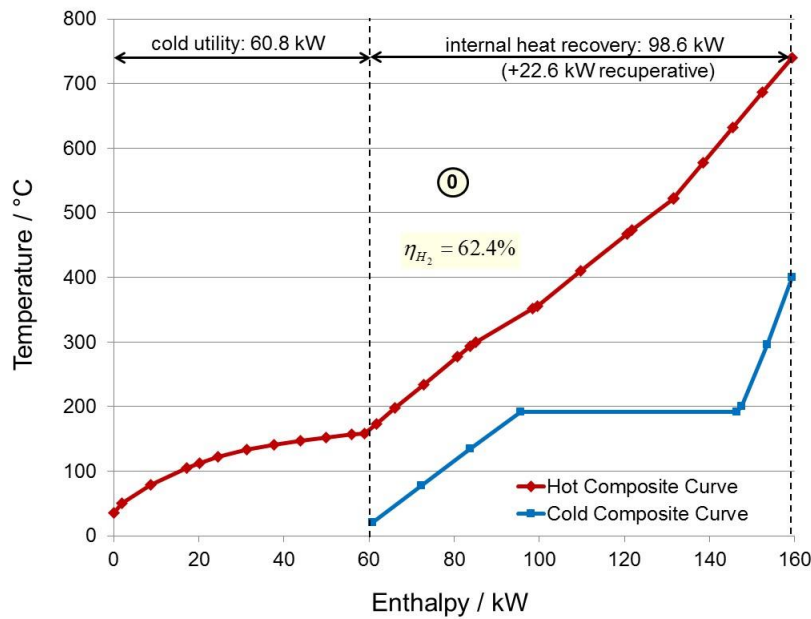
Figure 32 – Composite curves of Aspen Plus base case (=operating regime 0)

The maximum achievable burner air preheating temperature $T_{AIR-B,max}$ of the heat integrated system is limited by the enthalpy loads and related temperature levels of the available waste heat streams. For a given S/C ratio of 5 the maximum air preheating temperature $T_{AIR-B,max}$ can be determined iteratively (see Fig. A3) by targeting a minimum temperature approach (here: ΔT_{min}=15 °C) between the hot and cold composite curves with no additional external heating demand. By doing so, a maximum air preheating temperature of 472 °C is obtained at S/C=5 corresponding to a thermal system efficiency of 70.4 % (=operating regime 1, see Fig. 33 upper left side).

4.3.2.1 Effect of steam-to-carbon ratio on system efficiency

By lowering the S/C ratio stepwise from 5 (operating regime 1) to 4, 3 and 2.78 (operating regimes 2, 3, 4) $T_{AIR-B,max}$ can be raised to 545 °C, 617 °C and 632 °C, respectively (Fig. 33). At this point (operating regime 4), hereinafter referred to as the thermo-neutral point, no additional fuel is needed for the burner ($\dot{m}_{BD-B}$=0). Thus, the necessary heat for the endothermic reforming reaction is provided solely by the heating value of the PSA off-gas. From a technical point of view, this is highly advantageous since it eliminates the need of a dual fuel burner. Instead, a conventional gas burner can be used.

Moreover, Fig. 33 reveals an increasing energy turnover at higher S/C. Both the internal heat recovery and the external cooling demand increase (internal heat recovery: from 111.5 kW at S/C=2.78 to 126.0 kW at S/C=5, external cooling demand: from 7.9 kW at S/C=2.78 to 23.9 kW at S/C=5) resulting in a larger and more costly heat exchanger (HEX) network and increased energy costs. The higher energy turnover mainly arises from an increased heat demand for preheating and vaporization of water. Further taking into account the substantially reduced total fuel consumption (see Tab. 6) low S/C ratios appear highly favourable for heat-integrated DHG systems based on SR of biodiesel.
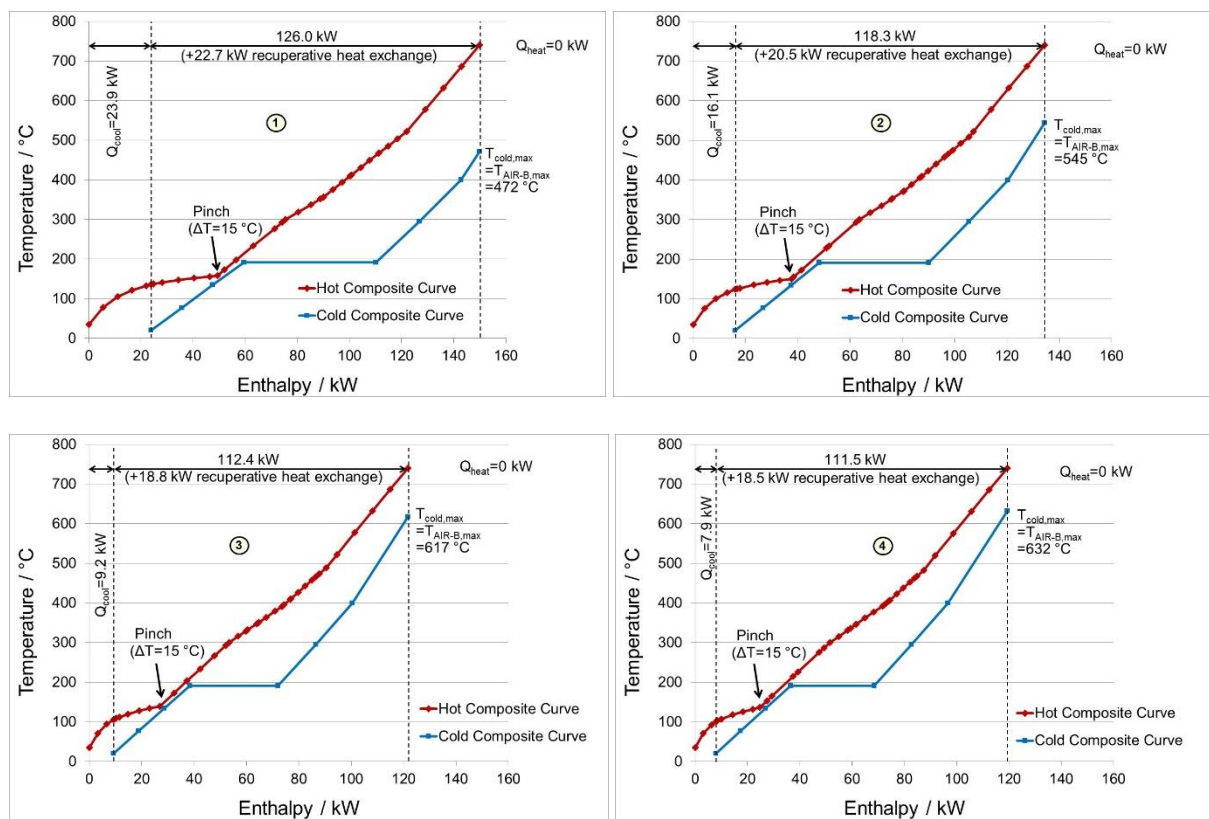

Figure 33 – Hot and cold composite curves of basic Aspen Plus flowsheet (upper left: S/C=5 corresponding to operating regime 1, upper right: S/C=4 corresponding to operating regime 2, bottom left: S/C=3 corresponding to operating regime 3, bottom right: S/C=2.78 corresponding to operating regime 4)

Figs. 34 – 36 summarize the effect of air preheating temperature and S/C on thermal system efficiency showing a positive effect of low S/C and high burner air preheating temperature. As can be seen from Fig. 35 the required biodiesel mass flow to the burner drops with decreasing S/C and increasing T_{AIR-B} up to a point where the biodiesel demand for the burner approaches zero (operating regime 4).
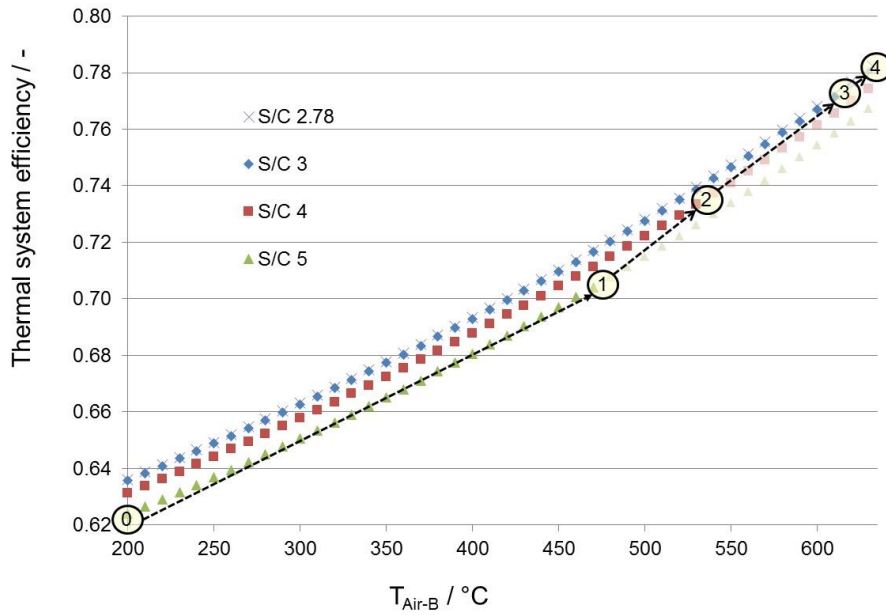
Figure 34 – Effect of S/C ratio and air preheating temperature $T_{AIR\text{-}B}$ on thermal system efficiency as defined by Eq. (29), operating regimes 1, 2, 3 and 4 (yellow-filled circles) represent the maximum achievable burner air preheating temperatures
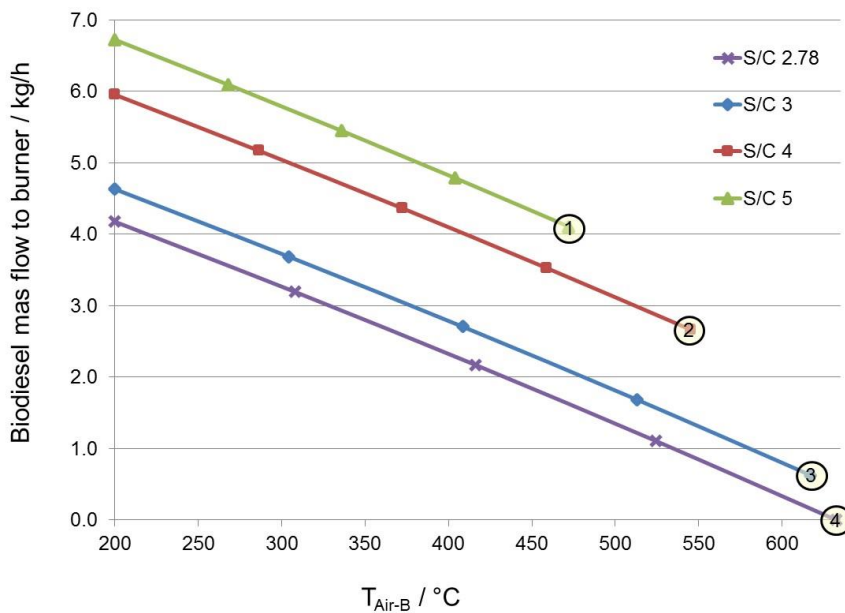
Figure 35 – Required biodiesel mass flow to the burner, operating regimes 1, 2, 3 and 4 (yellow-filled circles) represent the maximum achievable burner air preheating temperatures

The maximum thermal system efficiency (as corresponding to the maximum achievable burner air preheating temperature) of a heat integrated system increases linearly with decreasing S/C ratio up to the thermo-neutral point where PSA off-gas starts to emerge (Fig. 36). A maximum theoretical efficiency of 78.2 % is obtained.

Figure 36 – Maximum thermal system efficiency (as defined by Eq. (29)) as a function of S/C

Obviously, if the PSA off-gas surplus is vented, the system efficiency declines (=operating regime 5). Recycling the PSA off-gas would require gas compression from 1 bar to 13 bar. Taking into account th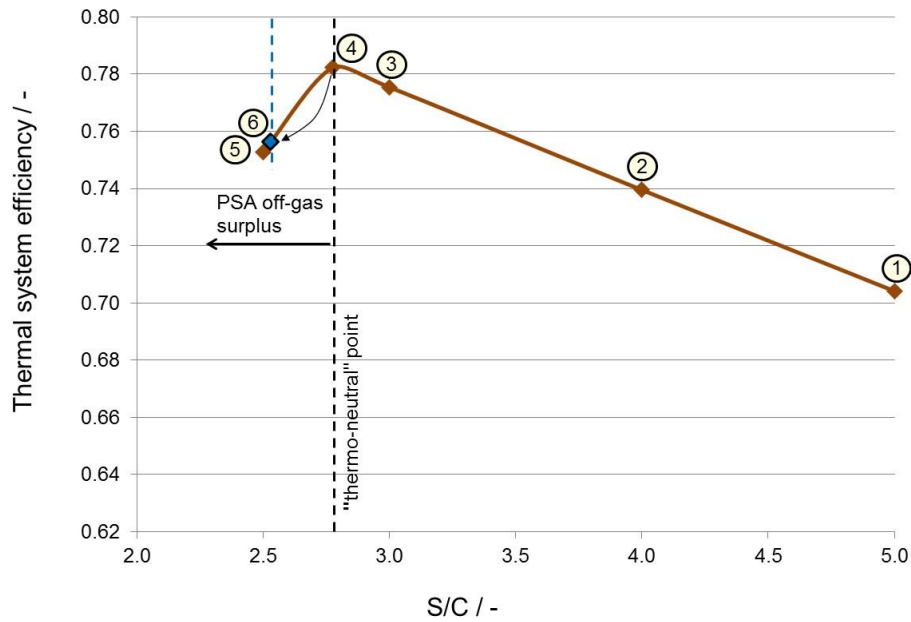at compressing gaseous feeds is energy intensive and considering that the PSA recycle ratio becomes extraordinary high at low S/C, the option of recycling the PSA off-gas was discarded. Tab. 6 summarizes the process characteristics of the considered operating regimes for a constant hydrogen output of 50 Nm^3/h.

Operating regime	S/C -	T_{AIR-B} (°C)	$\dot{m}_{BD-REF}$ (kg/h)	$\dot{m}_{BD-B}$ (kg/h)	$\dot{m}_{BD-Total}$ (kg/h)	η_{Syst} (%)	P_{el} (kW)
				Table 6 – Process characteristics of different operating regimes			
0	5.00	200.0	16.06	6.72	22.78	62.4	8.11
1	5.00	472.0	16.06	4.11	20.17	70.4	6.19
2	4.00	544.9	16.56	2.67	19.23	73.9	5.70
3	3.00	617.0	17.72	0.63	18.35	77.5	5.32
4	2.78	632.4	18.17	0.00	18.17	78.2	5.26
5	2.50	642.2	18.88	0.00	18.88	75.3	5.26
6	2.53	570.0	18.79	0.00	18.79	75.6	5.82

The highest theoretical efficiency is obtained under thermo-neutral conditions at S/C=2.78 (operating regime 4). Nonetheless, a heat integrated system based on these conditions would require a complex HEX network including several stream splits. In particular, the narrow section right above the pinch point and the initiation of water condensation during cooling of "WGS-1"-stream is detrimental to building up a HEX network. Even though we know from pinch theory that it is theoretically possible to set up a HEX network fulfilling the energy targets based on the composite curves at thermo-neutral conditions, the practicability of such a system must be questioned. Therefore a decision was taken to simplify the system by limiting the use of the "WGS-1" stream for heat integration purposes to a minimum value of 132 °C, which is the dew-point of the respective stream. Analogous to operating regime 4, thermo-neutral conditions were targeted for the simplified system (=operating regime 6).

4.3.2.2 Heat exchanger network of near-optimal system

The composite curves of the simplified, near-optimal system are depicted in Fig. 37. The minimum temperature approach between the hot and cold composite curve is 46.6 °C. 120.5 kW (102.1 kW + 18.4 kW) can be recovered within the system by matching hot and cold streams. No additional biodiesel $\dot{m}_{BD-B}$ is needed for the burner since the heating value of the PSA off-gas is sufficient for providing the necessary heat for the reforming reaction. An S/C of 2.53 has to be applied in order to ensure thermo-neutral conditions.
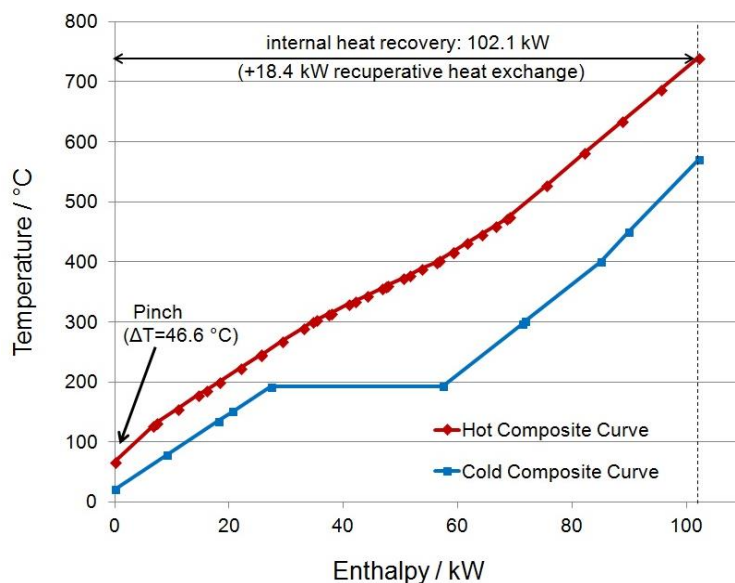

Figure 37 – Composite curves of near-optimal hydrogen generation system (=operating regime 6)

Based on the composite curves, a HEX network has been set up targeting a maximum internal heat recovery with no additional external cooling demand (except the cold utility which is required to cool down the WGS product gas stream from dew point temperature to PSA inlet temperature). A fully heat integrated system is obtained as depicted in Fig. 38.
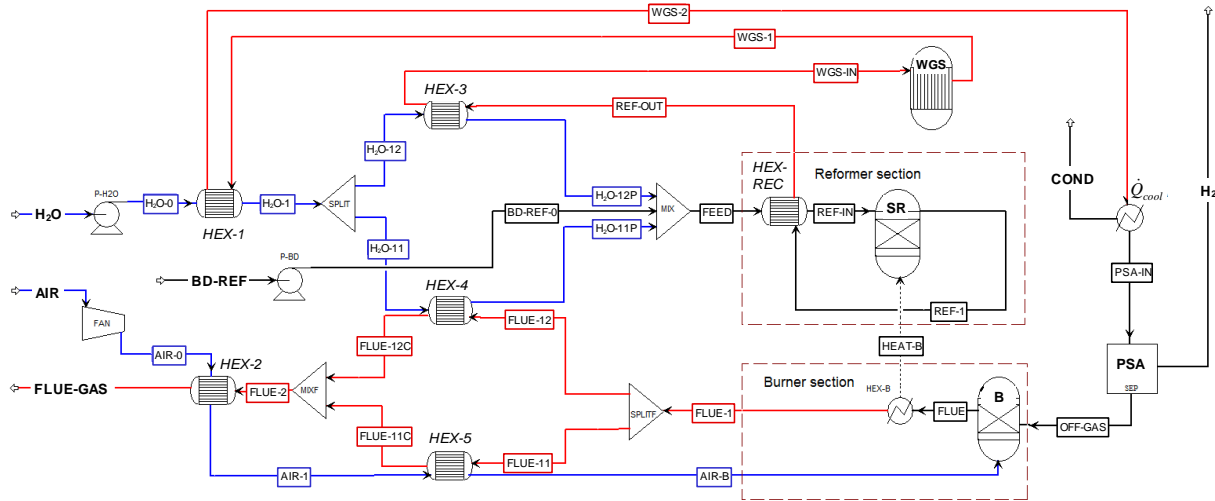

Figure 38 – Heat integrated 50 Nm^3/h hydrogen generation system based on SR of biodiesel

18.79 kg/h of biodiesel are consumed in order to generate 50 Nm^3/h (4.436 kg/h) of hydrogen. The system is operated at S/C 2.53 thus eliminating the need of feeding additional biodiesel to the burner. The endothermic heat demand for the steam reformer (47.6 kW) is provided by the burner, making use of the PSA off-gas. By splitting up the flue-gas stream "FLUE-1", the incoming air stream "AIR-1" is preheated to 570 °C ("AIR-B") before entering the burner. The preheated water "H2O-1" is split up similarly, one stream ("H2O-11") being heated up to 400 °C by making use of the "FLUE-12"-stream, the other stream ("H2O-12") being heated up to 400 °C by transferring waste heat from the "REF-OUT"-stream. Preheating of water ("H2O" to "H2O-1") is achieved by cooling down stream "WGS-1" to dew point temperature ("WGS-2"). Preheating of air ("AIR-0" to "AIR-1") is realized by making use of the remaining enthalpy of the flue-gas ("FLUE-2").

The system produces 5,391 l/h of hydrogen at 10 bar delivery pressure (corresponding to 50 Nm^3/h H$_2$ at standard conditions). The feed and product stream characteristics as well as the heat exchanger properties of the proposed fuel processor concept are depicted in Tabs. 7 and 8. In line with the energy targets derived from the composite curves (see Fig. 37), 120.5 kW can be recovered within the system by matching cold and hot streams. An additional electrical power

demand of 5.82 kW is required for cooling down the WGS product gas stream ("WGS-2") from dew point temperature to a PSA inlet temperature of 35 °C (assuming a glycol cooling circuit as used in the EU-project NEMESIS2[+] [2015]).

In conclusion, the minimum temperature approach of the heat integrated system is slightly lower than targeted (18.8 °C versus 46.6 °C) resulting in a near-optimal HEX network with a thermal system efficiency (as defined by Eq. (29)) of 75.6 %. Please note that the electrical power demand P_{el} is not included in the efficiency calculation. (When considering P_{el} as energy expenditure, the efficiency would decrease by approximately 2 %, see Fig. A4).

Table 7 – Feed and product stream characteristics of heat integrated fuel processor system						
	H2O	BD-REF	AIR	FLUE-OUT	COND	H2
$\dot{m}$ (kg/h)	54.9	18.8	335.4	384.0	20.6	4.436
$\dot{V}$ (l/h)	55.0	21.6	282,130	365,994	21.8	5,391
T (°C)	20	20	20	65.3	20	20

Table 8 – Heat exchanger properties ($\dot{Q}$: transferred heat; A : heat exchanger area; ΔT_{min} : minimum temperature approach), additional electrical power demand P_{el} : 5.82 kW						
	HEX-1	HEX-2	HEX-3	HEX-4	HEX-5	HEX-REC
$\dot{Q}$ (kW)	13.24	16.06	8.65	26.51	37.66	18.36
A (m²)	0.90	123.9	0.85	11.2	126.5	1.71
ΔT_{min} (°C)	112.0	20.5	74.9	18.8	20.5	175.0

4.3.3 Conclusions

The simulation study serves to evaluate a 50 Nm³/h hydrogen generation system based on steam reforming of biodiesel. Results show that it is vital in terms of improving system efficiency to apply a high system pressure and an optimum S/C ratio. The positive effect of pressure predominantly arises from an increased PSA efficiency at high pressures, which outweighs the adverse effect of equilibrium thermodynamics (lower syngas yield at higher pressure). The upper limit of the system pressure is hardware-dependent whereas the lower limit of the S/C ratio is

determined by the so-called thermo-neutral point. At this point, the heat for the steam reforming unit can be provided exclusively by burning the off-gas from the PSA, thus eliminating the need of a dual fuel burner. Further lowering the S/C ratio is not advisable since a PSA off-gas surplus starts to emerge, resulting in a decrease of the net system efficiency. Moreover, a low S/C ratio increases the risk of coke formation on the catalyst surface. Regarding practical applications, a trade-off between high catalyst durability and a sufficiently high system efficiency must be found.

Upon process optimization, proper heat integration of the system has been carried out resulting in a near-optimal heat exchanger network with a thermal system efficiency of 73.4 % (based on LHV, including power consumption). Compared to the results of Katikaneni et al. [2014] and Hulteberg et al. [2008], who reported system efficiencies of 65.2 % (58 %, respectively), significant improvement potential could be derived.

An additional techno-economic analysis of the proposed heat integrated fuel processor system has been carried out (not within the scope of this doctoral thesis) revealing a major impact of biodiesel price on hydrogen net production costs. 8.46 €/kg H_2 were calculated. By varying biodiesel prices, hydrogen production costs are considerably affected and amount to 5.77 €/kg and 11.15 €/kg for 40 % lower and higher market prices, respectively.
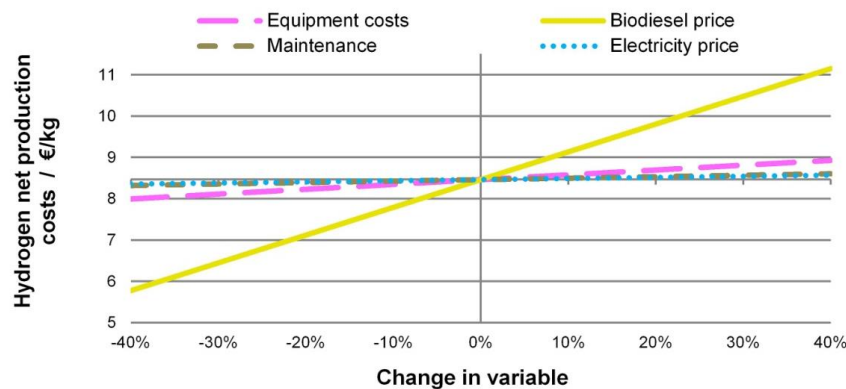

Figure 39 – Net hydrogen production costs of heat integrated fuel processor system (see Fig. 38) based on steam reforming of biodiesel (reference point: 8.46 €/kg, calculated for the 25th fuel processor unit based on learning curves [Martin 2016][3])

---

[3] responsible author of techno-economic evaluation: Friedemann G. Albrecht

5.   Comprehensive Discussion

Steam reforming of diesel and biodiesel involves hundreds of heterogeneously catalyzed chemical reactions, some of which can lead to coke deposition on the catalyst surface resulting in severe catalyst deactivation. From the experimental results of the current thesis it can be concluded that catalyst coking is the main reason for deactivation followed by sulphur poisoning and sintering.

5.1   Coke formation and deactivation

In chapter 4.1.1 results of coke deposition during SR of biodiesel using a ceramic catalyst substrate were shown (Figs. 12-14). Coke measurement was achieved by pulverizing the catalyst piece after the test and subsequently analyzing the deposited coke with an elemental analyzer. A decline of coke formation was observed with increasing temperature whereas the effect of S/C ratio in the considered range $(3-5)$ was found to be marginal. Concurrently, Wu et al. [2010], Frusteri et al. [2015] and Maximini et al. [2012] report a negative correlation between coke deposition and reforming temperature for SR of liquid fuels. The importance of temperature is further underlined by the results of Trabold et al. [2012] revealing that the temperature has by far the largest impact on carbon deposition during diesel reforming.

In particular, the experimental results of the current thesis indicate that catalyst deactivation is initiated at the catalyst front end, as shown by the axial temperature profile. After the start of the reforming reaction, the temperature at the front end drops due to the required heat demand. A stable temperature shows stable catalyst activity whereas a temperature rise indicates a gradual loss of catalyst activity due to a reduction of available active sites. As exemplarily shown in Fig. 40 the temperature minimum at the beginning is located at the front end, subsequently moving downstream in axial direction with increased test duration. Moreover, the temperature minimum levels increase in the order $TA < TB < TC$ which can be attributed to a constant heat input in flow direction from the electrical oven. The absolute level of the temperature minimum primarily results from the heat demand for the endothermic reaction and the radial heat transfer.
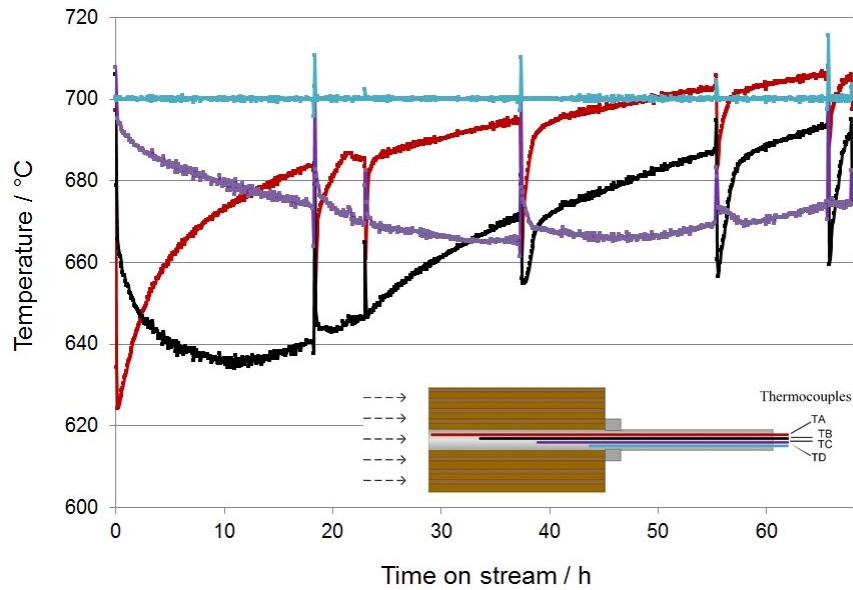
Figure 40 – SR of biodiesel, axial catalyst temperatures over time on stream, operating conditions: T_{Ref}=700 °C, S/C=5, p=3 bar, ceramic catalyst substrate

In order to further evaluate the relationship between coke deposition and progressive catalyst deactivation, a spent catalyst at similar operating conditions has been cut horizontally through the center line and analyzed via energy dispersive X-ray spectroscopy (EDX). As depicted in Fig. 41 the highest carbon concentration is measured at the catalyst front end. This coincides with an increase of temperature TA (located approximately at the position of measuring point A) soon after the start of the reaction (see Fig. 42, right side) indicating the initiation of catalyst deactivation.

EDX-Analysis	A	B	C	D
Ma. % C	36.4	6.7	3.8	3.7
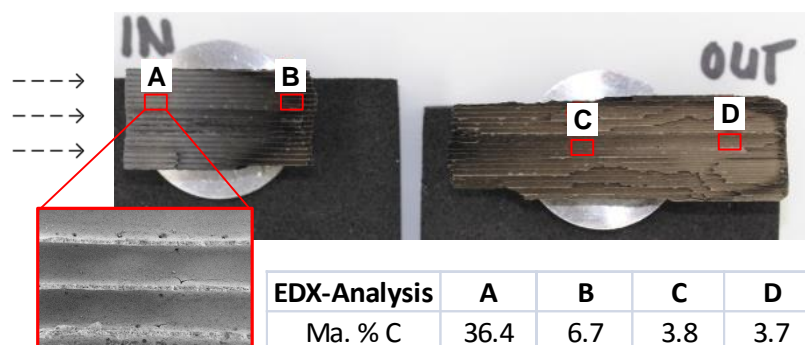
Figure 41 – Top view on catalyst surface (longitudinal cut) after test with diesel, T_{Ref}=700 °C, S/C=4, p=5 bar, test duration: 5 hours, (note: original catalyst piece was broken into two pieces for analysis purposes)
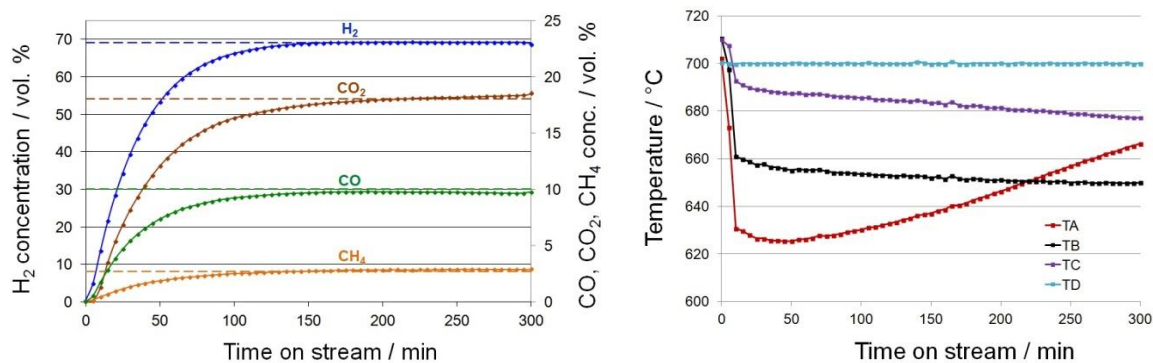
Figure 42 – Dry product gas composition (left side) and axial catalyst temperatures (right side), dashed lines: equilibrium product gas composition, test conditions: T_{Ref}=700 °C, S/C=4, p=5 bar, test duration: 5 hours, feed: diesel

Although coke deposition on the catalyst surface was observed (Fig. 41), the product gas composition approaches thermodynamic equilibrium (Fig. 42, left side). This can be attributed to the fact that after the given test period of 5 hours the number of active sites is still sufficient to ensure full conversion of diesel. However, at longer test durations a deterioration of the product gas composition (decrease of H_2, increase of CH_4, formation of light hydrocarbons) would be inevitable as the number of accessible active sites would be gradually reduced.

Summarizing the above it can be concluded that catalyst deactivation is closely related to carbon deposition. In particular, deactivation by coking is initiated at the catalyst front end, subsequently progressing in axial direction with increasing test duration.

It is widely agreed that carbon formation cannot be accurately predicted by thermodynamic equilibrium equations alone, especially at high S/C ratios [Lin 2014]. It is therefore assumed that the net coke formation rate is determined by a kinetic competition between coke deposition and coke elimination reactions [Bartholomew 1982, Christensen 1996, Wu 2010]. Based on this hypothesis, it is appropriate to maximize the rate of coke gasification reactions (which are known to be the slowest reactions of the entire chemical reaction system) in order to avoid initiation of coking, i.e. by increasing the temperature and/or increasing the partial pressure of H_2O [LeValley 2014, Trane 2012, Frusteri 2015]. A similar hypothesis has been derived within the current thesis revealing the importance of high reforming temperatures in order to avoid coke formation. In order to further test the carbon deposition – carbon elimination hypothesis, additional thermodynamic calculations are presented in the following chapter.

5.2   Thermodynamic considerations

A longevity test using a ceramic based catalyst monolith (chapter 4.1.2, Fig. 16) revealed catalyst deactivation due to coking from the beginning being initiated at the catalyst front end. At the given operating conditions (S/C=5, p=5 bar, T=800 °C) the temperature minimum occurred immediately behind the catalyst entrance. After the start, the temperature measured with thermocouple TA (located 1 mm behind the catalyst front end) drops from 800 °C to 723 °C due to the required endothermic heat demand of the steam reforming reaction. Although it is not possible to locate the exact position of the temperature minimum with the given number of thermocouples, the measured axial temperature profile indicates the approximate position of the temperature minimum.

The maximum possible temperature drop (T_0-T_1) at the catalyst front end (see Fig. 43) can be calculated according to Eq. (34) assuming a) adiabatic conditions, b) a homogeneous radial temperature profile, c) immediate reaction at chemical equilibrium and d) complete biodiesel conversion. It should be noted that the assumption of adiabatic conditions is a worst-case scenario which approximately applies for high feed mass flow rates and poor radial heat transfer.

$$\Delta \dot{H}_R(T_1) = -\dot{m} \cdot \int_{T_0}^{T_1} c_p \cdot dT \tag{34}$$

$\Delta \dot{H}_R$: heat of reaction (W), $\dot{m}$: feed mass flow (kg/s), c_p: constant pressure heat capacity (J kg^{-1} K^{-1}), T_0: gas inlet temperature (°C), T_1: adiabatic product gas temperature (°C)
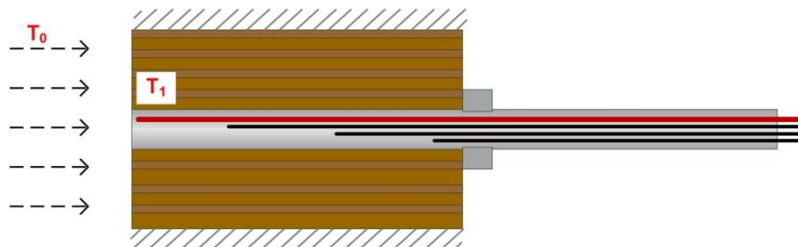

Figure 43 – Cross section of catalyst (visualization of adiabatic temperature drop from T_0 to T_1)

As can be seen from Fig. 44 the calculated adiabatic temperature drop raises linearly with increasing gas inlet temperature T_0 due to an increased endothermic heat demand for the overall steam reforming reaction. At T=800 °C a maximum temperature drop of 228 °C is obtained.

Gas inlet temperature T_0 / °C
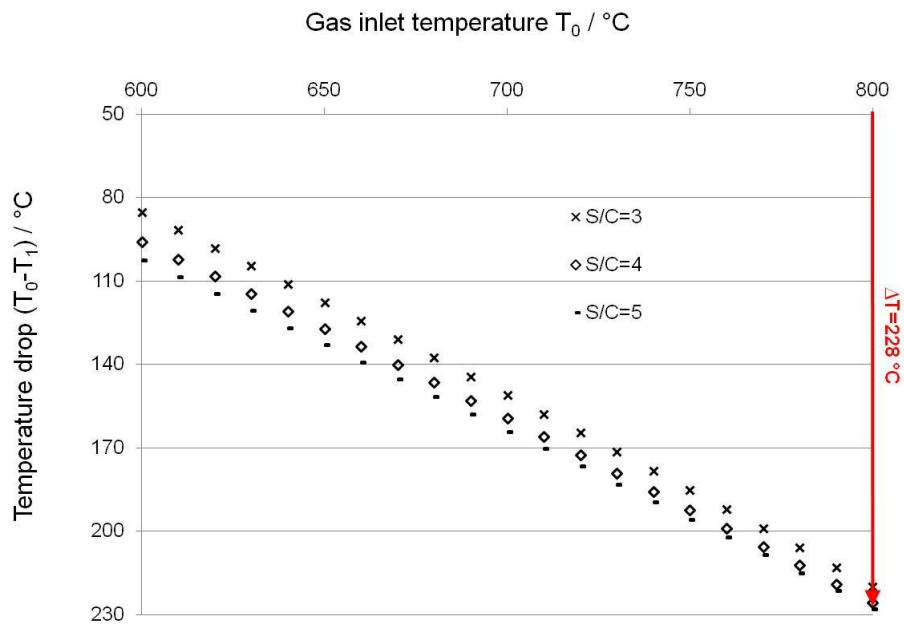
Figure 44 – Adiabatic temperature drop (T_0 - T_1) as a function of catalyst inlet temperature T_0, p=5 bar
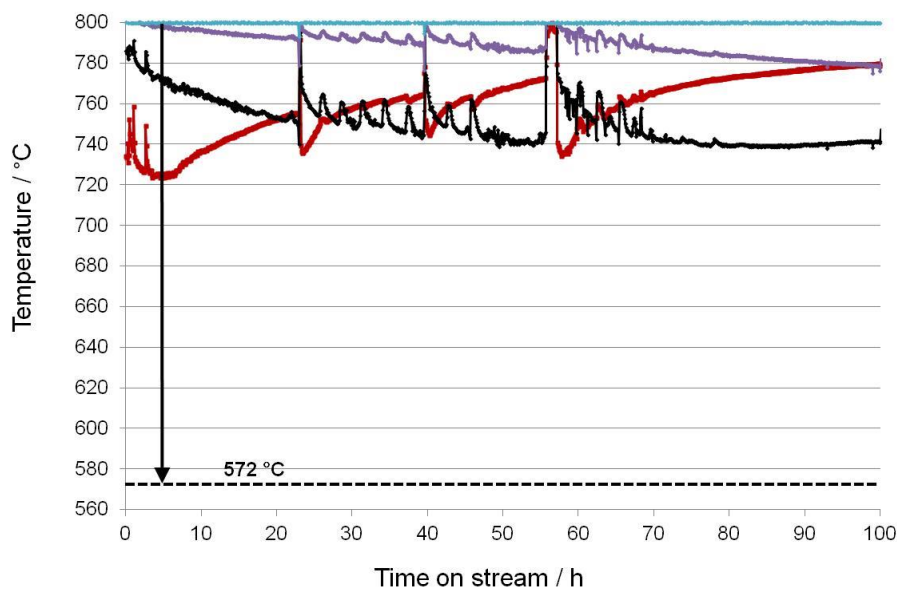
Figure 45 – Maximum theoretical temperature drop at boundary conditions of longevity test (S/C=5, p=5 bar, T=800 °C)

When applied to the longevity test at S/C=5, p=5 bar and T=800 °C (Fig. 16, right side) this means that a theoretical temperature minimum of 572 °C would be obtained (Fig. 45). Even at this hypothetical temperature (which can be considered as a worst-case assumption for coke deposition) no coke formation is expected under thermodynamic equilibrium conditions. In fact, coke formation at the given boundary conditions at chemical equilibrium would require

temperatures $< 50\,°C$ (calculated with Aspen Plus) which is significantly lower than the above derived theoretical minimum temperature of $572\,°C$ at the catalyst front end.

Thus, it can be concluded that the absence of coke at thermodynamic equilibrium is a necessary but not sufficient requirement in order to ensure coke-free operation. Coke formation may still occur under real operating conditions if the coke forming reactions are inherently faster than the gasification reactions. Taking into account that the gasification reactions with H_2O and CO_2 are the slowest reactions of the governing reaction system [Higman 2003], it is decisive to ensure high reforming temperatures in order to accelerate the rate of the gasification reactions. This is particularly important at the catalyst front end where coking is initiated. Concurrently, Trimm [1999] hypothesizes that the key to minimization of coke formation is to accelerate coke gasification reactions.

In the present work, stable long-term operation of biodiesel and diesel steam reforming was finally achieved by using a metallic catalyst monolith instead of a ceramic based monolith. Due to the improved heat transfer of the metallic monolith, the catalyst front end temperature could be raised above $800\,°C$ thus accelerating gasification reactions resulting in a mitigation of coke formation and a stable performance over 100 hours of on-stream exposure (Figs. 18, 19, 28). Concurrently, Kauppi et al. [2010] report a minimum of coke formation at $800\,°C$ for autothermal reforming of diesel model substance n-hexadecane which they attribute to an increased rate of reaction between carbon and steam at elevated temperatures.

This supports the previously expressed hypothesis that coke formation under real operating conditions results from a kinetic competition between carbon deposition and carbon elimination reactions, the actual rate of which strongly depends on the operating conditions and the type of catalyst used. With regard to practical applications a suitable temperature window must be determined which guarantees coke-free operation and prevents sulphur poisoning while at the same time avoids catalyst sintering. Both catalyst coking and sulphur poisoning can be effectively reduced by applying a high SR temperature. Especially in the high temperature range minimization of S/C ratio is essential since it is well known that a high partial pressure of steam strongly increases the risk of catalyst sintering (see chapter 2.5). To conclude, a trade-off in temperature must be found between increasing the rate of carbon gasification reactions and minimizing sintering effects.

5.3   Effect of fuel mass flow rate and type of fuel

In addition to the observed temperature effect, results show that the liquid fuel mass flow rate plays a crucial role for initiation of catalyst deactivation. In particular, a detrimental effect of high fuel mass flow rates on catalyst deactivation has been observed for SR of diesel and biodiesel (chapters 4.1.4, 4.2.4.). Furthermore, it has become clear that mass flow and temperature are not independent of each other: The maximum allowable fuel mass flow rate in order to ensure coke-free operation strongly correlates with temperature. High catalyst inlet temperatures allow for higher fuel mass flow rates.

Literature data on the influence of feed mass flow rate on catalyst deactivation is limited. Regarding diesel reforming (model compounds: n-tetradecane, 1-methylnaphtalene, decalin) using a Pt/γ-alumina catalyst Berry et al. [2003] report a production of olefins and aromatics at high space velocities leading to a drop in hydrogen yield and increased coke production. For ATR of diesel and biodiesel using commercially available Rh-containing ceramic based catalysts Lin et al. [2014] report the initiation of carbon formation at GHSV > 48,500 h^{-1} compared to > 44,000 h^{-1} for biodiesel (nitrogen was used to adjust the GHSV during the tests) indicating that biodiesel is even more sensitive to coking at high feed mass flow rates than diesel. Similarly, Maier et al. [2011] found for partial oxidation of iso-octane over a Rh/Al$_2$O$_3$ monolithic catalyst that coking tendency is related to the flow rate. More specifically, their results indicate the existence of an optimum flow rate for coke formation. They observed that the on-set of coke formation occurs at a certain position downstream the catalyst. In particular, the transition point moves upstream with decreasing flow rate. Concurrently, Hartmann et al. [2010] observed carbon deposition at a certain point downstream the catalyst monolith, the exact position of which depends on reactor temperature, catalyst loading and flow rate. According to the authors, initiation of carbon deposition always occurs in the first third of the catalyst and is typical for a fuel rich regime.

Within the present work, the effect of fuel mass flow rate on catalyst deactivation induced by coking has been evaluated for diesel and biodiesel. Additional tests have been carried out with feedstock bioethanol. Fig. 46 summarizes the effects of fuel mass flow rate and catalyst front end temperature (measured with a thermocouple located 1 mm behind the catalyst entrance in flow direction) on catalyst coking. In the upper left area conditions are such that coking is initiated

soon after the start of the reforming reaction (visible from the experiment by a raise of catalyst front end temperature) whereas in the bottom right area no coke deposition, thus no catalyst deactivation, occurs. As can be seen for feedstock bioethanol (orange filled rectangular points) there is an almost linear correlation between fuel mass flow rate at which coking is initiated and catalyst front end temperature. At 600 °C coking is initiated at an ethanol mass flow rate of 2.26 g/h. By increasing the temperature to 700 °C the maximum allowable ethanol mass flow can be raised by approximately factor 10 to 22.9 g/h. By extrapolating the trend line to higher temperature values the threshold fuel mass flow rates of ethanol, biodiesel and diesel at which coking is initiated can be directly compared at a benchmark temperature of 750 °C.

Obviously, there is a significant difference between the considered liquid fuels regarding coking tendency. At the given benchmark temperature of 750 °C the maximum allowable bioethanol mass flow is 33.1 g/h compared to 15 g/h for biodiesel and 7.5 g/h for fossil diesel. This finding is of particular importance regarding the practical operation of a steam reformer unit based on liquid fuels. Taking into account that a high throughput is economically favourable, bioethanol appears to be an interesting option for decentralized hydrogen production by means of SR. It should be noted that the presented values are only valid for the given operating conditions and the particular type of catalyst. However, a general trend is clear indicating that coking tendency increases in the order bioethanol < biodiesel < diesel.
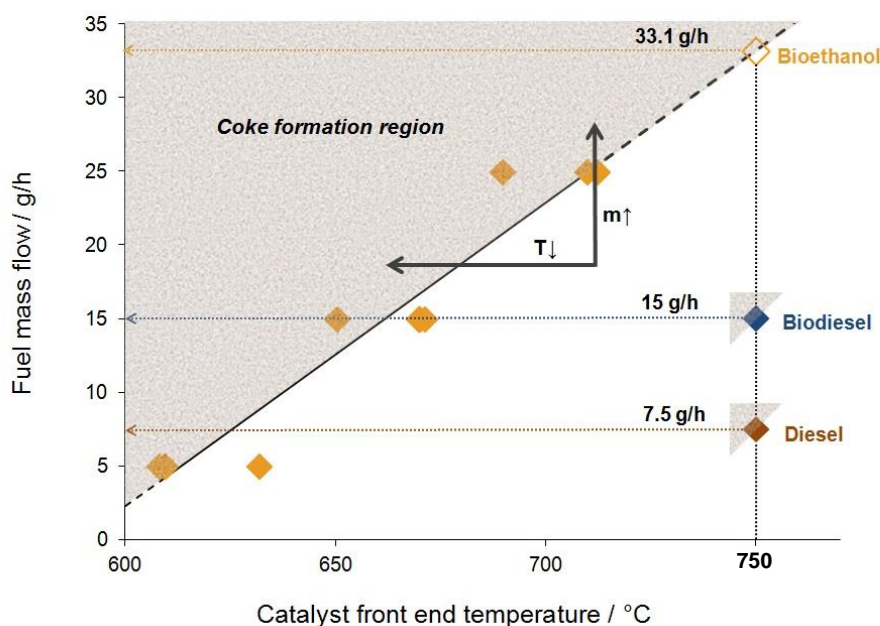

Figure 46 – Effect of fuel mass flow rate and catalyst front end temperature on catalyst deactivation induced by coking (p=5 bar)

Starting from any point in the coke-free region (Fig. 46), coke deposition is initiated if the catalyst front end temperature is decreased and/or the fuel mass flow rate is increased beyond a threshold value. The correlation between fuel mass flow and catalyst front end temperature varies from fuel to fuel. Regarding practical applications it has to be derived individually for each fuel and type of catalyst. In general, high fuel mass flows and low catalyst inlet temperatures favour the initiation of coking at the catalyst front end. With regard to feedstock bioethanol the influence of S/C ratio in the considered range $(3-5)$ on initiation of catalyst deactivation has been found to be insignificant [Schörner 2014]. Two opposing effects must be accounted for: A high S/C ratio (high partial pressure of H_2O) increases the rate of coke gasification reactions while at the same time it increases the GHSV, thus limiting the residence time. Taking into account that reducing the S/C ratio from 5 to 4 slightly affects the partial pressure of H_2O (4.55 bar versus 4.44 bar) and assuming that the coke gasification reaction rate it proportional to $p_{H2O}^{0.63}$ [Mann 2004] a slight decrease of gasification rate of 1.4 % is obtained. At the same time, reducing the S/C ratio from 5 to 4 leads to a reduction of GHSV by 18.2 %. In conclusion, under the given boundary conditions the two effects seem to neutralize each other. As shown by Lin et al. [2014], high values of GHSV caused by high S/C ratios can even outweigh the positive effect of enhanced partial pressures of H_2O resulting in increased coke formation.

In order to further evaluate the effect of fuel mass flow rate on initiation of coke deposition, the role of the flow regime (laminar/turbulent) shall be further considered. Assuming that the catalyst channels can be approximated by equilateral triangles (Fig. 47) the Reynolds number for the benchmark temperature (T=750 °C, see Fig. 46) can be calculated according to Eq. (35).
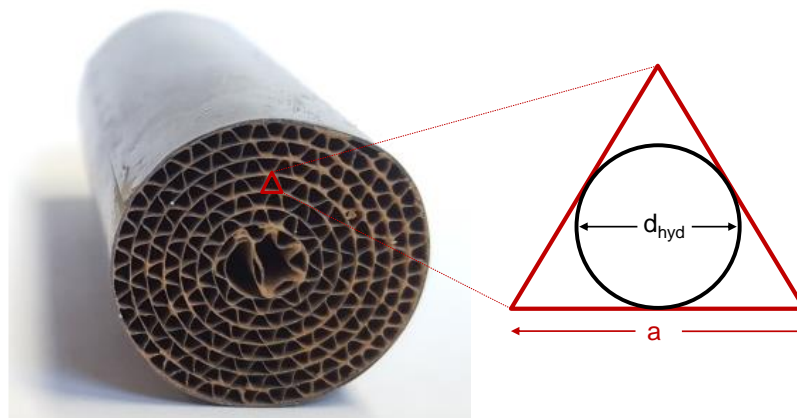

Figure 47 – Channel cross-section represented by equilateral triangle with uniform side length a=1mm, d_{hyd}: hydraulic diameter (=4*A/U)

$$Re = \frac{\bar{v} \cdot d_{hyd}}{\upsilon} = \frac{\bar{v} \cdot 4 \cdot a^2 \cdot \sqrt{3}}{\upsilon \cdot 3a \cdot 4} = \frac{\bar{v} \cdot a}{\upsilon \cdot \sqrt{3}} \tag{35}$$

$\bar{v}$: mean flow velocity (m/s), d_{hyd} : hydraulic diameter (m), υ : kinematic viscosity (m²/s), a : uniform side length of equilateral triangle (m)

Table 9 – Calculation of Reynolds number at benchmark temperature (T=750 °C) for different feeds

	$\dot{m}_{FUEL-REF}$ (g/h)	$\dot{m}_{H_2O}$ (g/h)	$\bar{v}$ (cm/s)	d_{hyd} (mm)	υ (m²/s)	Re
Bioethanol + H₂O	33.1	129.4	14.2	0.58	2.73·10⁻⁵	3.0
Biodiesel + H₂O	15	86.6	8.9	0.58	2.82·10⁻⁵	1.8
B7 Diesel + H₂O	7.5	48.0	4.9	0.58	2.95·10⁻⁵	1.0

From the calculated Reynolds numbers (Tab. 9) it becomes clear that the flow regime in the catalyst channels is laminar. In line, Schädel et al. [2009] and Xu et al. [2013] report laminar flow for reforming of liquid fuels using monolithic catalysts. In the present case, the observed increased coking tendency at higher fuel mass flow rates (see Fig. 46) thus cannot be explained by a transition from laminar to turbulent flow. However, according to the boundary layer theory which was first introduced by Ludwig Prandtl in the year 1904 there is a thin laminar layer in the immediate viscinity of the surface (here: surface of monolithic catalyst channel) where viscous forces are dominant. The boundary layer is characterized by a nonexistent velocity component perpendicular to the bounding surface with a fluid velocity of zero at the surface. According to Mauri [2015] the boundary layer thickness δ at laminar flow conditions decreases proportionally to the inverse of the square root of the Reynolds number:

$$\frac{\delta}{L} \approx \frac{1}{Re^{1/2}} \tag{36}$$

Mass transport from the bulk flow through the boundary layer to the surface occurs solely by diffusion. For practical applications the diffusive mass transport through the outer boundary layer (=film diffusion) is usually obtained from Eq. (37).

$$\dot{m}_{Diff} = \beta \cdot A \cdot (c_\infty - c_0) \tag{37}$$

$\dot{m}_{Diff}$: diffusive mass flow rate; β : film diffusion coefficient; A : outer surface area, c_∞ : concentration in the bulk flow; c_0 : solute concentration on the surface

In particular, the diffusive mass flow through the outer boundary layer depends on the film diffusion coefficient β which in turn correlates to the thickness of the boundary layer δ. According to Eq. (36) δ decreases as Re (and thus fluid velocity) increases. In the context of the previously discussed carbon deposition - carbon elimination kinetic model (chapters 2.2 and 5.1) which states that the coke formation on the catalyst surface results from a kinetic competition between carbon deposition and carbon elimination reactions this raises the question if increased carbon deposition at high fuel mass flow rates can be explained by transport phenomena, in particular by a mass transport limitation through the outer boundary layer. Assuming that the film diffusion is the rate limiting step in the considered high temperature range which is also indicated by the work of Hartmann et al. [2010] the following hypothesis can be derived: At higher fuel mass flow rates the diffusive mass transport of hydrocarbon molecules through the outer boundary layer with subsequent coke deposition on the catalyst surface is favoured over the coke elimination reaction due to a decreased thickness of the boundary layer. This implies that the film diffusion of H_2O with subsequent adsorption and chemical reaction is not the rate limiting step. This assumption appears to be justified since a) the analysis starts from a point where coking does not occur, thus the gasification of intermediary formed carbon is obviously sufficiently fast for a given constant temperature and b) the diffusive mass transport of H_2O through the boundary layer is (according to Eq. (37)) substantially faster due a considerably higher concentration difference $(c_\infty - c_0)$ (in case of biodiesel at S/C=5 and p=5 bar the partial pressure of steam in the bulk flow is 4.95 bar compared to 0.05 bar for biodiesel). Thus, it is assumed that the film diffusion limitation is in particular relevant for the mass transport of fuel molecules through the boundary layer to the catalyst surface subsequently affecting coke deposition on the catalyst surface.

It can be concluded that at a given catalyst front end temperature the coking tendency is mainly influenced by the fuel mass flow rate and is only marginally affected by the S/C ratio (in the considered range of S/C=3 − 5). It should be noted however that the effects of temperature and fuel mass flow rate cannot be strictly separated. Increasing the fuel mass flow rate also affects the level and axial position of the temperature minimum. In fact, both effects point into the same direction: Increasing the fuel mass flow rate results in a lower temperature minimum level, thus a lower coke gasification rate. At the same time it enhances the diffusive fuel mass flow through the outer boundary layer, thus favouring the subsequent heterogeneous coke deposition reaction.

5.4   Thermal hydrogen efficiency

As discussed in the previous chapter, a high fuel mass flow rate has a detrimental effect on catalyst deactivation induced by coke deposition. However, the threshold fuel mass flow rate appears to be inadequate for evaluating different fuels since it does not include information about the energy content nor on the hydrogen yield. Therefore the fuels investigated within this study shall be further assessed in terms of hydrogen yield and thermal hydrogen efficiency.
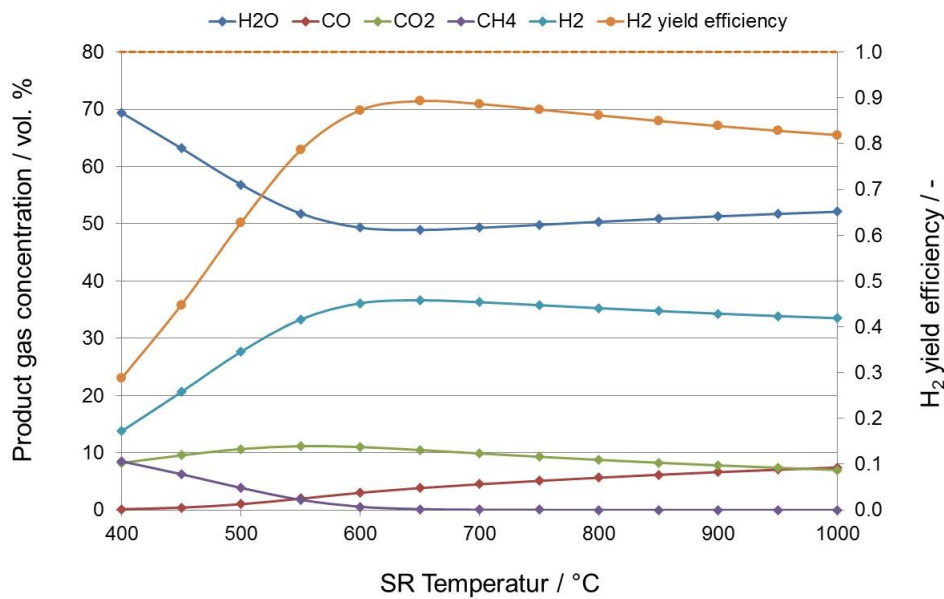

Figure 48 – Equilibrium gas composition after reformer (biodiesel SR, S/C=5, p=1 bar)
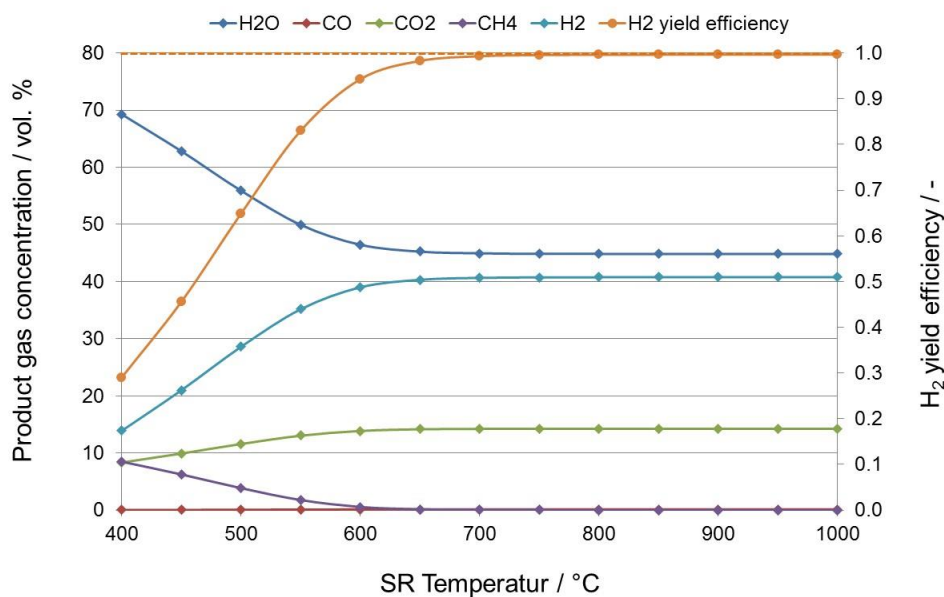

Figure 49 – Equilibrium gas composition after reformer + WGS (biodiesel SR, S/C=5, p=1 bar, T_{WGS}=250 °C)

The equilibrium product gas composition of biodiesel SR is shown exemplarily in Figs. 48 and 49 for S/C=5 and p=1bar (see Figs. A5 and A6 for product gas composition of diesel and bioethanol). At a given S/C ratio the H_2 concentration raises with temperature up to a point where CH_4 vanishes and the H_2 concentration reaches a maximum.

For comparison reasons the H_2 concentration is insufficient since it strongly depends on the operating conditions and the dilution with other gases. Instead the H_2 yield, defined as the generated amount of hydrogen divided by the required amount of fuel, should be used. The maximum H_2 yield for diesel, biodiesel (model substance methyl-oleate) and bioethanol is given by Eqs. (11), (38) and (39). As graphically shown in Fig. 50 the generated hydrogen predominantly originates from the water feed stream. In case of bioethanol the hydrogen equally originates from the water and the fuel stream.
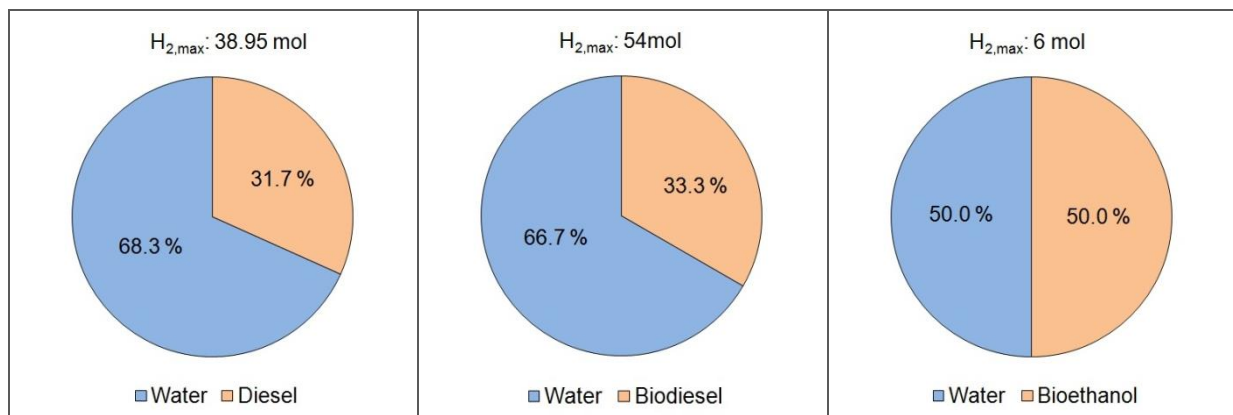
$$\text{max. } H_2 \text{ yield methyl-oleate: } C_{19}H_{36}O_2 + 36\,H_2O \rightarrow 19\,CO_2 + 54\,H_2 \tag{38}$$

$$\text{max. } H_2 \text{ yield bioethanol: } \quad C_2H_6O + 3\,H_2O \rightarrow 2\,CO_2 + 6\,H_2 \tag{39}$$
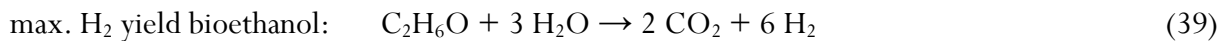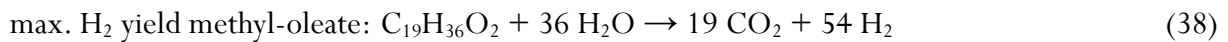
Figure 50 – SR of diesel, biodiesel and bioethanol: H_2 origin (as percentage) from water and fuel feed stream assuming full conversion of fuel into CO_2 and H_2

Accordingly, a minimum S/C ratio can be determined in order to fully convert the liquid fuels into CO_2 and H_2. The values obtained are 1.89 for biodiesel, 2 for diesel and 1.5 for bioethanol. Under real conditions the maximum hydrogen yield can be reached by ensuring a high SR temperature and a high S/C ratio (thus avoiding the formation of methane) and by using a separate downstream WGS unit in the low temperature range, thereby converting the remaining CO into CO_2. In the present case, the H_2 yield efficiency (percentage of the maximum yield) approaches 100 % if the reformer temperature exceeds 700 °C (Fig. 49).

Figure 51 – Thermal hydrogen yield of different liquid fuels at S/C=5, p=1 bar for a system consisting of reformer + WGS (dashed lines: maximum thermal H$_2$ yield)

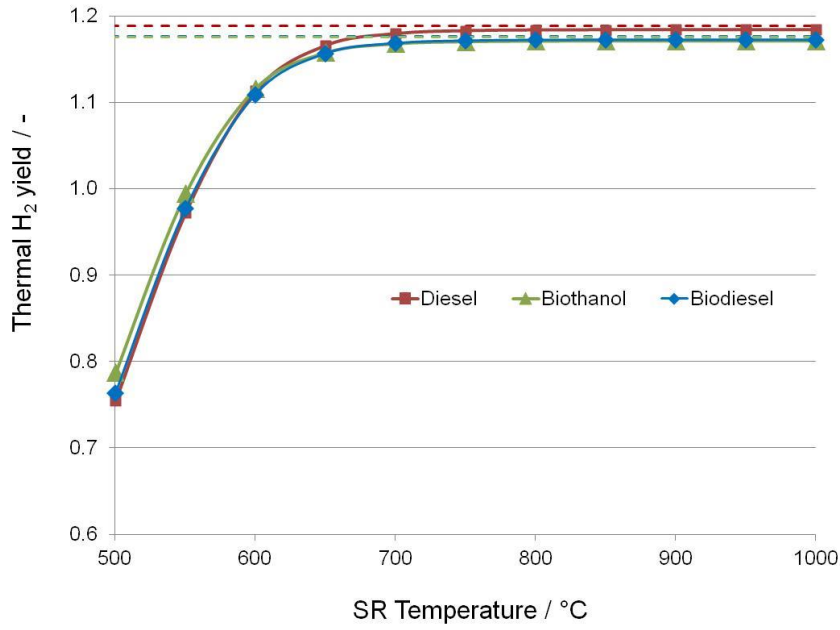When comparing the thermal H$_2$ yield (as defined by Eq. (40)) of diesel, bioethanol and biodiesel, it can be seen that the considered fuels behave similarly (Fig. 51). The thermal H$_2$ yield increases with temperature and reaches a plateau at 700 °C. The slight deviations from the maximum obtainable thermal H$_2$ yield arise from the fact that CO is not completely eliminated during the WGS stage owing to the thermodynamic equilibrium of the reaction.

$$\eta'_{H_2} = \frac{\dot{m}_{H_2} \cdot LHV_{H_2}}{\dot{m}_{FUEL-REF} \cdot LHV_{FUEL-REF}} \tag{40}$$

The thermal H$_2$ yield is a suitable evaluation parameter when waste heat at high temperature is freely available (thus must not be accounted for as energy expenditure). In this particular case, an upgrade of the liquid fuel can be achieved by transforming the thermal energy of the waste heat stream into chemical energy of the reformate gas stream. However, in the majority of the industrial applications high temperature waste heat is not freely available. Hence, an additional burner is required in order to supply the necessary heat for the endothermic SR reaction. Taking into account the additional fuel demand for the burner the thermal net H$_2$ efficiency becomes:

$$\eta'_{H_2,net} = \frac{\dot{m}_{H_2} \cdot LHV_{H_2}}{(\dot{m}_{FUEL-REF} + \dot{m}_{FUEL-B}) \cdot LHV_{FUEL}} \tag{41}$$

	maximum H$_2$ yield		LHV	$\eta'_{H_2,max}$	$\eta'_{H_2,net}$
Table 10 – Key parameters of hydrogen production from diesel, biodiesel and bioethanol by means of SR					
	$\dfrac{\dot{n}_{H_2}}{\dot{n}_{FUEL-REF}}$	$\dfrac{\dot{m}_{H_2}}{\dot{m}_{FUEL-REF}}$	MJ / kg	%	%
Diesel	38.95	0.425	42.93	118.8	76.5 [Samsun 2015]
Biodiesel	54	0.367	37.44	117.7	75.6 [Martin 2011], 75.6 (chapt. 4.3)
Bioethanol	6	0.263	26.80	117.5	76.3 [Martin 2011], 73.7 [Benito 2007]

Tab. 10 summarizes the key parameters of the SR hydrogen production process from diesel, biodiesel and bioethanol. Despite major differences in the chemical composition of the individual fuels (see chapter 3.1), the calculated maximum thermal H$_2$ yield is similar, varying in a narrow range of 117.5 % (bioethanol) to 118.8 % (diesel). Even if taking into account the additional fuel demand for the burner, there is no significant difference between the fuels ($\eta'_{H_2,net}$). This leads to an important conclusion: With regard to thermal net H$_2$ efficiency (Eq. (41)) there is no reason to favour one particular fuel over the others, which further underlines the importance of catalyst coking induced by high feed mass flow rates and low catalyst inlet temperatures.

	$\dot{m}_{FUEL-REF}$	$\dot{m}_{FUEL-B}$	$\dot{m}_{FUEL-TOT} \cdot LHV$	$\dot{m}_{H_2} \cdot LHV$	Factor
Table 11 – Comparison of energy content at benchmark conditions (assumption: $\eta'_{H_2,net}$ = const.= 0.76)					
	g/h	g/h	W	W	-
Diesel	7.5	4.23	139.9	106.3	1
Biodiesel	15	8.22	241.5	183.5	1.73
Bioethanol	33.1	18.09	381.1	289.6	2.72

For given threshold fuel mass flow rates (maximum fuel mass flow rate to reformer at the benchmark temperature of T=750 °C in order to ensure coke-free operation, see Fig. 46) the energy content of the total fuel stream ($\dot{m}_{FUEL-TOT} \cdot LHV$) allows for direct comparison of the fuels. Please note that a constant thermal net H$_2$ efficiency of 0.76 is assumed (based on Tab 10). As shown in Tab. 11 the energy content of the total bioethanol (biodiesel) mass flow corresponding to the threshold fuel mass flow rate to the reformer at the benchmark temperature is by factor 2.72 (1.73) higher than for diesel.

In economic terms this renders bioethanol and biodiesel favourable feedstocks for hydrogen production by means of SR since the amount of produced hydrogen per energy equivalent of total fuel is significantly higher compared to diesel.

5.5   Simulation study: Assumptions and limitations

The preceding experimental investigation of biodiesel SR (chapter 4.1) served as a basis to evaluate a 50 Nm³/h hydrogen generation system comprising a steam reformer (SR), a water gas shift stage (WGS), a pressure swing adsorption unit (PSA) and a dual fuel burner (chapter 4.3). The chosen capacity arises due to the current market demand for decentralized hydrogen production plants reported by the National Hydrogen Association [2010] and the U.S. Department of Energy [2015]. Accordingly, the typical size of small hydrogen generation units at fueling stations ranges between 30 Nm³/h and 100 Nm³/h. In line, Katikaneni et al. [2014] present a roadmap for on-site hydrogen generation at commercial scale, starting with a small size hydrogen refueling station of 50 Nm³/h.
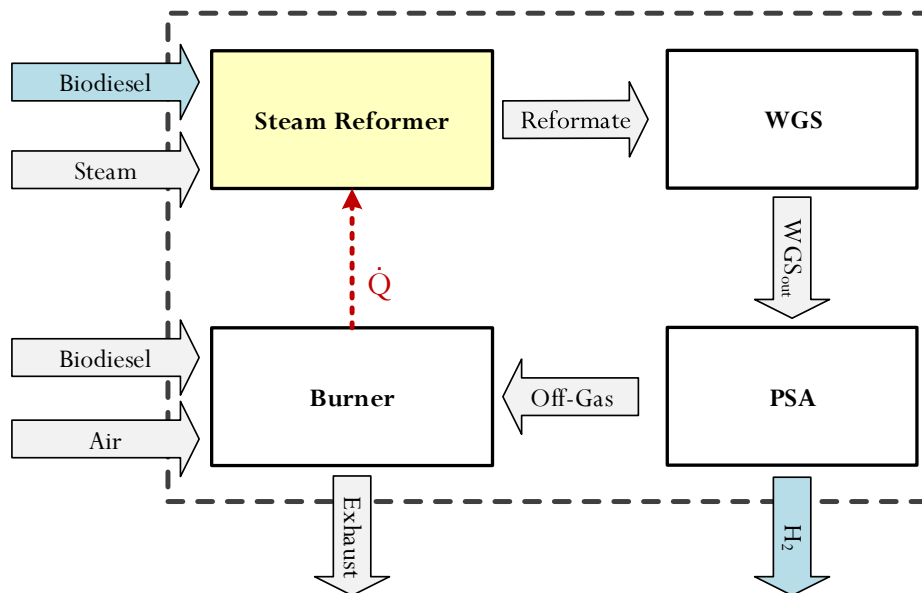
Figure 52 – Components of 50 Nm³/h hydrogen generation system based on biodiesel SR

The Aspen Plus simulation study is based on the assumption that SR, WGS and burner product gas composition are at chemical equilibrium. As for the burner the assumption is well-founded since the burner is operated in the high temperature region (1100 °C) resulting in a high rate of reaction. Regarding the WGS stage literature data shows that for an adiabatically operated

medium temperature WGS at typical space velocities the product gas composition reaches chemical equilibrium [Scheuerecker 2013]. With regard to biodiesel SR the experimental results derived within the present work proved that the reformate gas is at chemical equilibrium (Fig. 16, left side, Fig. 18) providing a sufficient amount of catalyst. Concerning the PSA-efficiency, a linear correlation between the H_2 recovery rate and system pressure was assumed (Fig. A7) the maximum efficiency (78.3 %) of which is in good agreement with literature data [Sircar 2000].

Further boundary conditions of the simulation study as laid down in Tab. 4 (chapter 3.3.2) are mainly based on experimentally derived values of the FCH JU project NEMESIS2$^+$ [2015] based on a modified tubular reforming technology. Thus, it is not possible to apply the current Aspen Plus model of the 50 Nm^3/h hydrogen generation unit to a larger scale without adjusting the underlying boundary conditions. Moreover, variation of operating conditions of the proposed heat integrated system (Fig. 38) is limited due to the fact that the minimum temperature approach of the heat exchangers (in particular HEX-2, HEX-4 and HEX-5, see Tab. 8) is already small, thus increasing the risk of temperature crossovers. It should be noted however, that the primary goal of the simulation study is to show a theoretical maximum system efficiency based on process optimization. Clearly, stream splitting and recombination poses certain challenges regarding practical operation of the heat integrated system. The technical feasibility of the proposed system remains to be shown.

6. Summary

Within the present work steam reforming (SR) of biodiesel, diesel and bioethanol has been investigated experimentally and on process level targeting stable process conditions and a high system efficiency. The experimental investigations aim at a better understanding of catalyst deactivation at varying operating conditions. In particular, the initiation of coke deposition on the catalyst surface has been evaluated in detail using a laboratory test rig. As a result, macroscopic properties were derived allowing to assess carbon formation. The experimental work was complemented by a simulation study using Aspen Plus, the main emphasis of which was placed on maximizing system efficiency through process optimization. Based on the results of process optimization, a novel heat-integrated fuel processor concept based on biodiesel SR is proposed which possesses significant improvement potential as compared to existing on-site hydrogen generation plants.

In agreement with literature data, the experimental investigations revealed that catalyst deactivation is closely related to carbon deposition on the catalyst surface leading to a gradual blockage of the active sites. More specifically, increased coke formation was observed with decreasing temperature whereas the effect of S/C ratio in the given range ($3-5$) was marginal. By placing several thermocouples along the center line of the catalyst piece, the position of the axial temperature profile could be tracked over time on stream, thereby providing valuable information on the deactivation front.

Axial temperature profiles reveal that coke deposition on the catalyst surface is induced at the catalyst front end, subsequently moving downstream in axial direction up to a point where the catalyst is completely deactivated. In this way, it is possible to detect catalyst deactivation long before a deterioration of the product gas composition (caused by a limitation of the active catalyst sites) appears.

Moreover, the present work shows that carbon formation at elevated S/C ratios and low reforming temperatures cannot be predicted by thermodynamic equilibrium calculations. In fact,

coke deposition being induced at the catalyst front end results from a kinetic competition between coke deposition and coke elimination reactions. Results support the hypothesis that the heterogeneous gas solid reactions (in particular the reaction of coke with H_2O and CO_2) are the rate limiting step. Thus, in order to avoid initiation of catalyst coking it is decisive to accelerate the gasification reactions by ensuring a high temperature level at the catalyst inlet.

In addition to the observed temperature effect, the experiments reveal a detrimental effect of high fuel mass flow rates on catalyst deactivation induced by coking. Most importantly, the two effects are not independent of each other: The maximum allowable fuel mass flow rate which guarantees coke-free conditions strongly correlates with temperature. High catalyst inlet temperatures allow for higher fuel mass flow rates.

Significant differences were found between the considered liquid fuels. In particular, coking tendency increases in the order bioethanol < biodiesel < diesel. The detrimental effect of high fuel mass flow rate on catalyst deactivation can be attributed to mass transport phenomena. It is assumed that the diffusive mass transport of fuel molecules through the outer boundary layer with subsequent adsorption is enhanced at higher fuel mass flow rates, thus favouring the coke deposition reactions over the coke gasification reactions.

Catalyst deactivation which is induced by coke deposition at the catalyst front end can be assessed based on the macroscopic properties temperature and fuel mass flow rate. By contrast, the commonly used gas hourly space velocity (GHSV) is considered inadequate for evaluating coking tendency during SR of liquid fuels since the GHSV does not include specific information on the operating conditions at the catalyst front end (where deactivation is initiated).

By ensuring a high catalyst inlet temperature (T > 800 °C) and applying a sufficiently low fuel mass flow rate per open area of catalyst ($\sim$2 g h^{-1} cm^{-2}), stable biodiesel SR (100 hours) has been achieved, which has not yet been shown in the scientific literature. Similarly, stable SR of fossil diesel (100 hours) has been demonstrated, indicating a positive effect of fuel desulphurization on catalyst activity. Slight sintering effects were observed for both biodiesel and diesel which were not detrimental for the catalyst performance in the given time range.

The experimental work has been complemented by a simulation study, the aim of which was to evaluate a 50 Nm^3/h hydrogen generation system based on biodiesel SR. Results show a positive effect of pressure on thermal system efficiency being mainly attributed to an improved PSA-efficiency. Furthermore, calculations with Aspen Plus revealed an S/C optimum of 2.78 at the given operating conditions. At this point, the required heat for the steam reforming unit can be provided solely by using the PSA off-gas, thereby eliminating the need for a dual fuel burner. Based on process optimization a near-optimum heat exchanger network has been derived. The proposed hydrogen generation system consumes 21.6 l/h biodiesel and 55.0 l/h water in order to generate 50 Nm^3/h H$_2$, corresponding to a thermal system efficiency of 75.6 %.

Outlook

Further work should be dedicated to quantify the correlation of threshold temperature and feed mass flow rate (in order to guarantee coke-free operation) for different operating conditions and different types of catalyst, targeting a dimensionless parameter which allows the prediction of catalyst deactivation induced by coking more precisely. Regarding system simulation, the derived near-optimum hydrogen generation system based on biodiesel SR should be evaluated in more detail including an assessment of system behaviour at varying operating conditions, functional design of subcomponents and appropriate measures for system control.

Summarizing, the results of the current thesis show that hydrogen generation via SR of liquid fuels is technically feasible. The widespread deployment of on-site hydrogen generators based on logistic fuels such as biodiesel, diesel and bioethanol within the upcoming years could greatly accelerate the market introduction of fuel cell electric vehicles, thereby paving the way to a future hydrogen economy.

Bibliography

Abatzoglou N, Fauteux-Lefebvre C, Braidy N, Biodiesel reforming with a $NiAl_2O_4/Al_2O_3$-YSZ catalyst for the production of renewable SOFC fuel, WIT Transactions on Ecology and the Environment 143, (2011), 145–155

Achouri I E, Abatzoglou N, Fauteux-Lefebvre C, Braidy N, Diesel steam reforming: Comparison of two nickel aluminate catalysts prepared by wet-impregnation and co-precipitation, Catalysis Today 207, (2013), 13–20

Ahmed S, Krumpelt M, Hydrogen from hydrocarbon fuels for fuel cells, International Journal of Hydrogen Energy 26, (2001), 291–301

Alvarez-Galvan M C, Navarro R M, Rosa F, Briceño Y, Gordillo Alvarez F, Fierro J L G, Performance of La,Ce-modified alumina-supported Pt and Ni catalysts for the oxidative reforming of diesel hydrocarbons, International Journal of Hydrogen Energy 33, (2008), 652–663

Argyle M D, Bartholomew C H, Heterogeneous Catalyst Deactivation and Regeneration: A Review, Catalysts 5, (2015), 145–269

Aspen Technology Inc., Aspen Energy Analyzer, Reference Guide, V7.1, 2009

Aspen Technology Inc., Aspen Physical Property System, Physical Property Methods, version V7.2, 2010

Audesirk T, Audesirk G, Biology, Life on Earth, 5th Ed., Prentice-Hall, 1999

Bartholomew C H, Carbon Deposition in Steam Reforming and Methanation, Catalysis Reviews, 24:1, (1982), 67–112

Bartholomew C H, Farrauto R J, Fundamentals of industrial catalytic processes, Second edition Wiley, 2006

Benito M, Padilla R, Sanz J L, Daza L, Thermodynamic analysis and performance of a 1 kW bioethanol processor for a PEMFC operation, Journal of Power Sources 169, (2007), 123–130

Berry D A, Shekhawat D, Gardner T H, Development of Reaction Kinetics for Diesel-Based Fuel Cell Reformers, American Institute of Chemical Engineers, Hydrogen, Fuel Cells and Infrastructure Technologies, FY Progress Report, 2003

Blasi A, Fiorenza G, Freda C, Steam reforming of biofuels for the production of hydrogen-rich gas, Woodhead Publishing Limited, (2014), 145–181

Bolat P, Thiel C, Hydrogen supply chain architecture for bottom-up energy systems models. Part 2: Techno-economic inputs for hydrogen production pathways, International Journal of Hydrogen Energy 39, (2014), 8898–8925

Boon J, van Dijk E, de Munck S, van den Brink R, Steam reforming of commercial ultra-low sulphur diesel, Journal of Power Sources 196, (2011), 5928–5935

Brown L F, A comparative study of fuels for on-board hydrogen production for fuel-cell-powered automobiles, International Journal of Hydrogen Energy 26, (2001), 381–397

Carmo M, Fritz D L, Mergel J, Stolten D, A comprehensive review on PEM water electrolysis, International Journal of Hydrogen Energy 38, (2013), 4901–4934

Chaubey R, Sahu S, James O O, Maity S, A review on development of industrial processes and emerging techniques for production of hydrogen from renewable and sustainable sources, Renewable and Sustainable Energy Reviews 23, (2013), 443–462

Christensen T S, Adiabatic prereforming of hydrocarbons – an important step in syngas production, Applied Catalysis A: General 138, (1996), 285–309

Colucci J A, Hydrogen production using autothermal reforming of biodiesel and other hydrocarbons for fuel cell applications, ASME International Solar Energy Conference, (2006), 483–484

Contreras J L, Fuentes G A, Sintering of Supported Metal Catalysts, in: Sintering – Methods and Products, edited by Volodymyr Shatokha, InTech, 2012

Davies H S, Humphries K J, Hebden D, Percy D A, Applications and development of the catalytic rich gas process, Inst. Gas Eng. J. 7, (1967), 707–719

Depeyre D, Flicoteaux C, Chardaire C, Pure n-Hexadecane Thermal Steam Cracking, Industrial & Engineering Chemistry Process Design and Development 24, (1985), 1251–1258

Dincer I, Acar C, Review and evaluation of hydrogen production methods for better sustainability, International Journal of Hydrogen Energy 40, (2015), 11094–11111

Diop D, Blanco M, Flammini A, Schlaifer M, Kropiwnicka M A, Mautner-Markhof M, Assessing the impact of biofuels production on developing countries from the point of view of Policy Coherence for Development, The European Union's Framework Contract Commission 2011, Final Report, 2013

Dutta S, A review on production, storage of hydrogen and its utilization as an energy resource, Journal of Industrial and Engineering Chemistry 20, (2014), 1148–1156

Engelhardt P, Maximini M, Beckmann F, Brenner M, Integrated fuel cell APU based on a compact steam reformer for diesel and a PEMFC, International Journal of Hydrogen Energy 37, (2012), 13470–13477

Ersoz A, Olgun H, Ozdogan S, Reforming options for hydrogen production from fossil fuels for PEM fuel cells, Journal of Power Sources 154, (2006), 67–73

Eßmann C, Untersuchung der Verkokung von Rhodiumkatalysatoren während der Wasserdampfreformierung von Erdgas, Dissertation, Fakultät für Chemie und Biowissenschaften, Karlsruher Institut für Technologie (KIT), 2011

Fauteux-Lefebvre C, Abatzoglou N, Blanchard J, Gitzhofer F, Steam reforming of liquid hydrocarbons over a nickel-alumina spinel catalyst, Journal of Power Sources 195, (2010), 3275–3283

Fauteux-Lefebvre C, Abatzoglou N, Braidy N, Achouri I E, Diesel steam reforming with a nickel-alumina spinel catalyst for solid oxide fuel cell application, Journal of Power Sources 196, (2011), 7673–7680

Forzatti P, Lietti L, Catalyst deactivation, Catalysis Today 52, (1999), 165–181

Frusteri F, Bonura G, Hydrogen production by reforming of bio-alcohols, Compendium of Hydrogen Energy, Elsevier, (2015), 109–136

Gautam R, Seider W D, Computation of phase and chemical equilibrium, Part II. Phase-splitting, AIChE Journal 25(6), (1979), 999–1006

Gonzalez A V, Pettersson L J, Full-scale autothermal reforming for transport applications: The effect of diesel fuel quality, Catalysis Today 210, (2013), 19–25

Goud S K, Whittenberger W A, Chattopadhyay S, Abraham M A, Steam reforming of n-hexadecane using a Pd/ZrO_2 catalyst: Kinetics of catalyst deactivation, International Journal of Hydrogen Energy 32, (2007), 2868–2874

Grote M, Maximini M, Yang Z, Engelhardt P, Köhne H, Lucka K, Brenner M, Experimental and computational investigations of a compact steam reformer for fuel oil and diesel fuel, Journal of Power Sources 196, (2011), 9027–9035

Hartmann M, Maier L, Minh H D, Deutschmann O, Catalytic partial oxidation of iso-octane over rhodium catalysts: An experimental, modeling, and simulation study, Combustion and Flame 157, (2010), 1771–1782

Higman C, van der Burgt M, Gasification, Elsevier Science, 2003

Hoguet J C, Karagiannakis G P, Valla J A, Agrafiotis C C, Konstandopoulos A G, Gas and liquid phase fuels desulphurization for hydrogen production via reforming processes, International Journal of Hydrogen Energy 34, (2009), 4953–4962

Holladay J D, Hu J, King D L, Wang Y, An overview of hydrogen production technologies, Catalysis Today 39, (2009), 244–260

Hulteberg P C, Burford H, Duraiswamy K, Porter B, Woods R, A cost effective steam reformer for a distributed hydrogen infrastructure, International Journal of Hydrogen Energy 33, (2008), 1266–1274

Hulteberg C, Sulphur-tolerant catalysts in small-scale hydrogen production, a review, International Journal of Hydrogen Energy 37, (2012), 3978–3992

Kabadi V N, Danner R P, A Modified Soave-Redlich-Kwong Equation of State for Water-Hydrocarbon Phase Equilibria, Industrial & Engineering Chemistry Process Design and Development 24, (1985), 537–541

Kang I, Carstensen H H, Dean A M, Impact of gas-phase reactions in the mixing region upstream of a diesel fuel autothermal reformer, Journal of Power Sources 196, (2011), 2020–2026

Katikaneni S P, Al-Muhaish F, Harale A, Pham T V, On-site hydrogen production from transportation fuels: An overview and techno-economic assessment, International Journal of Hydrogen Energy 39, (2014), 4331–4350

Kauppi E I, Kaila R K, Linnekoski J A, Krause A O I, Niemela M K V, Temperature-programmed oxidation of coked noble metal catalysts after autothermal reforming of n-hexadecane, International Journal of Hydrogen Energy 35, (2010), 7759–7767

Kaynar A D D, Dogu D, Yasyerli N, Hydrogen production and coke minimization through reforming of kerosene over bi-metallic ceria–alumina supported Ru–Ni catalysts, Fuel Processing Technology 140, (2015), 96–103

Kemp I C, Pinch Analysis and Process Integration, Elsevier Ltd (2007), Second Edition

Kırtay E, Recent advances in production of hydrogen from biomass, Energy Conversion and Management 52, (2011), 1778–1789

Kolb G, Hofmann C, O'Connell M, Schürer J, Microstructured reactors for diesel steam reforming, water-gas shift and preferential oxidation in the kiloWatt power range, Catalysis Today 147S, (2009), S176–S184

Koo K Y, Park M G, Jung U H, Kim S H, Yoon W L, Diesel pre-reforming over highly dispersed nano-sized Ni catalysts supported on MgO-Al$_2$O$_3$ mixed oxides, International Journal of Hydrogen Energy 39, (2014), 10941–10950

Kraaij G J, Specchia S, Bollito G, Mutri L, Wails D, Biodiesel fuel processor for APU applications, International Journal of Hydrogen Energy 34, (2009), 4495–4499

Lakhapatri S L, Abraham M A, Deactivation due to sulfur poisoning and carbon deposition on Rh-Ni/Al2O3, catalyst during steam reforming of sulfur-doped n-hexadecane, Applied Catalysis A: General 364, (2009), 113–121

LeValley T L, Richard A R, Fan M, The progress in water gas shift and steam reforming hydrogen production technologies - A Review, International Journal of Hydrogen Energy 39, (2014), 16983–70000

Lide D R (ed.), CRC Handbook of Chemistry and Physics, 85th Edition, CRC Press, Boca Raton, Florida, Section 14, Geophysics, Astronomy, and Acoustics; Abundance of Elements in the Earth's Crust and in the Sea, 2005

Lin J, Trabold T A, Walluk M R, Smith D F, Autothermal Reforming of Biodiesel-Ethanol-Diesel Blends for Solid Oxide Fuel Cell Applications, Energy & Fuels 27(8), (2013), 4371–4385

Lin J, Trabold T A, Walluk M R, Smith D F, Bio-fuel reformation for solid oxide fuel cell applications. Part 1: Fuel vaporization and reactant mixing, International Journal of Hydrogen Energy 38, (2013), 12024–12034

Lin J, Trabold T A, Walluk M R, Smith D F, Bio-fuel reforming for solid oxide fuel cell applications. Part 2: Biodiesel, International Journal of Hydrogen Energy 39, (2014), 183–195

Lindermeir A, Kah S, Kavurucu S, Mühlner M, On-board diesel fuel processing for an SOFC-APU - Technical challenges for catalysis and reactor design, Applied Catalysis B: Environmental 70, (2007), 488–497

Linnhoff B, Lenz W, Wärme-Integration und Prozeßoptimierung, Chemie Ingenieur Technik 59, Nr. 11, (1987), 851–857

Maier L, Hartmann M, Tischer S, Deutschmann O, Interaction of heterogeneous and homogeneous kinetics with mass and heat transfer in catalytic reforming of logistic fuels, Combustion and Flame 158, (2011), 796–808

Mann M D, Knutson R Z, Erjavec J, Jacobsen J P, Modeling reaction kinetics of steam gasification for a transport gasifier, Fuel 83, (2004) 1643–1650

Martin S, Wörner A, On-board reforming of biodiesel and bioethanol for high temperature PEM fuel cells: Comparison of autothermal reforming and steam reforming, Journal of Power Sources 196, (2011), 3163–3171

Martin S, Kraaij G, Ascher T, Wails D, Wörner A: An experimental investigation of biodiesel steam reforming, International Journal of Hydrogen Energy 40, (2015), 95–105

Martin S, Kraaij G, Ascher T, Karagiannakis G, Baltzopoulou P, Wails D, Wörner A: Direct steam reforming of diesel and diesel-biodiesel blends for distributed hydrogen generation, International Journal of Hydrogen Energy 40, (2015), 75–84

Martin S, Albrecht F G, van der Veer P, Lieftink D, Dietrich R U: Evaluation of on-site hydrogen generation via steam reforming of biodiesel: Process optimization and heat integration, International Journal of Hydrogen Energy 41, (2016), 6640–6652

Mauri R, Fluid Mechanics and its Applications, Volume 112, Transport Phenomena in Multiphase Flows, Springer International Publishing Switzerland, 2015

Maximini M, Engelhardt P, Grote M, Brenner M, Further development of a microchannel steam reformer for diesel fuel, International Journal of Hydrogen Energy 37, (2012), 10125–10134

Mieville R L, Coking Characteristics of Reforming Catalysts, Journal of Catalysis 100, (1986), 482–488

Ming Q, Healey T, Allen L, Irving P, Steam reforming of hydrocarbon fuels, Catalysis Today 77, (2002), 51–64

Moseley F, Stephens R W, Stewart K D, Wood J, The poisoning of a steam hydrocarbon gasification catalyst, Journal of Catalysis 24, (1972), 18-39

Moulijn J A, van Diepen A E, Kapteijn F, Catalyst deactivation: Is it predictable? What to do? Applied Catalysis A: General 212, (2001), 3–16

Nahar G A, Hydrogen rich gas production by the autothermal reforming of biodiesel (FAME) for utilization in the solid-oxide fuel cells: A thermodynamic analysis, International Journal of Hydrogen Energy 35, (2010), 8891–8911

Nahar G A, Madhani S S, Thermodynamics of hydrogen production by the steam reforming of butanol: Analysis of inorganic gases and light hydrocarbons, International Journal of Hydrogen Energy 35, (2010), 98–109

Nahar G A, Dupont V, Hydrogen via steam reforming of liquid biofeedstock, Biofuels 3, (2012), 167–191

Nahar G, Dupont V, Twigg M V, Dvininov E, Feasibility of hydrogen production from steam reforming of biodiesel (FAME) feedstock on Ni-supported catalysts, Applied Catalysis B: Environmental, 168-169, (2015), 228–242

National Hydrogen Association, Hydrogen and Fuel Cells: The U.S. Market Report, Washington (2010), http://www.ttcorp.com/pdf/marketReport.pdf (accessed 20/05/2016)

Navarro Yerga R M, Alvarez-Galvan M C, Mota N, Villoria de la Mano J A, Al-Zahrani S M, Fierro J L G, Catalysts for Hydrogen Production from Heavy Hydrocarbons, ChemCatChem 3, (2011), 440–457

NEMESIS2[+] website, http://www.nemesis-project.eu/ (accessed 20/05/2016)

Neumann P, von Linde F, Options for economical supply of hydrogen, MPT International 2, (2003), 72–75

Norinaga K, Deutschmann O, Detailed Kinetic Modeling of Gas-Phase Reactions in the Chemical Vapor Deposition of Carbon from Light Hydrocarbons, Industrial & Engineering Chemistry Research 46, (2007), 3547–3557

Ogden J M, Review of small stationary reformers for hydrogen production, Princeton University Center for Energy and Environmental Studies, Report for the International Energy Agency, Task 16, (2001), 1–49

Parmar R D, Kundu A, Karan K, Thermodynamic analysis of diesel reforming process: Mapping of carbon formation boundary and representative independent reactions, Journal of Power Sources 194, (2009), 1007–1020

Pereira C, Bae J M, Ahmed S, Krumpelt M, Liquid Fuel Reformer Development: Autothermal Reforming of Diesel Fuel, Argonne National Laboratory, Electrochemical Technology Program, 2000

Persson T, Simulation of small-scale hydrogen production, Department of Chemical Engineering Lund University, Master Thesis, 2007

Pfropfe B, Kreyenberg D, Wind J, Schmid S, Market penetration analysis of electric vehicles in the German passenger car market towards 2030, International Journal of Hydrogen Energy 38, (2013), 5201–5208

Piwetz M M, Larsen J S, Christensen T S, Hydrodesulfurization and Prereforming of Logistic Fuels for Use in Fuel Cell Applications, Fuel Cell Seminar Program and Abstracts, 1996

Qi A, Peppley B, Karan K, Integrated fuel processors for fuel cell application: A review, Fuel Processing Technol 88, (2007), 3–22

Rostrup-Nielsen J R, Acitivity of Nickel Catalysts for Steam Reforming of Hydrocarbons, Journal of Catalysis 31, (1973), 173–199

Rostrup-Nielsen J R, Christensen T S, Dybkjaer I, Steam reforming of liquid hydrocarbons, Studies in Surface Science and Catalysis Volume 113, (1998), 81–95

Rostrup-Nielsen J, Steam reforming of hydrocarbons. A historical perspective, Studies in Surface Science and Catalysis 147, (2004), 121–125

Rostrup-Nielsen J, Christiansen L J, Concepts in Syngas Manufacture, Catalytic Science Series, Volume 10, Imperial College Press, 2011

Sahin Z, Experimental and Theoretical Investigation of the Effects of Gasoline Blends on Single-Cylinder Diesel Engine Performance and Exhaust Emissions, Energy & Fuels 22, (2008), 3201–3212

Samsun R C, Pasel J, Peters R, Stolten D, Fuel cell systems with reforming of petroleum-based and synthetic-based diesel and kerosene fuels for APU applications, International Journal of Hydrogen Energy 40, (2015), 6405–6421

Schädel B T, Duisberg M, Deutschmann O, Steam reforming of methane, ethane, propane, butane, and natural gas over a rhodium-based catalyst, Catalysis Today 142, (2009), 42–51

Scheuerecker T, Untersuchung der Grobreinigung von Kohlenmonoxid mit einem Wassergas-Shift-Reaktor im Reformatgas eines mit Biodiesel betriebenen Dampfreformers, Masterarbeit, Hochschule Amberg-Weiden, 2013

Schjølberg I, Hulteberg C, Yasuda I, Nelsson C, Small scale reformers for on-site hydrogen supply, Energy Procedia 29, (2012), 559–566

Schörner M, Experimentelle Untersuchung der Dampfreformierung von Bioethanol, Bachelorarbeit, Hochschule Mannheim, 2015

Sgroi M, Bollito G, Saracco G, Specchia S, BIOFEAT: Biodiesel fuel processor for a vehicle fuel cell auxiliary power unit, Study of the feed system, Journal of Power Sources 149, (2005), 8–14

Shekhawat D, Berry D A, Gardner T H, Haynes D J, Spivey J J, Effects of fuel cell anode recycle on catalytic fuel reforming, Journal of Power Sources 168, (2007), 477–483

Shi L, Bayless D J, Prudich M, A model of steam reforming of iso-octane: The effect of thermal boundary conditions on hydrogen production and reactor temperature, International Journal of Hydrogen Energy 33, (2008), 4577–4585

Shiratori Y, Quang-Tuyen T, Umemura Y, Kitaoka T, Sasaki K, Paper-structured catalyst for the steam reforming of biodiesel fuel, International Journal of Hydrogen Energy 38, (2013), 11278–11287

Shiratori Y, Quang-Tuyen T, Sasaki K, Performance enhancement of biodiesel fueled SOFC using paper-structured catalyst, International Journal of Hydrogen Energy 38, (2013), 9856–9866

Siefert N S, Shekhawat D, Smith M W, Haynes D J, Bergen R M, Robey E H, Gemmen R S, Berry D A, Operation of a solid oxide fuel cell on a reformed FAME mixture, Biomass & Bioenergy 47, (2012), 362–371

Sircar S, Golden T C, Purification of Hydrogen by Pressure Swing Adsorption, Separation Science and Technology 35(5), (2000), 667–687

Soave G, Equilibrium constants from a modified Redlich-Kwong equation of state, Chemical Engineering Science 27, (1972), 1197–1203

Specchia S, Tillemans F W A, van den Oosterkamp P F, Saracco G, Conceptual design and selection of a biodiesel fuel processor for a vehicle fuel cell auxiliary power unit, Journal of Power Sources 145, (2005), 683–690

Specchia S, Fuel processing activities at European level: A panoramic overview, International Journal of Hydrogen Energy 39, (2014), 17953–17968

Sterner M, Stadler I, Energiespeicher – Bedarf, Technologien, Integration, Springer Viehweg Berlin Heidelberg, 2014

Thormann J, Maier L, Pfeifer P, Kunz U, Deutschmann O, Schubert K, Steam reforming of hexadecane over a Rh/CeO$_2$ catalyst in microchannels: Experimental and numerical investigation, International Journal of Hydrogen Energy 34, (2009), 5108–5120

Thormann J, Pfeifer P, Kunz U, Dynamic performance of hexadecane steam reforming in a microstructured reactor, Chemical Engineering Journal 191, (2012), 410–415

Trabold T A, Lylak J S, Walluk M R, Lin J F, Troiani D R, Measurement and analysis of carbon formation during diesel reforming for solid oxide fuel cells, International Journal of Hydrogen Energy 37, (2012), 5190–5201

Trane R, Dahl S, Skjøth-Rasmussen M S, Jensen A D, Catalytic steam reforming of bio-oil, International Journal of Hydrogen Energy 37, (2012), 6447–6472

Trimm D L, Coke formation and minimization during steam reforming reactions, Catalysis Today 37, (1997), 233–238

Trimm D L, Catalysts for the control of coking during steam reforming, Catalysis Today 49, (1999), 3–10

U.S. Department of Energy, Fuel Cell Technologies Market Report 2014, Washington, 2015, http://energy.gov/sites/prod/files/2015/10/f27/fcto_2014_market_report.pdf (accessed 20/05/2016)

Wang X, Gorte R J, A study of steam reforming of hydrocarbon fuels on Pd/ceria, Applied Catalysis A: General 224, (2002), 209–218

Wu C, Liu R, Carbon deposition behavior in steam reforming of bio-oil model compound for hydrogen production, International Journal of Hydrogen Energy 35, (2010), 7386–7398

Xu L, Mi W, Su Q, Hydrogen production through diesel steam reforming over rare-earth promoted Ni/γ-Al$_2$O$_3$ catalysts, Journal of Natural Gas Chemistry 20, (2011), 287–293

Xu X, Li P, Shen Y, Small-scale reforming of diesel and jet fuels to make hydrogen and syngas for fuel cells: A review, Applied Energy 108, (2013), 202–217

Xuan J, Leung M K H, Leung D Y C, Ni M, A review of biomass-derived fuel processors for fuel cell systems, Renewable and Sustainable Energy Reviews 13, (2009), 1301–1313

Yeh G T, Kao Y L, Yang S Y, Rei M H, Yan Y Y, Lee P C, Low cost compact onsite hydrogen generation, International Journal of Hydrogen Energy 39, (2014), 20614–20624

Yoon S, Kang I, Bae J, Effects of ethylene on carbon formation in diesel autothermal reforming, International Journal of Hydrogen Energy 33, (2008), 4780–4788

Yoon S, Kang I, Bae J, Suppression of ethylene-induced carbon deposition in diesel autothermal reforming, International Journal of Hydrogen Energy 34, (2009), 1844–1851

Yuan W, Hansen A C, Zhang Q, Vapor pressure and normal boiling point predictions for pure methyl esters and biodiesel fuels, Fuel 84, (2005), 943–950

Zheng Q, Janke C, Farrauto R, Steam reforming of sulfur-containing dodecane on a Rh-Pt catalyst: Influence of process parameters on catalyst stability and coke structure, Applied Catalysis B: Environmental 160-161, (2014), 525–533

Zyryanova M M, Badmaev S D, Belyaev V D, Amosov Y I, Snytnikov P V, Kirillov V A, Sobyanin V A, Catalytic Reforming of Hydrocarbon Feedstocks into Fuel for Power Generation Units, Catalysis in Oil Refining 5, (2013), 312–317
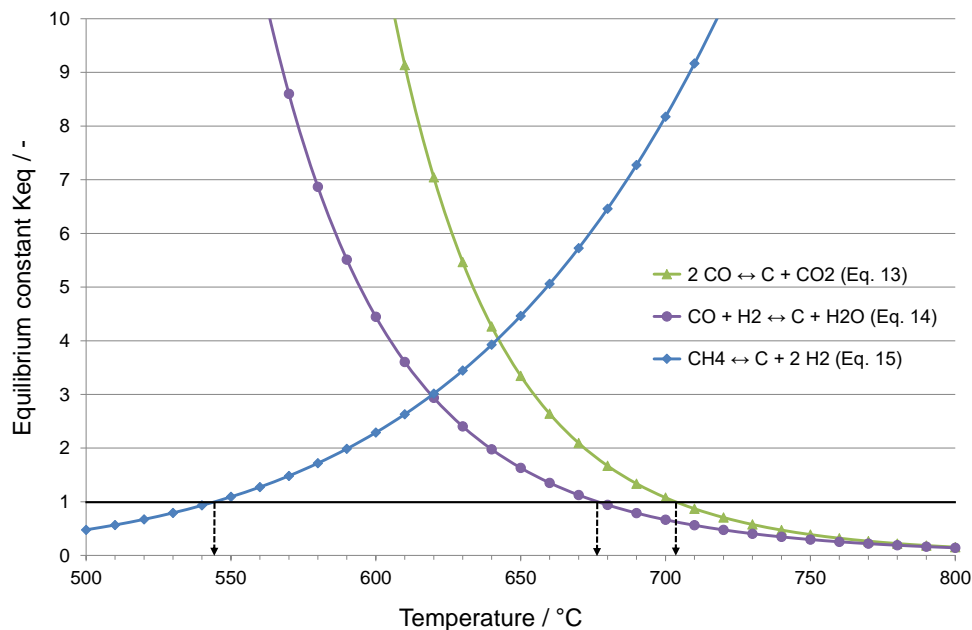
Annex

Figure A1 — Equilibrium constants Keq (calculated with Aspen Plus) of selected carbon formation reactions

Table A1 – Equilibrium constants Keq of selected carbon formation reactions (see Fig. A1)

T (°C)	Keq (Eq. (13))	Keq (Eq. (14))	Keq (Eq. (15))	T (°C)	Keq (Eq. (13))	Keq (Eq. (14))	Keq (Eq. (15))
500	252.3	49.0	0.5	660	2.6	1.4	5.1
510	179.3	37.5	0.6	670	2.1	1.1	5.7
520	128.6	28.9	0.7	680	1.7	0.9	6.5
530	93.0	22.4	0.8	690	1.3	0.8	7.3
540	67.8	17.5	0.9	700	1.1	0.7	8.2
550	49.8	13.7	1.1	710	0.9	0.6	9.2
560	36.9	10.8	1.3	720	0.7	0.5	10.3
570	27.5	8.6	1.5	730	0.6	0.4	11.5
580	20.7	6.9	1.7	740	0.5	0.3	12.8
590	15.7	5.5	2.0	750	0.4	0.3	14.2
600	11.9	4.4	2.3	760	0.3	0.3	15.8
610	9.1	3.6	2.6	770	0.3	0.2	17.5
620	7.0	2.9	3.0	780	0.2	0.2	19.3
630	5.5	2.4	3.4	790	0.2	0.2	21.3
640	4.3	2.0	3.9	800	0.2	0.1	23.5
650	3.3	1.6	4.5				

Table A2 – Bioethanol properties

Parameter	Test Method	Unit	Actual value	Specification
Ethanol	DIN 12803	wt. %	99.9	min. 99.9
Water	DIN EN ISO 12937	ppm	507	max. 2000
Density at 20 °C	DIN 12803	kg/m³	789.9	$789.2 - 792.3$
Methanol	GC Verbio-Method	ppm	49	max. 300
Higher alcohols (C3-C5)	GC Verbio-Method	ppm	1452	max. 2000
Ester (calculated as ethylacetate)	GC-Verbio-Method	ppm	228	max. 500
Aldehydes (calculated as acetaldehyde)	GC-Verbio-Method	ppm	179	max. 500
Acidity (calculated as acetic acid)	DIN EN ISO 11885	ppm	24	max. 40
Chloride	ASTM 4929 B	ppm	< 1.0	max. 1.0
Sulphur	DIN EN ISO 11885	ppm	< 1.0	max. 1.0
Sodium	DIN EN ISO 11885	ppm	< 1.0	max. 1.0
Iron	DIN EN ISO 11885	ppm	< 1.0	max. 1.0
Nitrogen as NH_3	ASTM D1614-03	ppm	< 1.0	max. 1.0
Copper	DIN EN ISO 11885	ppm	< 0.1	max. 1.0
Phosphorus	DIN EN ISO 11885	ppm	< 0.5	max. 0.5
Insoluble matter	ASTM D 1353:2003	mg/100 ml	< 10	max. 10

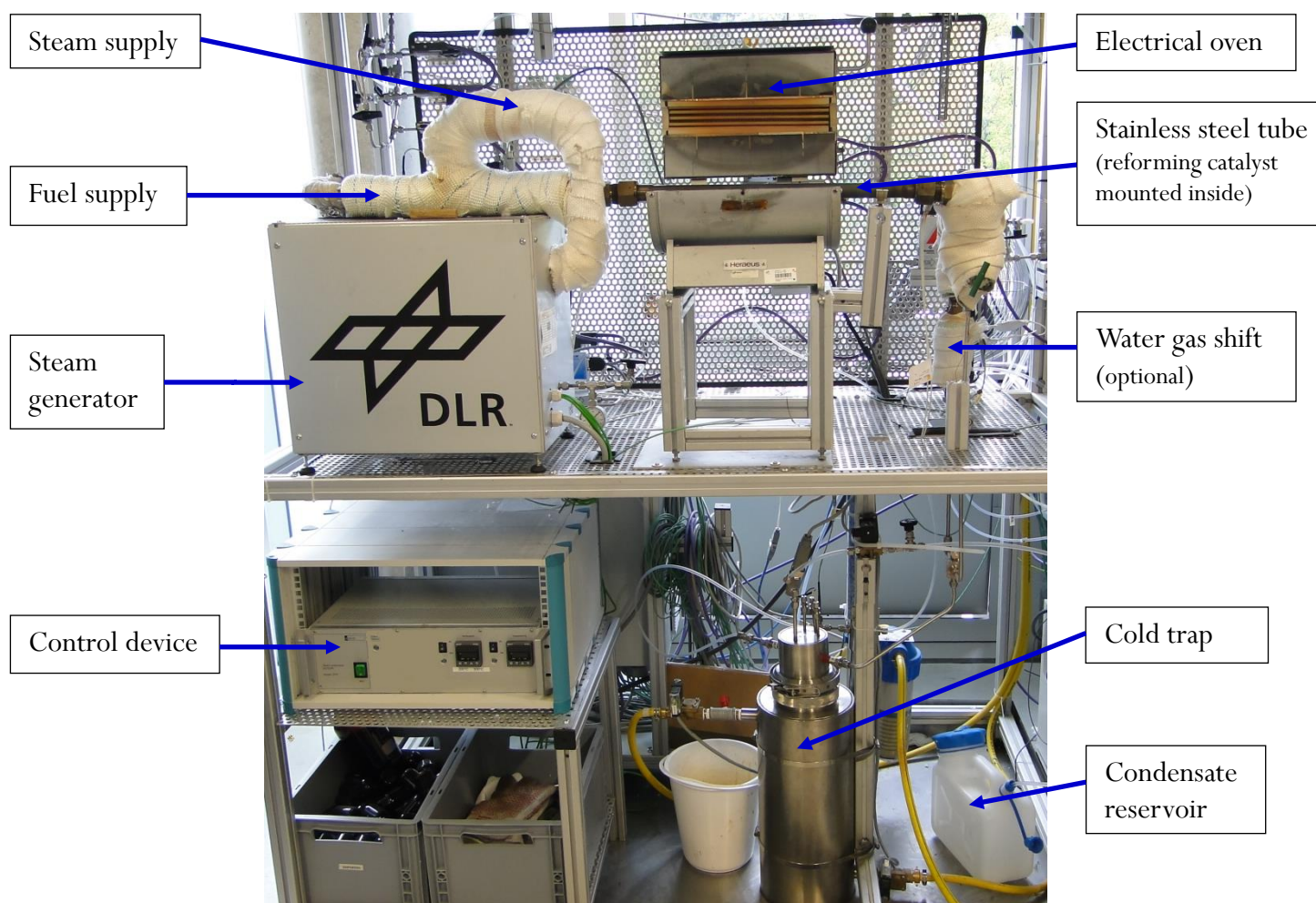* denatured with 0.3 g denatonium benzoat per 100 l and 1 vol. % methyl-ketone

Figure A2 — Photographic view of laboratory test rig for steam reforming of liquid fuels

Table A3: Details on measurement equipment

Measuring device	Measured variable	Range	Accuracy
Rosemount Analytical NGA 2000 MLT	CO, CO_2, CH_4	0-100 %	$\pm$ 1 % FS
Mess- und Analysetechnik GmbH: Thermo-FID	H_2	0-100 %	$\pm$ 1 % FS
ABB URAS 14, Advanced Optima AO 2020	CO, CO_2, CH_4, H_2	0-100 %	$\pm$ 0.5 % FS
Varian Micro GC CP-4900	H_2, CO, CO_2, CH_4, N_2, O_2, C_1-C_4	0-100 %	$\pm$ 0.1 % FS
Mass Flow Meter El-Flow, F-201CV, Bronkhorst	Reformate mass flow	max. 5 l_N/min	$\pm$ 0.5 % FS
Pressure Controller El-Press, Bronkhorst	System Pressure	max. 10 bar	$\pm$ 0.1 % FS
Elemental Analyzer EA 5000, Jena Analytik	C_{solid}	dependent on weight of sample	dependent on quality of calibration
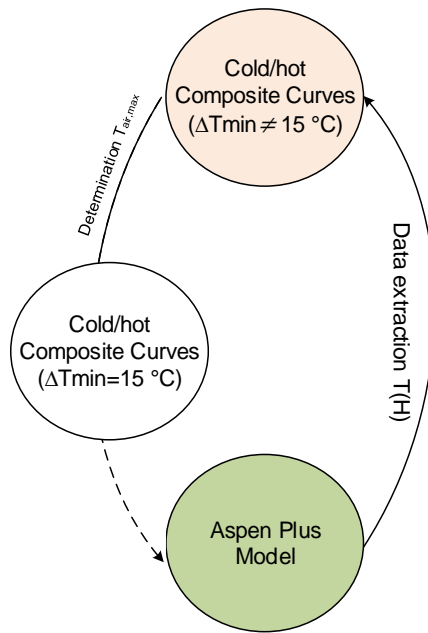
Figure A3 – Iterative procedure for determining the maximum air preheating temperature of heat integrated hydrogen generation system based on biodiesel SR
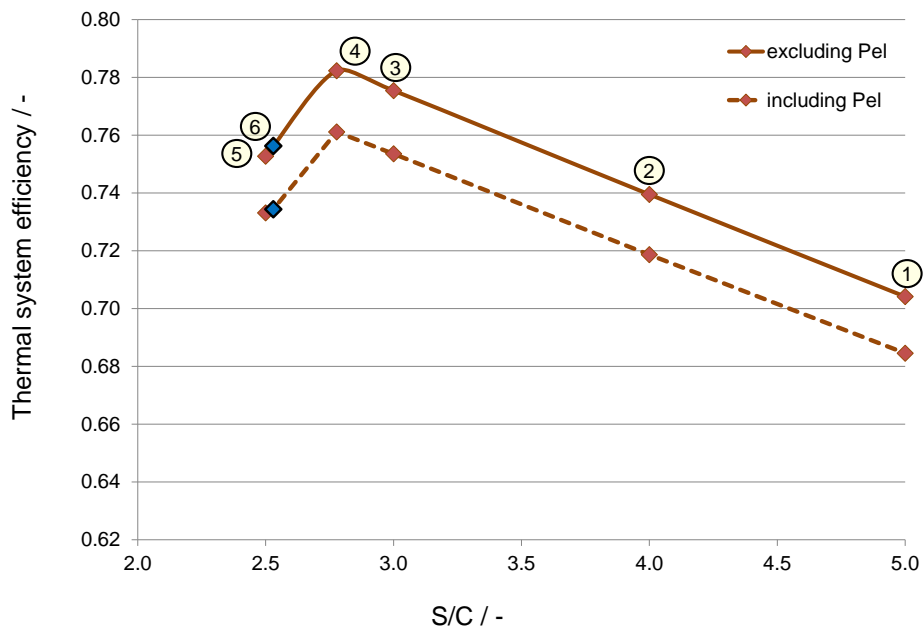

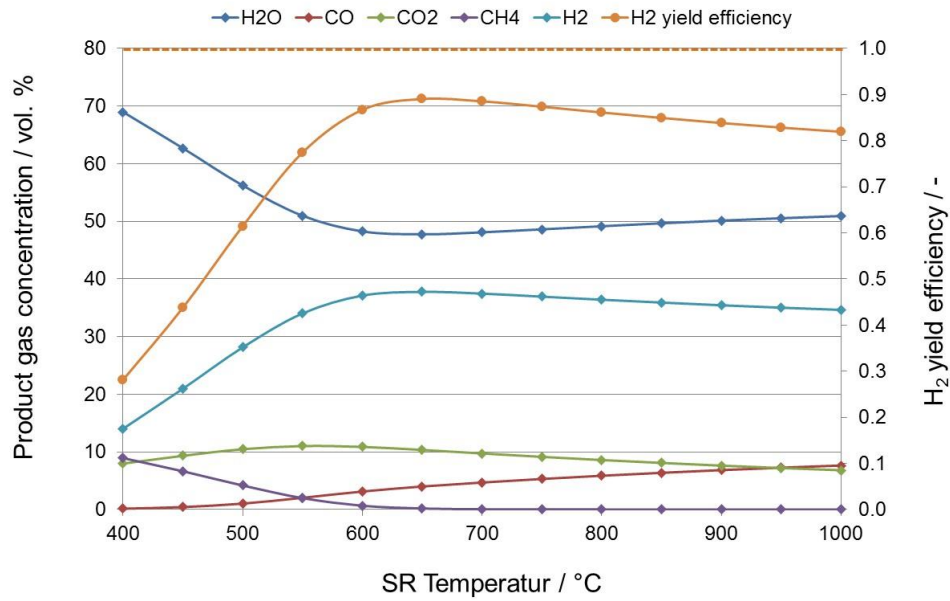**Figure A4 –** Thermal system efficiency including and excluding P_{el}

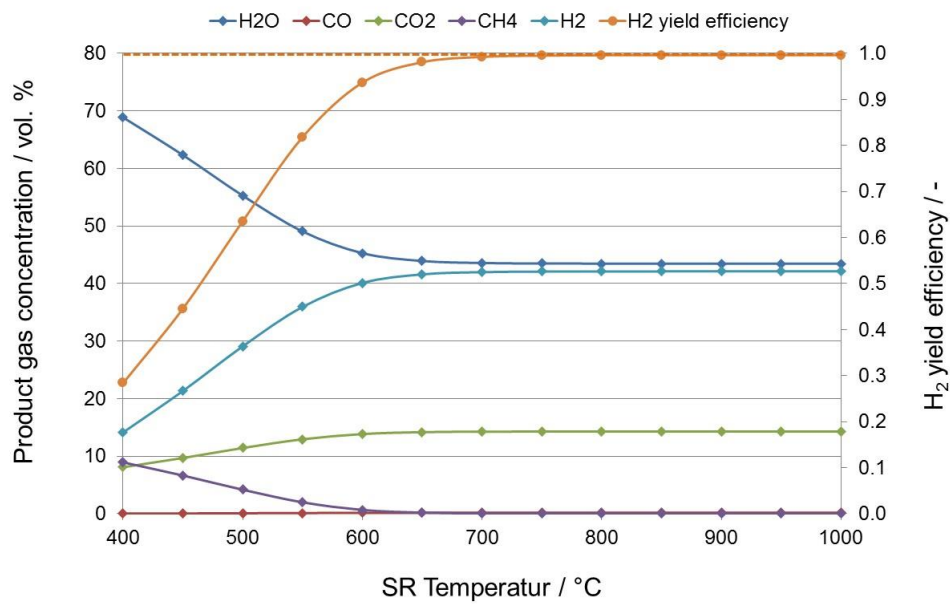**Figure A5a** – Equilibrium gas composition after reformer (diesel SR, S/C=5, p=1 bar)

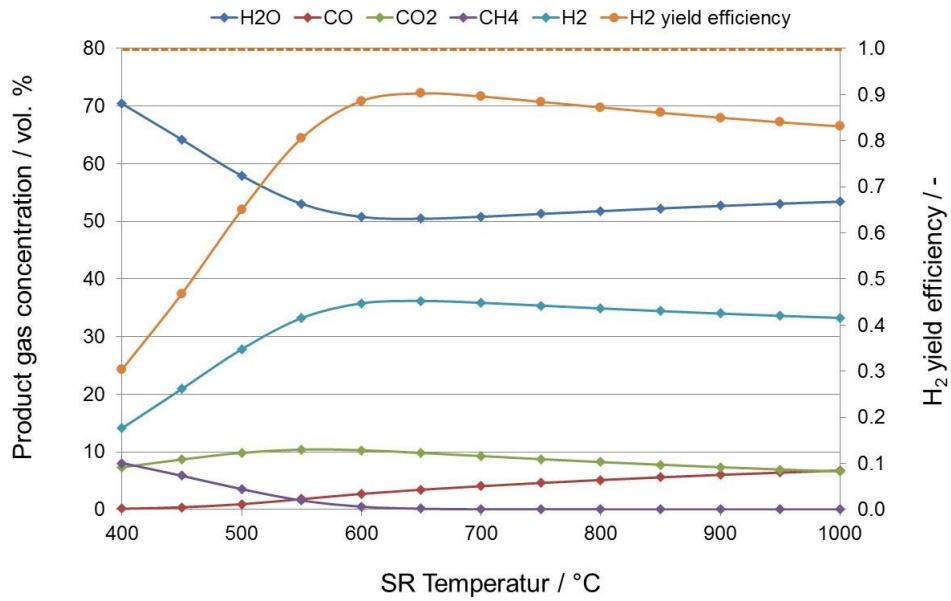**Figure A5b** – Equilibrium gas composition after reformer + WGS (diesel SR, S/C=5, p=1 bar, T_{WGS}=250 °C)

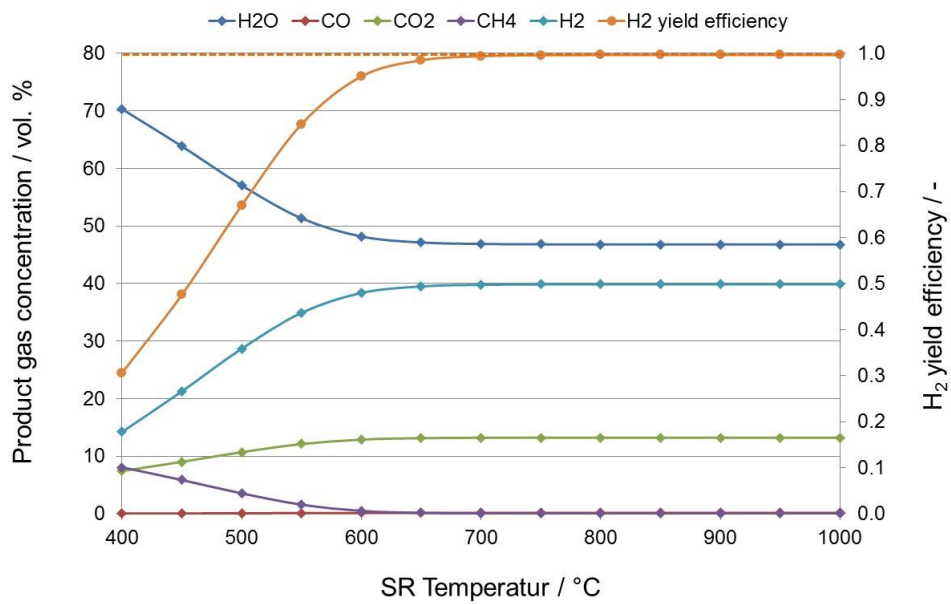**Figure A6a** – Equilibrium gas composition after reformer (bioethanol SR, S/C=5, p=1 bar)

Figure A6b – Equilibrium gas composition after reformer + WGS (bioethanol SR, S/C=5, p=1 bar,
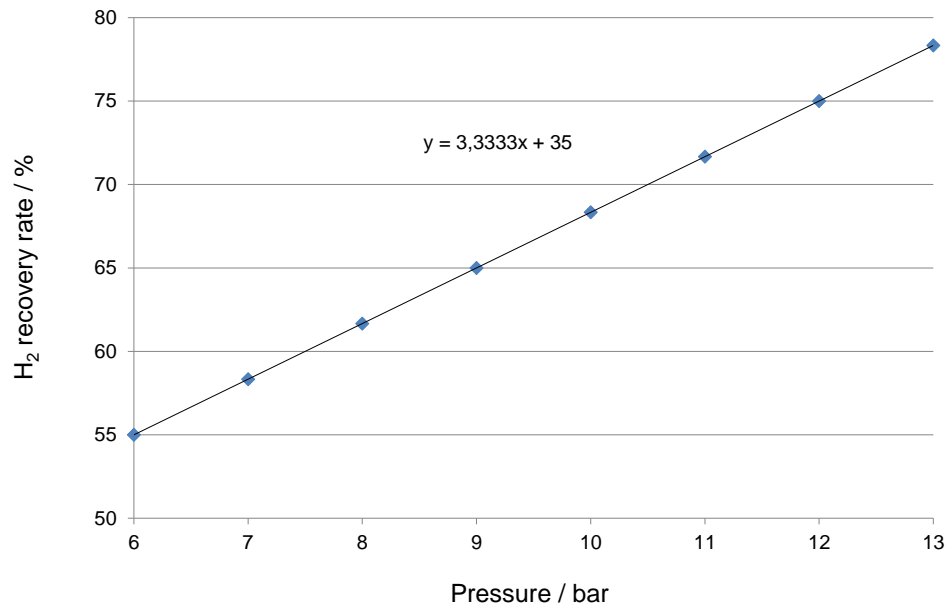
T_{WGS}=250 °C)

$y = 3,3333x + 35$

Figure A7 – PSA-efficiency: H_2 recovery rate in the pressure range p=6 bar – 13 bar

Table A4 – PSA-efficiency: H_2 recovery rate in the pressure range p=6 bar – 13 bar (see Fig. A7)

Pressure (bar)	H_2 recovery (%)
6	55.0
7	58.3
8	61.7
9	65.0
10	68.3
11	71.7
12	75.0
13	78.3